State of Wyoming
Department of Transportation

WY-2201F

FINAL REPORT

Source: WYDOT Road Information System

Characterization of Blow Over Risk in the Wyoming Highway System

Department of Civil and Architectural Engineering
University of Wyoming
1000 E. University Avenue, Dept. 3295
Laramie, WY 82071

Department of Civil Engineering
Gonzaga University
502 E Boone Ave, AD 26
Spokane, WA 99258

November 30, 2021

Disclaimer Notice:

This document is disseminated under the sponsorship of the Wyoming Department of Transportation (WYDOT) in the interest of information exchange. WYDOT assumes no liability for the use of the information contained in this document. WYDOT does not endorse products or manufacturers. Trademarks or manufacturers' names appear in this report only because they are considered essential to the objective of the document.

Quality Assurance Statement

WYDOT provides high-quality information to serve government, industry, and the public in a manner that promotes public understanding. Standards and policies are used to ensure and maximize the quality, objectivity, utility, and integrity of its information. WYDOT periodically reviews quality issues and adjusts its programs and processes to ensure continuous quality improvement.

Copyright

No copyrighted material, except that which falls under the "fair use" clause, may be incorporated into a report without permission from the copyright owner, if the copyright owner requires such.

Prior use of the material in a WYDOT or governmental publication does not necessarily constitute permission to use it in a later publication.

- Courtesy – Acknowledgment or credit will be given by footnote, bibliographic reference, or a statement in the text for use of material contributed or assistance provided, even when a copyright notice is not applicable.
- Caveat for Unpublished Work – Some material may be protected under common law or equity even though no copyright notice is displayed on the material. Credit will be given and permission will be obtained as appropriate.
- Proprietary Information – To avoid restrictions on the availability of reports, proprietary information will not be included in reports, unless it is critical to the understanding of a report and prior approval is received from WYDOT. Reports containing such proprietary information will contain a statement on the Technical Report Documentation Page restricting availability of the report.

Creative Commons

The report is covered under a Creative Commons, CC-BY-SA license. When drafting an adaptive report or when using information from this report, ensure you adhere to the following:

- Attribution – You must give appropriate credit, provide a link to the license, and indicate if changes were made. You may do so in any reasonable manner, but not in any way that suggests the licensor endorses you or your use.
- ShareAlike – If you remix, transform, or build upon the material, you must distribute your contributions under the same license as the original.
- No additional restrictions – You may not apply legal terms or technological measures that legally restrict others from doing anything the license permits.

Foreword

This report provides technical documentation of probabilistic quantification of blow over risk based on high-frequency wind monitoring data in the State of Wyoming.

Noriaki Ohara, P.E. Ph.D., Associate Professor
Department of Civil and Architectural Engineering
University of Wyoming
1000 E. University Avenue, Dept. 3295
Laramie, Wyoming 82071

Technical Report Documentation Page

1. Report No. WY-2201F	2. Government Accession No.	3. Recipient's Catalog No.	
4. Title and Subtitle Characterization of Blow Over Risk in the Wyoming Highway System		5. Report Date November 2021	
		6. Performing Organization Code	
7. Author(s) Noriaki Ohara, P.E. Ph.D. (0000-0002-7829-0779), Adarsha Neupane (0000-0001-8533-7806), Rhonda Young, P.E. Ph.D. (0000-0001-6745-5008), Antonio Roman Campos (0000-0002-5027-5104)		8. Performing Organization Report No.	
9. Performing Organization Name and Address University of Wyoming 1000 East University Avenue, Dept. 3295 Laramie, WY 82070		10. Work Unit No.	
		11. Contract or Grant No. RS07219	
12. Sponsoring Agency Name and Address Wyoming Department of Transportation (WYDOT) 5300 Bishop Blvd. Cheyenne, Wyoming 82001		13. Type of Report and Period Covered Final Report	
		14. Sponsoring Agency Code WYDOT	
15. Supplementary Notes Project Champions: Kathy Ahlenius and Clifford Spoonemore, WYDOT Field Operations and Maintenance Services			
16. Abstract: Blow over crashes caused by severe crosswinds are a common problem on Wyoming highways, as well as roadways elsewhere that are subject to high wind conditions. To characterize blow over-inducing wind gusts, a high-frequency wind monitoring system was installed at a known hazard area along Interstate 25 just north of the Colorado-Wyoming state line. Data collected from this high-frequency system were analyzed along with data from the Wyoming Department of Transportation's (WYDOT) traditional systems including a Portable Weather Instrument Station (PWIS) and an existing Road Weather Information System (RWIS). Using data collected from these sources and a static vehicle stability model that integrates major influencing factors, the critical vehicle speed for the blow over condition was statistically modeled by distribution fitting. Through this investigation, the exp-gamma distribution was found to be the most appropriate to model the stochastic process of vehicle blow over risk. Applications using historical, statewide RWIS Environmental Sensor Station (ESS) data demonstrated the predictive capability of this developed tool for historical blow over crashes. Furthermore, the sensitivity analysis of this vehicle stability model characterizes the blow over risk of vehicles with various attributes. Finally, blow over hazard maps were produced based on reconstructed historical maximum and mean wind fields using a Weather Research and Forecasting (WRF) model. This dynamic risk-assessing tool, founded in the technology developed herein, will provide significant additional information to traveler information systems and roadway agencies managing roads with frequent high wind conditions.			
17. Key Words Blow over crash, blow over risk, tractor-trailer, high winds, extreme weather events, Wyoming	18. Distribution Statement This document is available through the National Transportation Library and the Wyoming State Library.		
19. Security Classification. (Of this report) Unclassified	20. Security Classification. (Of this page) Unclassified	21. No. of Pages 92	22. Price

SI* (MODERN METRIC) CONVERSION FACTORS

APPROXIMATE CONVERSIONS TO SI UNITS

Symbol	When You Know	Multiply By	To Find	Symbol
		LENGTH		
in	inches	25.4	millimeters	mm
ft	feet	0.305	meters	m
yd	yards	0.914	meters	m
mi	miles	1.61	kilometers	km
		AREA		
in^2	square inches	645.2	square millimeters	mm^2
ft^2	square feet	0.093	square meters	m^2
yd^2	square yard	0.836	square meters	m^2
ac	acres	0.405	hectares	ha
mi^2	square miles	2.59	square kilometers	km^2
		VOLUME		
fl oz	fluid ounces	29.57	milliliters	mL
gal	gallons	3.785	liters	L
ft^3	cubic feet	0.028	cubic meters	m^3
yd^3	cubic yards	0.765	cubic meters	m^3
	NOTE: volumes greater than 1000 L shall be shown in m^3			
		MASS		
oz	ounces	28.35	grams	g
lb	pounds	0.454	kilograms	kg
T	short tons (2000 lb)	0.907	megagrams (or "metric ton")	Mg (or "t")
		TEMPERATURE (exact degrees)		
°F	Fahrenheit	5 (F-32)/9 or (F-32)/1.8	Celsius	°C
		ILLUMINATION		
fc	foot-candles	10.76	lux	lx
fl	foot-Lamberts	3.426	$candela/m^2$	cd/m^2
		FORCE and PRESSURE or STRESS		
lbf	poundforce	4.45	newtons	N
lbf/in^2	poundforce per square inch	6.89	kilopascals	kPa

APPROXIMATE CONVERSIONS FROM SI UNITS

Symbol	When You Know	Multiply By	To Find	Symbol
		LENGTH		
mm	millimeters	0.039	inches	in
m	meters	3.28	feet	ft
m	meters	1.09	yards	yd
km	kilometers	0.621	miles	mi
		AREA		
mm^2	square millimeters	0.0016	square inches	in^2
m^2	square meters	10.764	square feet	ft^2
m^2	square meters	1.195	square yards	yd^2
ha	hectares	2.47	acres	ac
km^2	square kilometers	0.386	square miles	mi^2
		VOLUME		
mL	milliliters	0.034	fluid ounces	fl oz
L	liters	0.264	gallons	gal
m^3	cubic meters	35.314	cubic feet	ft^3
m^3	cubic meters	1.307	cubic yards	yd^3
		MASS		
g	grams	0.035	ounces	oz
kg	kilograms	2.202	pounds	lb
Mg (or "t")	megagrams (or "metric ton")	1.103	short tons (2000 lb)	T
		TEMPERATURE (exact degrees)		
°C	Celsius	1.8C+32	Fahrenheit	°F
		ILLUMINATION		
lx	lux	0.0929	foot-candles	fc
cd/m^2	$candela/m^2$	0.2919	foot-Lamberts	fl
		FORCE and PRESSURE or STRESS		
N	newtons	0.225	poundforce	lbf
kPa	kilopascals	0.145	poundforce per square inch	lbf/in^2

*SI is the symbol for the International System of Units. Appropriate rounding should be made to comply with Section 4 of ASTM E380.
(Revised March 2003)

Table of Contents

Executive Summary 1

Chapter 1 - Introduction 3

1.1 Problem Description 3

1.2 Literature Review 8

1.2.1 Vehicle Stability Affected by Strong Wind 8

1.2.2 Blow Over Risk Model in Wyoming 9

1.2.3 Mitigation in Practice 9

1.2.4 Implications 10

1.3 Objectives 11

Chapter 2 - Observation of Wind Fields 13

2.1 Installation of the High-Frequency Wind Monitoring System 13

2.2 Comparison of the Wind Direction and Wind Speed from the Three Observation Systems 14

Chapter 3 - Blow Over Risk Analysis 21

3.1 Vehicle Stability Model 21

3.1.1 Forces Acting on Vehicle 21

3.1.2 Static Force Balance for Blow Over Condition 22

3.1.1 Roadside Wind Field Estimation 24

3.2 Stochastic Model for Blow over Crash 28

3.2.1 Probability of Blow Over Crash 28

3.2.2 Statistical Distributions for Extreme Value 29

3.2.3 Distribution of the Critical Vehicle Speed 32

3.2.4 Parametric Exp-gamma Distribution 33

3.2.5 Estimation of the Mean Critical Vehicle Speed from the Mean Wind Speed 34

3.2.6 Estimation of the SD from the Gust Wind Speed and Average Wind Speed 35

3.2.7 Parameter Estimation Algorithm for the Critical Wind Speed Distribution 36

3.2.8 Validation of the Parametric Distribution 36

3.3 Model Performance Demonstration 38

3.3.1 Baseline Vehicle Type and the Model Parameters 38

3.3.2 Computational Efficiency of the Blow over Model 43

3.3.3 Case Studies: Three Observed Blow Over Crashes in the Wyoming Hill Study Area 44

3.3.3.2 November 13, 2020 Crash 44
Chapter 4 – Blow Over Risk Assessment in Wyoming 49
4.1 Blow Over Risk Assessment System 49
4.2 Road Geometry Parameter Database 50
4.3 Implementation of the Blow Over Risk Assessment System 53
4.3.1 Ground-Based Wind Data 53
4.3.2 Spatial Distribution of Blow Over Risk During November 13, 2020 Crash Period 54
4.3.3 Other Historical Blow Over Crashes 57
4.3.4 Factor of Safety (FOS) Selection 59
4.3.5 Performance Evaluation of the Blow Over Risk Assessment System 61
4.3.6 Real time Implementation of the Configured Blow Over Risk Evaluation System 62
4.4 Blow Over Hazard Maps based on Simulated Wind Data 63
4.2.1 Model-Based Historical Wind Data 63
4.4.2 Historical Mean Wind Records and Blow Over Risk 67
4.4.3 Historical Maximum Wind and Blow Over Risk 68
Chapter 5 – Integration of Results into WYDOT Traveler Information Systems and Recommendations 71
5.1 Road Weather Information Dissemination 71
5.2 Generating Road Weather Information 73
5.2.1 Pikalert® System 74
5.2.2 CV Pilot Spot Weather Impact Warning 77
5.3 Incorporating Findings into Road Weather Systems 78
Chapter 6- Products 81
6.1 Demonstrative Real Time Implementation of the Blow Over Risk Evaluation System 81
6.2 GIS map of road geometry (shapefile and csv) 81
6.3 Blow Over Hazard Map (shapefile and csv) 82
6.4 Blow Over Sensitivity Analysis Source Code for General Characterization for Practice (Python code) 82
6.5 Blow Over Hazard Map Source Code (Python code) 83
6.6 Excel spreadsheet for critical vehicle velocity 83
6.7 Publications on the Blow Over Risk Evaluation Methodology 83
6.8 Opportunities for Training and Professional Development 84
Chapter 7 – Conclusions and Recommendations 85

References.. 87
Appendix: Variable Glossary.. 92

List of Figures

Figure 1: Statewide blow over crashes from 2012-2017 4

Figure 2. Location of Wyoming Hill project location..... 5

Figure 3: Aerial view and elevation profile of Wyoming Hill project location..... 6

Figure 4: Cross Section of Wyoming Hill Project Location..... 6

Figure 5: Street view of Wyoming Hill project location..... 7

Figure 6: Diagram of project data sources and their purposes..... 8

Figure 7: Definition of blow over risk operationalized in this study 12

Figure 8: Map of Wyoming Hill project area. There are two crash sites denoted by black stars at MP 3.8 (Nov 13 &15, 2020 crashes) and at MP 3.3 (Jan 1, 2020 crash) 13

Figure 9: Assembled high-frequency wind monitoring system in the UW Water Resources Lab 14

Figure 10: Installed system near exit 4 on I-25 (MP 4.5) 14

Figure 11: Wind rose diagrams based on different wind sensors in the study area, January 2020..... 16

Figure 12: Time series of the observed 10-minute average and maximum wind speeds on November 13, 2020 (Subfigure A,B), and their linear relation to the winds from RWIS station (Subfigure C,D)..... 18

Figure 13: Definitions of axes for static blow over analysis..... 22

Figure 14: Various forces acting on a vehicle..... 23

Figure 15: Wind profile, wind height adjustment, and road elevation adjustment 25

Figure 16: Computation of headwind and crosswind components from wind and vehicle azimuth angles25

Figure 17: Sensitivity analysis of wind azimuth angle to the critical vehicle speed with a gust wind speed of 60 mph and the definitions of the angles as shown 27

Figure 18: Sensitivity analysis of vehicle weight to the critical vehicle speed with a gust wind speed of 60 mph 27

Figure 19: Example PDF of the critical vehicle speed during Jan 1, 2020, at the I-25 study section..... 29

Figure 20: Example of fitted distribution and actual data of critical vehicle speed (Time step 163 of 15-minute data for March) 32

Figure 21: Annual average RMSE values, 2020..... 33

Figure 22: The relation between the mean of V_c by statistical analysis of high-frequency wind data within 15-minute and the V_c calculated from average wind and average wind direction during the corresponding periods..... 34

Figure 23: The relationship between the standard deviation of V_c and Vc computed from the wind gust. Red dots are the outliers..... 35

Figure 24: The relationship between the difference in V_c from 15-minute average and gust speed and standard deviation of V_c. Red dots are the outliers. 36

Figure 25: The annual average RMSE value of the parametric distributions for those 15-minute instances with an average V_c less than 105 mph. 37
Figure 26: The PDF of the actual data with their associated parametric distributions. 37
Figure 27: The CDF of the actual data with their associated parametric distributions. 38
Figure 28: Sensitivity analysis of the blow over risk model with respect to wind speed. Both average and maximum speeds influence the blow over risk. 39
Figure 29: Sensitivity analysis of the blow over risk model with respect to wind direction for the heavier vehicle (20000 kg). 40
Figure 30: Sensitivity analysis of the blow over risk model with respect to wind direction for a lighter vehicle (15000 kg). 41
Figure 31: Sensitivity analysis of the blow over risk model with respect to vehicle weight and travel speed on a straight road. 42
Figure 32: Sensitivity analysis of the blow over risk model with respect to vehicle weight and travel speed on a curved road. 43
Figure 33: Estimated blow over risk evolution and the corresponding PDF of critical vehicle speed V_c during January 1st, 2020 44
Figure 34: Photographs of the Nov 13 blow over crash from the webcam at the Wyoming Hill RWIS ESS and the map of the incident 45
Figure 35: The critical vehicle speed on the day of reported blow over crash at the crash site 46
Figure 36: The blow over risk probability calculated based on the fitted distribution 47
Figure 37: Flowchart for blow over risk (BO risk or P(A)) assessment system 49
Figure 38: Road points established at each tenth of a mile in the Wyoming highway system. 50
Figure 39: Computed elevation in MASL around the study area (MP 3-5) of I-25 51
Figure 40: Estimated relative road surface elevation in the study area and the historical blow over crash sites. 52
Figure 41: Example parameters associated with the road point database. 53
Figure 42: RWIS Stations with Buffer of 10 km Around them in Wyoming 54
Figure 43: Blow over risk map at four different times on November 13, 2020. Size of dots, as well as color, reflects blow over risk severity. 56
Figure 44: Model Analysis of windy period from January 18, 2012. Size of dots, as well as color, reflects blow over risk. 59
Figure 45: The FOS used in the model vs the efficiency of the model at different time intervals. 60
Figure 46: Statewide real time blow over risk maps 62
Figure 47: The nesting domains of the WRF model for wind field reconstruction (Ohara, 2017) 64
Figure 48: Beaufort scale for various wind speed units 66

Figure 49: Estimated blow over risk using the historical average wind on the highway network of Wyoming based on the WRF simulation. 67

Figure 50: Estimated blow over risk at the historical maximum wind on the highway network of Wyoming based on the WRF simulation. 68

Figure 51: Estimated blow over risk at the historical maximum wind on the highway network of southeast Wyoming based on the WRF simulation. Black circles denote historical blow over crash sites. 69

Figure 52: Estimated blow over risk at the historical maximum wind and the 10 km coverage of the RWIS ESS network in Wyoming 70

Figure 53: WYDOT Cheyenne Traffic Management Center (TMC) 72

Figure 54: Example of an extreme blow over risk traveler message from Wyoroad.info 72

Figure 55: Diagram of weather data feeding into vehicle data translator module's line of communication 74

Figure 56: Diagram of connected vehicles communicating road conditions and changes in road maintenance 75

Figure 57: Pikalert® Blow over Algorithm 75

Figure 58: CV Pilot spot weather impact warning application (SWIW) 77

Figure 59: CV Pilot Project HMI for traveler information messages 78

List of Tables

Table 1: Common statistical distributions for extreme value modeling 31

Table 2: Baseline parameter values for sensitivity analysis..... 38

Table 3: The historical days with high frequencies of blow over crashes 57

Table 4: Results based on the distance to the nearest RWIS ESS. 61

Table 5: Efficiency of the model based on the crashes within 10 km (6.2 miles) of RWIS. 62

List of Abbreviations

AASHTO	American Association of State Highway and Transportation Officials
ABS	Anti-lock Braking System
ASOS	Automated Surface Observing System
BSM	Basic Safety Message
CDF	Cumulative Distribution Function
CFD	Comuptational Fluid Dynamics
CV	Connected Vehicle Pilot Deployment Project
CVOP	Commercial Vehicle Operator Portal
DEM	Digital Elevation Model
DOT	Department of Transportation
DMS	Dynamic Messaging Signs
ESS	Environmental Sensor Station
FOS	Factor of Safety
GEV	General Extreme Value
GIS	Geographic Information System
HAR	Highway Advisory Radio
HMI	Human-Machine Interface
HRRR	High Resolution Rapid Refresh
IEM	Iowa Environmental Mesonet
MASL	Meters Above Sea Level
MAW	Motorist Advisory and Warning System
MLE	Maximum Likelihood Estimation
MP	Mile Post
NARR	North American Regional Reanalysis
NCAR	National Center for Atmospheric Research
NCEP	National Centers for Environmental Prediction
NED	National Elevation Dataset
NHS	National Highway System
NWP	Numerical Weather Prediction
OBU	Onboard Unit
PBL	Planetary Boundary Layer
PDF	Probability Density Function
PWIS	Portable Weather Instrument Station
RMSE	Root Mean Square Error
ROCA	Road Curvature Analyst
RWA	Road Weather Alert
RWIS	Road Weather Information System
SD	Standard Deviation
SWIW	Spot Weather Impact Warning
TIMs	Traveler Information Messages
TMC	Traffic Management Center
TRR	Transportation Research Record

USGS	United States Geological Survey
UW	University of Wyoming
WHP	Wyoming Highway Patrol
WRF	Weather Research and Forecasting
WYDOT	Wyoming Department of Transportation

Executive Summary

This study quantified blow over crash risk in terms of temporal probability from road geometry, wind fields, vehicle types, and vehicle speeds. The rapid and robust model developed herein was applied to every 0.1-mile segment along highways in Wyoming.

The high-frequency wind monitoring system, University of Wyoming (UW) station, near milepost (MP) 4.5 of Interstate 25 (I-25) provided the essential information for gust wind characterization used by this project. The site of this location is locally known as Wyoming Hill, and it has been historically known for frequent blow over crashes. The collected data from the UW station, as well as Wyoming Department of Transportation's (WYDOT) Portable Weather Instrument Station (PWIS) and the Road Weather Information System (RWIS) Environmental Sensor Station (ESS) sites nearby, have been analyzed. The developed vehicle stability model, which integrates major influencing factors, has been significantly improved in robustness with consideration given to the relative road elevation and both side rollover axes. This computationally efficient model can transform the multi-variate problem into a univariate problem in terms of the critical vehicle speed, which is the maximum travel speed that may be maintained without a blow over crash. Additionally, the critical vehicle speed for the blow over condition was statistically modeled by distribution fitting for the computed quantities. The exp-gamma distribution was found to be the most appropriate for modeling the stochastic process of vehicle blow over risk. A practical method was developed for parameter estimation from the commonly available wind measurements, including average and maximum windspeed.

Applications using the historical roadside wind record available in the RWIS ESS network that covers the entire state of Wyoming demonstrated the predictive capability of this developed tool for historical blow over crashes. The percentage of historical crashes successfully predicted was termed the "efficiency" of the model. The efficiency of the model was analyzed based on the distance to the nearest RWIS ESS. The factor of safety (FOS) of this model was then updated to a value of 5.5 from 3.5 used in a previous study with high-frequency data to improve model performance.

The sensitivity analysis of the new vehicle stability model characterizes the blow over risk of a vehicle with various attributes. For example, it was illustrated that road curvature results in an asymmetry in blow over risk associated with wind direction, and it was found that the weight of a vehicle is crucially important to blow over risk.

The next phase of the research took the previous work on vehicle stability and blow over risk, and applied it statewide to develop blow over hazard maps. These maps were produced based on the reconstructed historical maximum and mean wind fields using the WRF model.

The last phase of model development demonstrated the potential of calculating risk in real time using the mapped statewide RWIS readings. This map was created to illustrate what a decision support tool and driver alert system using these results could look like.

The final task was to look at how the research presented in this report could be integrated within WYDOT's existing Road Weather Management System, including both infrastructure and vehicle-based technologies to provide information to passenger and freight vehicles about current and forecasted high wind events.

Chapter 1 - Introduction

1.1 Problem Description

Blow over (also known as "rollover").[1] crashes caused by extreme crosswinds are a severe problem on Wyoming highways, as well as roadways throughout the world that are subject to severe wind conditions. Because of these crosswinds, Wyoming has the largest number of truck and bus crashes per population in the United States (U.S. Department of Transportation, 2018). Some notable events include November 20, 2017, when dangerous wind gusts toppled 14 tractor-trailers along Interstate 25 (I-25) in southern Wyoming and northern Colorado (e.g., Kull, 2017 Wyoming Tribune Eagle). As a result of this wind event, the Transportation Management Center (TMC), in conjunction with Colorado Department of Transportation (CDOT), closed I-25 in both directions between Wellington, Colorado, and Cheyenne, Wyoming. Another high-profile event occurred on February 7, 2017, when a Wyoming Highway Patrol cruiser was destroyed when a semi-truck rolled onto it on I-80 near Elk Mountain, Wyoming. In total, there were 316 blow over crashes reported in 6 years (2012-17), in Wyoming, for an average of 52.7 incidents per year. In addition to the immediate safety concerns associated with these rollover crashes, there are additional impacts resulting from frequent and long road closures during high wind conditions (WYDOT 2016a). Thus, it is evident that blow over or rollover crashes due to wind gusts are a considerable problem for travelers on the Wyoming sections of national major corridors, such as I-25 and I-80.

Furthermore, high wind events and their resulting blow over crash concerns are not limited to Wyoming. Many coastal areas throughout the world also experience frequent high winds. Areas prone to severe storms, such as hurricanes or typhoons, also have blow over crash concerns. Quantification of blow over risk during a hurricane is an important consideration when managing evacuation routes in advance of a storm. Wind speeds have been increasing worldwide since 2010 and climate change models continue to predict a further escalation of high wind events (Zeng et al., 2019).

The state of Wyoming is often windy during winter months as wind speeds reach 30 to 40 mph, with wind gust speeds of 50 to 60 mph (Curtis and Grimes, 2004). Liesman (2005) identified the most hazardous wind locations in the state based on high frequencies of overturning truck crashes. This was accomplished using three geographic information systems (GIS) models that included the Grid Model, the Sliding Scale Model, and the Advanced Grid Model, all of which were based on records from January 1994 to June 2007. The most hazardous regions in Wyoming were identified as:

- On I-80, approximately 35 miles west of Laramie, near Arlington.
- On I-25, north of Cheyenne, about 10 miles south of Wheatland (Bordeaux).
- On I-80, west of Evanston.
- At the I-80 and I-25 interchange in Cheyenne.

[1] In this report, the term "blow over" that implies a rollover caused by strong wind is used, while "rollover" may still be chosen for general vehicle stability.

Among these sections, Young (2010) found the most hazardous section to be between MP 70.00 and MP 71.00, along I-25, known locally as Bordeaux. Additionally, WYDOT (2016a) empirically identified common blow over "hot spots" in Wyoming as follows:

- Wyoming Hill (I-25, District 1, MP 3-5).
- Bordeaux (I-25, District 2, MP 60-80).
- Arlington (I-80, District 1, MP 272-274).
- Cooper Cove-Strouss Hill (I-80, District 1, MP 278-284).
- Casper's Outer Drive (Hwy 258, District 2, near I-25).

These five hot spots are also outlined in Figure 1, which mapped blow over crashes from 2012-2017.

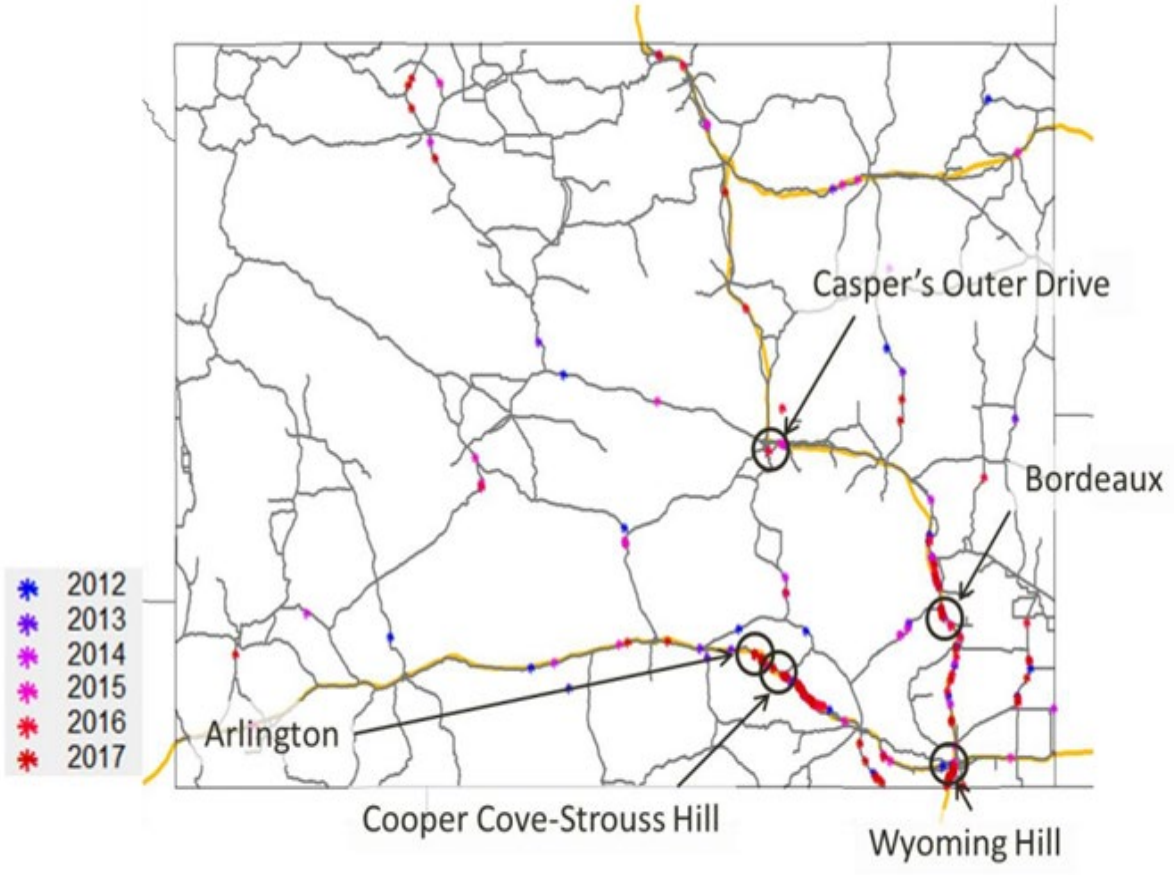

Source: Wyoming Geolibrary and WYDOT

Figure 1: Statewide blow over crashes from 2012-2017

Many of these locations are situated downwind of mountain gaps where the Bernoulli Effect (mountain gap wind effect) augments wind speeds; however, according to the recent blow over crash record, crashes can also occur outside of these hotspots. Therefore, it is important to improve current understandings of the blow over crash mechanism in order to implement better risk management.

While the hazards created from high blow over risk are far from ideal, the frequency and concentration of these blow over crashes do provide a unique opportunity to research the characterization of this risk. This project used the Wyoming Hill hot spot location to collect high frequency wind data along with the more

standard wind data from both permanent and portable RWIS equipment. The Wyoming Hill site is located between MP 3 and MP 5, on I- 25, just north of the Colorado-Wyoming state line, as indicated in Figure 2. The study site is a few miles south of the City of Cheyenne and the junction of Interstates 80 and 25.

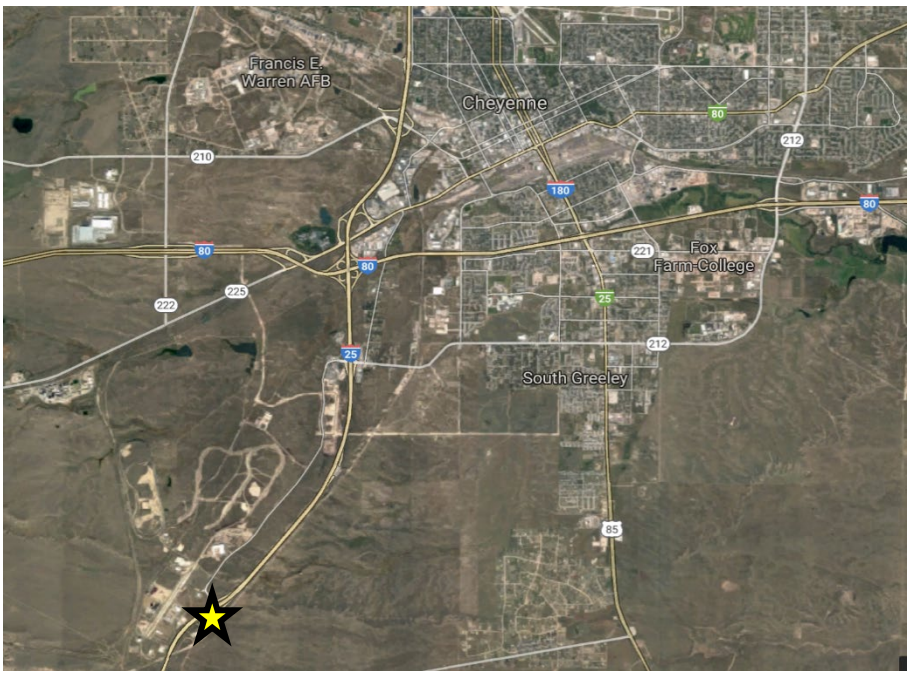

Source: Adapted from Google Maps

Figure 2. Location of Wyoming Hill project location

The topography of the study site is shown in Figure 3 from Google Earth, indicating the corridor is around 6,350 feet above sea level. The major dips in the profile are locations of railroad underpasses where the interstate section passes overhead on a bridge structure. The effect of the bridge will be incorporated into the blow over risk estimation as a locally elevated road surface as discussed in later section.

Source: Adapted from Google Earth

Figure 3: Aerial view and elevation profile of Wyoming Hill project location

Figure 4 and Figure 5 below show more detail of the existing roadway. The project segment is a typical rural interstate facility with two 12-foot lanes accompanied by 10-foot side-shoulders in both directions. The surrounding land use is predominately ranchland and grassland.

Source: Google Earth

Figure 4: Cross Section of Wyoming Hill Project Location

Source: Google Earth

Figure 5: Street view of Wyoming Hill project location

The objective of this report is to fill in existing gaps between operational practices by utilizing weather data from RWIS ESS, the risk available from high-resolution modeled data, and the high-frequency wind observation system. The physical process of blow over crashes has been thoroughly investigated through computational fluid dynamics (CFD) and wind tunnel experiments; however, the process in the real world has rarely been analyzed since field measured wind gusts data at the time and location of a crash are either lacking or incomplete. Because of these data deficiencies, characterization of wind gusts using high-frequency wind monitoring at one known hotspot (Wyoming Hill location on I-25, MP 4) is essential for the prediction and prevention of blow over crashes. To meet this demand, a roadside wind observation system, complete with three-dimensional sonic anemometer (CSAT3B-NC), was installed to evaluate the effect of local topography on the gust wind direction and the blow over crashes. In sum, vehicle stability analysis integrated wind data from the high-frequency observation system, the nearby PWIS, the RWIS, and the WRF model (Figure 6).

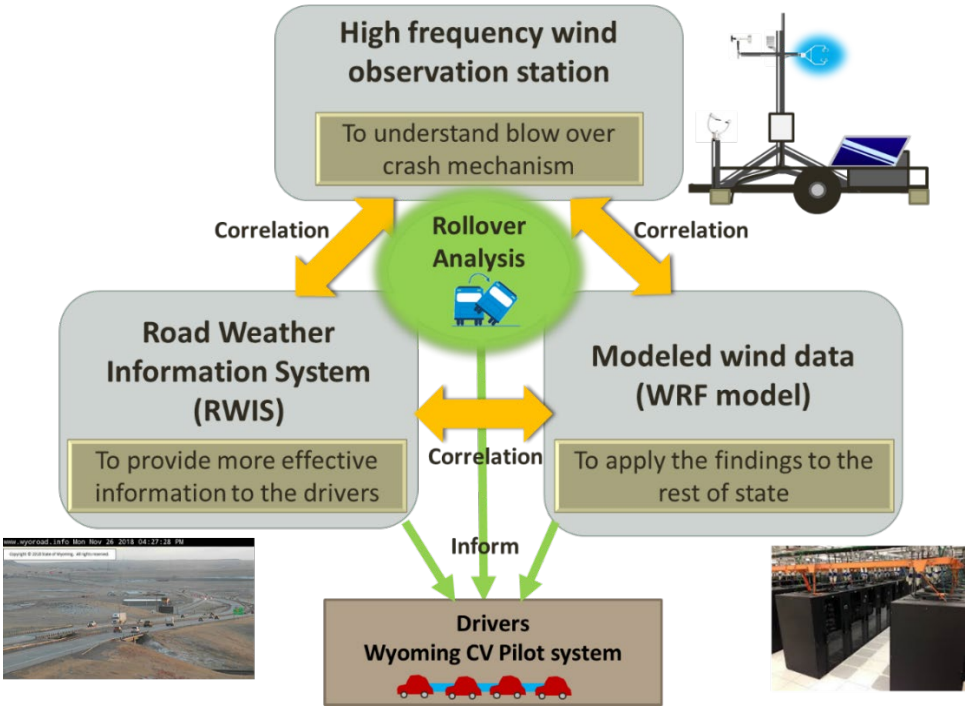

Figure 6: Diagram of project data sources and their purposes

Thanks to its diversity of data sources and analysis techniques, this project provided a better understanding of wind, vehicle speed, load weights, and road geometry characteristics for blow over crash risk. The outcome of this research aims to improve operational practices related to weather-responsive road management, such as the current Wyoming connected vehicle (CV) pilot project. Thus, this research is aligned with WYDOT's strategic goals to improve safety in the state transportation system through education, engineering, enforcement, and other innovative methods.

1.2 Literature Review

1.2.1 Vehicle Stability Affected by Strong Wind

A series of studies for quantifying blow over risk of high-sided vehicles was conducted by Baker, et al., in the United Kingdom (Baker, 1988, 1994; Coleman and Baker, 1994; Baker and Reynolds, 1992). In this inquiry, the blow over mechanism was investigated using models that calculated the accidental (critical) wind speed by solving for aerodynamic and inertial forces. Researchers simulated severe storms in 1990 that caused blow overs in different parts of the United Kingdom using wind tunnel experiments to determine the aerodynamic coefficients for calculating forces. Baker and Reynolds (1992) concluded that wind gusts of 17 to 20 m/s (38 to 45 mph) can initiate a vehicle blow over.

Saiidi and Maragakis (1995) developed an algorithm for the Nevada Department of Transportation to identify the critical wind speeds that lead to blow overs based on vehicle loads and their profiles. The model, when applied by Young et al. (2010), yielded a critical wind speed of 62 mph for an empty single 5-axle tractor-trailer with a weight of 30.000 lbs, and 84 mph when a weight of 55.000 lbs was used. These results highlighted the importance of the weight of vehicles in blow over crashes. Balsom et al. (2006), through the use of instruments that measured the lateral accelerations of trucks, further showed

that these accelerations increased significantly during high wind speed events. Young and Liesman (2007b) also described four levels of operational strategies for large vehicles in high-wind conditions based on vehicle weight, wind speed, and surface conditions.

Snæbjörnsson et al. (2007) used a probabilistic model developed from a reliability approach for assessing road vehicle stability in windy conditions. Chen and Cai (2004) developed a deterministic vehicle accident model for vehicles on long-span bridges considering the excitations from the bridge and including some driver behavior parameters. The coupled vehicle-bridge-wind system was also applied by Wang and Xu (2015) to examine the safety and behavior of road vehicles passing by a bridge tower and subject to crosswinds. Chen and Chen (2010) developed a deterministic model that assessed the safety of vehicles against hazardous winds in terms of critical driving speed and critical sustained time. The study carried out by Hou et al. (2019) performed safety analysis on stochastic traffic patterns in crosswinds. Finally, Chen et al. (2019) used a driving simulator experiment to examine the safety of trucks on a bridge-tunnel section in crosswinds. The stability of trucks, in this case, was based on driving behaviors as a response to crosswinds. and was quantified by truck yawing rate and steering angle.

1.2.2 Blow Over Risk Model in Wyoming

Blow over risks have also been assessed using quantitative statistical models. Young and Liesman (2007) used historical crash data with wind records from the nearest weather station to find the probability of blow over crashes based on wind conditions. In this research, a binary logic model was used to determine the correlation between the weather station data and the likelihood of the crash being a blow over crash. This study found wind speed and wind differential to be the most significant weather station parameters. Alrejjal et al. (2021) employed a correlated random parameter logic model to investigate the influence of contributing factors on rollover risk. Furthermore, a blow over algorithm developed using fuzzy logic (McNeill et al., 1994) was integrated within the Pikalert® System (Anderson et al., 2016), which is used on Interstate 80 as part of the WYDOT CV Pilot Program (Welch, 2018). This algorithm produces interest values for blow over risk ranging from -1 to 1 based on a set of interest functions. The weights assigned to these functions were initially based on studies by Baker et al. (2008) and were later refined by Welch (2018), based on historical blow over crash data in Wyoming.

Guided both by these different models and a case-by-case basis, traffic managers currently decide when interstate traffic needs to be halted due to wind conditions, and such decisions to halt travel are mostly based on wind speeds. The wind speed cutoff currently used in other states becomes economically infeasible because it is met too frequently in the State of Wyoming (Young and Liesman, 2007b). Therefore, in Wyoming specifically, strong wind warnings are issued when winds exceed 40 mph, and movement of light, high-profile vehicles are halted when wind gusts exceed 60 mph (WYDOT, 2016b). The long-term trend analysis conducted by Ohara (2017) suggests Wyoming is getting windier, indicating that blow over crashes will remain an important issue in the Wyoming transportation system for decades to come. Overall, quantifying blow over risk is important as it provides the responsible agency with an additional tool for making decisions regarding controlling the movement of traffic.

1.2.3 Mitigation in Practice

There is a consensus that lowering driving speed is an effective measure for lowering accident risk (e.g., Chen and Cai, 2004, Young, 2010). Therefore, setting a suitable driving speed limit is important to decrease the likeliness of accident occurrence.

The Nevada Department of Transportation applied a high wind warning system on a seven-mile section of US Route 395 because this highway segment was subjected to high-speed crosswinds. The system components of this high wind warning system included two parts: an ESS and two Dynamic Message Signs (DMS) located at either end of the corridor. Both wind speed and wind gust speed were used as decision factors, and the threshold value of wind gust speeds to prohibit high-profile vehicles on the road was 40 mph. Another motorist warning system was implemented by the Idaho Department of Transportation on a 100-mile section of Interstate 84 in southeast Idaho and northwest Utah (Kyte, Shannon, and Kitchener, 2000).

Young (2010) pointed out that high wind hazardous highway segments in Wyoming usually suffer from yet higher wind speeds (above 30 mph), and wind gust speeds (above 50 mph) than the aforementioned corridors in Nevada and Idaho. Chen and Cai (2004) stated that extremely high wind speeds inevitably cause overturning for high-sided vehicles like trucks and tractor-trailers. However, Young and Liesman (2007) found that speed limit reductions improved safety only when wind speeds were above 37 mph. Moreover, Young and Liesman outlined four levels of operational strategies in the high wind warning system (Young and Liesman, 2007), as follows:

- Level 1. Wind and surface variable thresholds for advisory messages for DMS.
- Level 2. Wind and surface variable thresholds to determine road closure for all vehicles.
- Level 3. Wind, surface, and vehicle profile variable thresholds to determine road closure for all high-profile vehicles only.
- Level 4. Wind, surface, vehicle profile, and vehicle weight variable thresholds to determine road closure for all high-profile, lightweight vehicles only.

As an alternative to this model, ground-based facilities, such as wind fences, were also reported to be effective. Imai (2002) demonstrated the effect of wind fences and embankments against wind hazards on train operations in 1996 along the Nemuro Line in Japan. Similarly, Alonso-Estébanez et al. (2017) demonstrated the effectiveness of the wind fence and embankment system using the Reynolds-averaged Navier–Stokes equations along with the turbulence model.

1.2.4 Implications

The quantitative wind hazard models that have been developed rely on wind measurements from weather stations that are often located far from crash sites. The timing of crashes recorded are often only approximations at best. On the other hand, most of the deterministic studies are to specific to some sites (bridges or some specific sections of roads) and vehicles, which is unacceptable due to the significant variability in vehicle specifications and road corridors. The aerodynamic coefficients used in certain studies are also primarily based on wind tunnel tests and computational fluid models. This all combines to present a great deal of uncertainty and computational effort when applying models at larger scales. Moreover, models quantifying blow over risks are often based on uniform crosswinds, which are not realistic.

To avert these insufficiencies, the framework developed in this study makes use of both deterministic and stochastic approaches. A deterministic vehicle stability model incorporates major factors, such as wind direction, road alignment, the radius of road curves, cant angle (superelevation), and vehicle weights, thereby generating an output in terms of critical vehicle speed. This is the speed of a vehicle at which an additional increase of vehicle speed would cause the vehicle to blow over. Keeping scalability and

computational effort in consideration, various simplifying assumptions were required in the vehicle stability model, as there are considerable uncertainties and variabilities in vehicle specifications, local aerodynamics, driver behaviors, and road surface conditions. Thus, a relatively large FOS must be included in the model parameterization even for the probabilistic or stochastic approaches.

The stochastic approach was employed using a suitable probability distribution from the high-frequency wind records from the sonic anemometer stationed as a part of this study. In large trucks, failure to adjust speed to conditions was understood to be a key factor in blow over crashes (McKnight and Bahouth, 2009). Thus, based on the selected distribution, the blow over risk could be quantified as the probability of having a critical vehicle speed below the posted speed limit. The risk of blow over calculated using this method would find the blow over risk considering the variation of wind conditions in real life. Furthermore, this study used multiple sensors in the study area to check consistency among the roadside wind measurements and the wind measured from the existing ESS so that blow over risk could be quantified with wind data from the conventional anemometers. The developed decision support tool thereby informs operators of blow over probability in real time. Ideally, this will enable operators to better handle traffic movements during high wind periods.

1.3 Objectives

The main goal of this research project was to quantify the blow over risk associated with vehicle speed, load weight, wind field, and road geometry. One high-frequency wind monitoring tower was used to characterize the wind conditions around the 2017 multiple blow overs crash site at I-25, between MP 3 and MP 5, known as Wyoming Hill. The field observed wind speed data measured during high wind events at this location was then used to improve the understanding of the blow over crash mechanism under adverse weather conditions. The field data and the high-resolution modeled data helped to fill the gap between the RWIS ESS weather data and the blow over risk.

Additional, specific project objectives are listed below:

- Improvement of understanding concerning the vehicle blow over mechanism from the data collected using the high-frequency wind monitoring system (UW station), WYDOT's PWIS, and the RWIS ESS.
- Development of the blow over model integrating road geometry, vehicle specifications, and wind field.
- Assessment of blow over risk in Wyoming using the developed model.
- Exploration of how the results can be incorporated into existing traveler information and road weather management systems.

Overall, this project assessed the risk of blow over crashes for high-profile, light-weight vehicles, such as semi-trailer trucks, commonly found on Wyoming highways. The blow over risk in this study was the probability that critical vehicle speed dipped beneath actual travel speed or posted speed limit. Figure 7, below, illustrates the definition of blow over risk operationalized for this study.

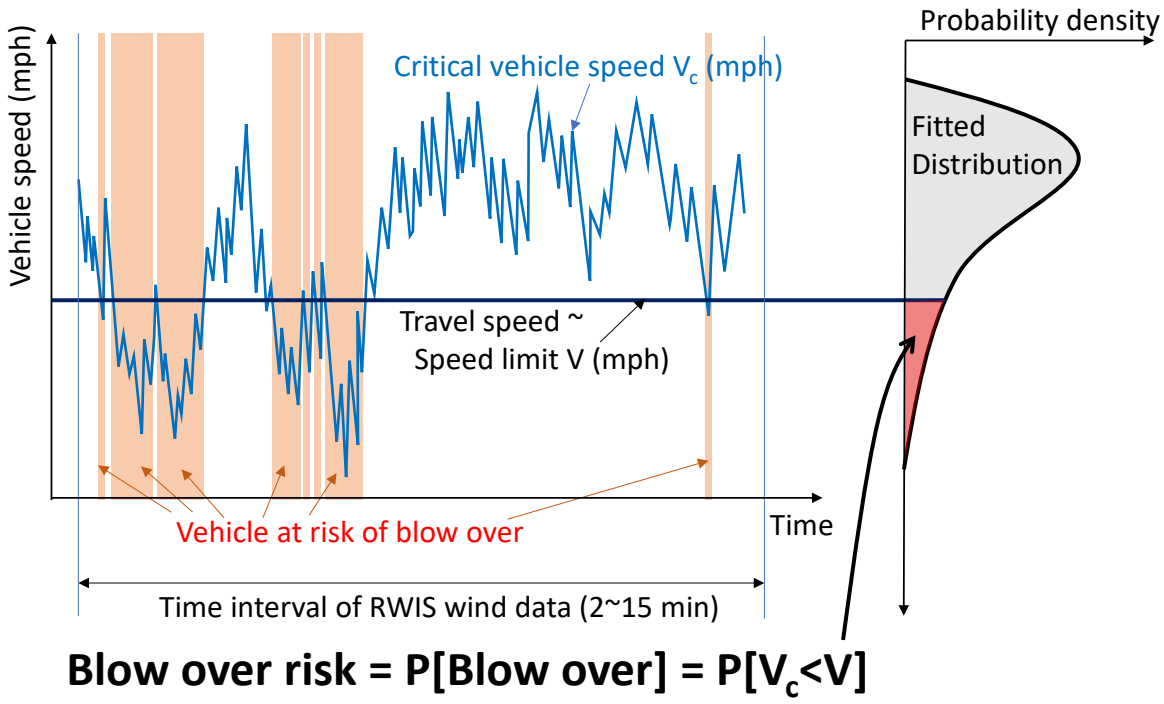

Figure 7: Definition of blow over risk operationalized in this study

The critical vehicle speed, which depends mainly on wind speed, wind angle, road geometry, and vehicle weight, is highly dynamic with considerable uncertainty. This study focused on the temporal variabilities of blow over risk within a time interval of measurement frequency used by conventional mechanical wind sensors, such as the RWIS ESS.

The spatial resolution of the analysis was set at 0.1 miles in order to resolve the road geometry and wind azimuth angle variabilities. In addition to the field observed wind data, simulated high wind conditions were prepared in the previous study, "Historical Winter Weather Assessment for Snow Fence Design using a Numerical Weather Model" (WY-17/03F). Therefore, this developed blow over model can extrapolate the blow over risks verified in the Wyoming Hill area to the major highways in Wyoming using statewide historical weather data.

Chapter 2 - Observation of Wind Fields

This research was conducted at a known high winds hotspot located along a two-mile stretch from MP 3 to MP 5, of I-25 south of Cheyenne, Wyoming. Three blow over crash events were identified in the study section: one incident in January 2020 close to MP 3.3, and two more incidents in November 2020 close to MP 3.8 (Figure 8).

2.1 Installation of the High-Frequency Wind Monitoring System

A mobile, high-frequency, wind monitoring system was deployed to characterize the wind field that initiated blow over crashes around the known hotspot. The system was installed just south of Exit 4, on I-25 (approximately MP 4.5, denoted "UW Station" in Figure 8), on November 11, 2019, and it was securely anchored to the ground on November 19, 2019. In addition to the new high-frequency observation system (UW station), there are also PWIS and RWIS units that take wind measurements in the study area.

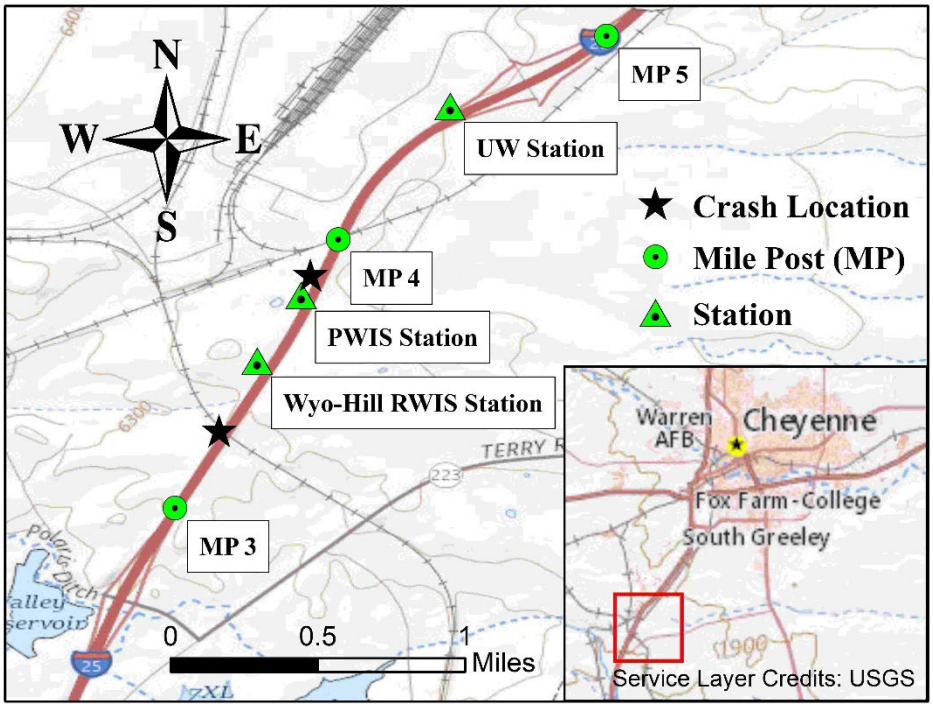

Basemap source: USGS topographic map via ArcGIS

Figure 8: Map of Wyoming Hill project area. There are two crash sites denoted by black stars at MP 3.8 (Nov 13 &15, 2020 crashes) and at MP 3.3 (Jan 1, 2020 crash)

The UW Station system consists of a 3D sonic anemometer, a mechanical anemometer, temperature and humidity sensors, a visibility sensor, a data logger, an enclosure, three large solar panels, four batteries, a power control unit, and a mounting tower. The system was assembled at the Water Resources Laboratory (B115 room, Engineering Building), University of Wyoming (Figure 9). At the same time, the software for the data logger was developed to record wind speed, direction, visibility, temperature, and relative

humidity at excellent temporal resolution. It took three weeks to assemble the system in October of 2019, plus two additional weeks to adjust the system at the Laramie Plains site, south of Laramie. The final measurement frequency for the sonic anemometer was set at one second, and those for the other instruments were set at one minute.

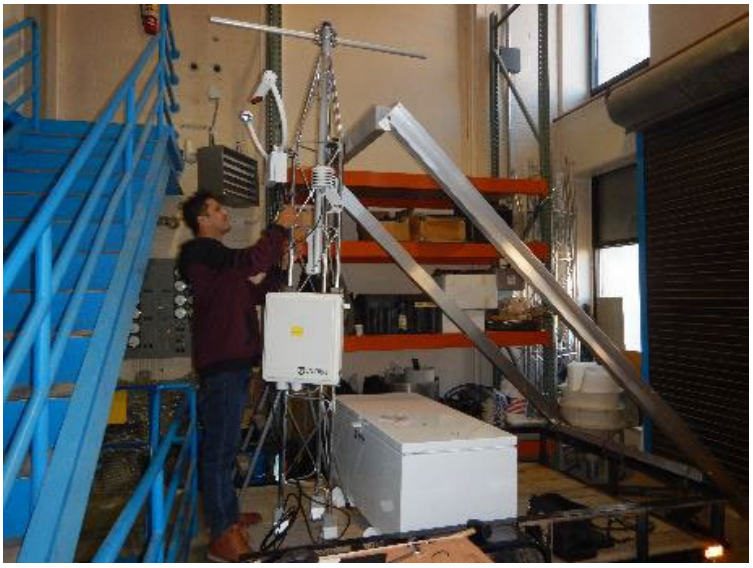

Figure 9: Assembled high-frequency wind monitoring system in the UW Water Resources Lab

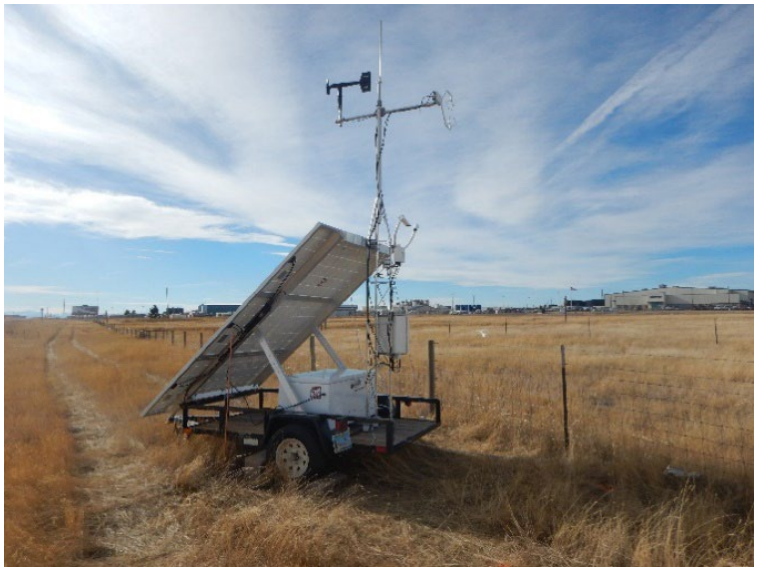

Figure 10: Installed system near exit 4 on I-25 (MP 4.5)

2.2 Comparison of the Wind Direction and Wind Speed from the Three Observation Systems

Ideally, wind characteristics are measured at locations directly adjacent to roadways for blow over analysis. However, RWIS stations, the most common wind monitoring systems in the US, are often positioned at a distant and elevated location from the roadway. Therefore, it is important to compare the wind measurements from the roadside stations and the RWIS stations. The wind records from the nearest

RWIS station, Wyoming Hill, and the other two roadside stations nearby were compared using wind rose diagrams for January 2020, as well as a time series of wind speeds and gusts on November 15, 2020.

The wind direction measurements from different sensors are visualized in the wind rose diagrams, in Figure 11. The measurements from sensors from both of the roadside stations, PWIS and UW sensors (sonic and mechanical), showed westerly winds as the most dominant wind direction in January 2020. The dominant direction from the RWIS station deviates slightly to the north. The difference in elevation of wind measurement of PWIS and RWIS sensors is around 50 ft (~15.3 m). Therefore, given the proximity of the PWIS and RWIS stations, this deviation in dominant wind direction can be attributed to the difference in elevation of wind measurement between the stations. Certainly, wind direction is crucial to the blow over model developed in this study, so it was important to keep in mind the spatiotemporal uncertainty of observed wind fields. Nevertheless, it was encouraging to see lesser deviations in dominant wind directions even with considerable elevation and location differences in wind measurement apparatuses.

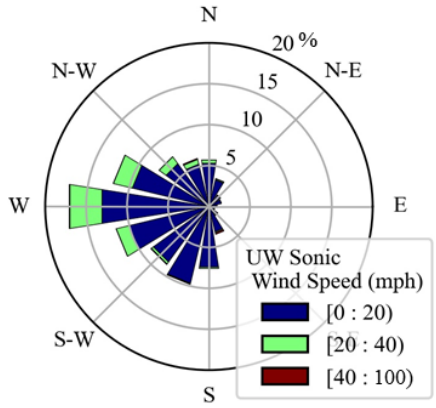

Subfigure A

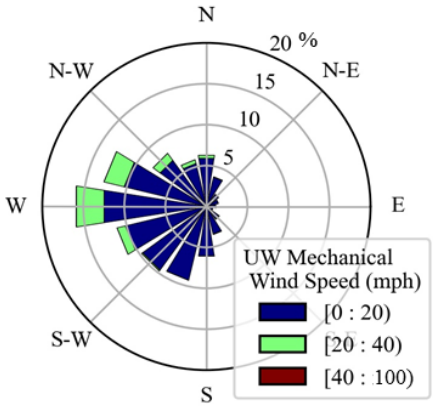

Subfigure B

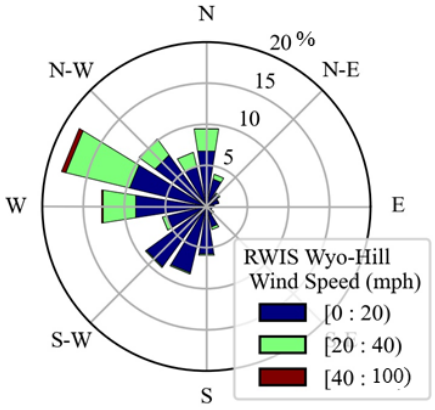

Subfigure C

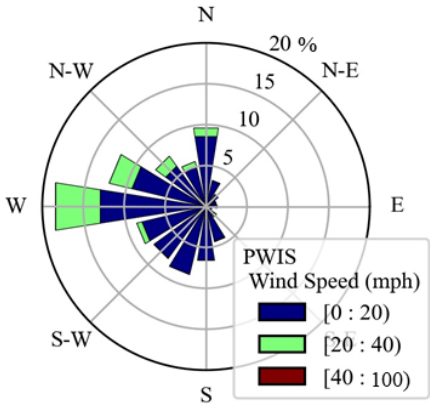

Subfigure D

Figure 11: Wind rose diagrams based on different wind sensors in the study area, January 2020.

The time series of 10-minute average winds and maximum winds from the different sensors on November 13, 2020, is shown in Figure 12 (Subfigure A,B). The height of the wind measurement is highest for the RWIS station followed by PWIS and UW stations. The average wind speeds measured decreased via the same pattern, a fact that can also be seen proportionally among the stations in Figure 12 (Subfigure C,D). The associated wind rose diagrams also show a higher percentage of winds above 20 mph recorded by the RWIS sensors (Figure 11). This proportionality in wind measurements implies the use of a log-profile to adjust the wind measurement highs for the blow over model. The wind gusts from the mechanical sensors follow a similar pattern to the average wind. The mechanical sensor placed at the same elevation as the sonic sensor in the UW station verifies the capability of a conventional mechanical sensor to capture aspects of a wind field including mean wind speeds and directions. Subfigure D of Figure 12 indicates that the mechanical anemometers slightly underestimated wind gust speeds.

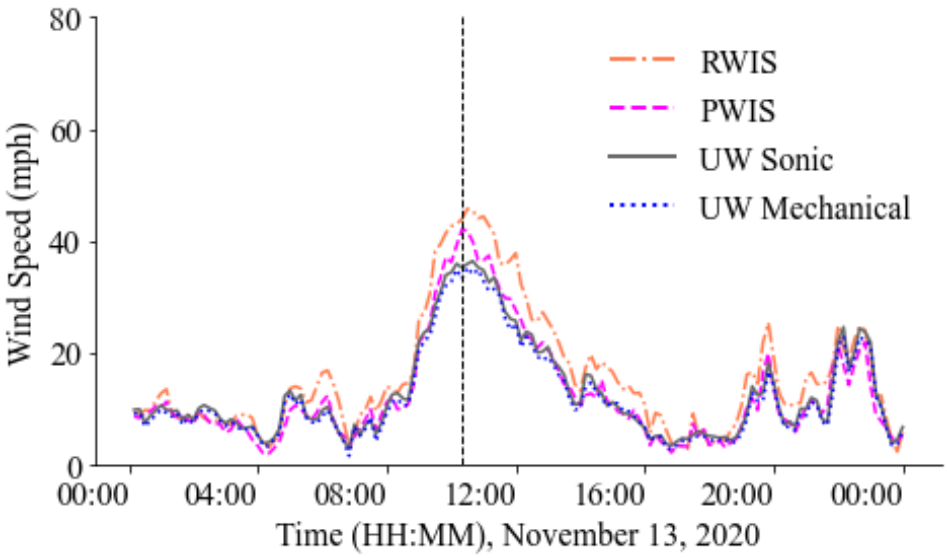

Subfigure A

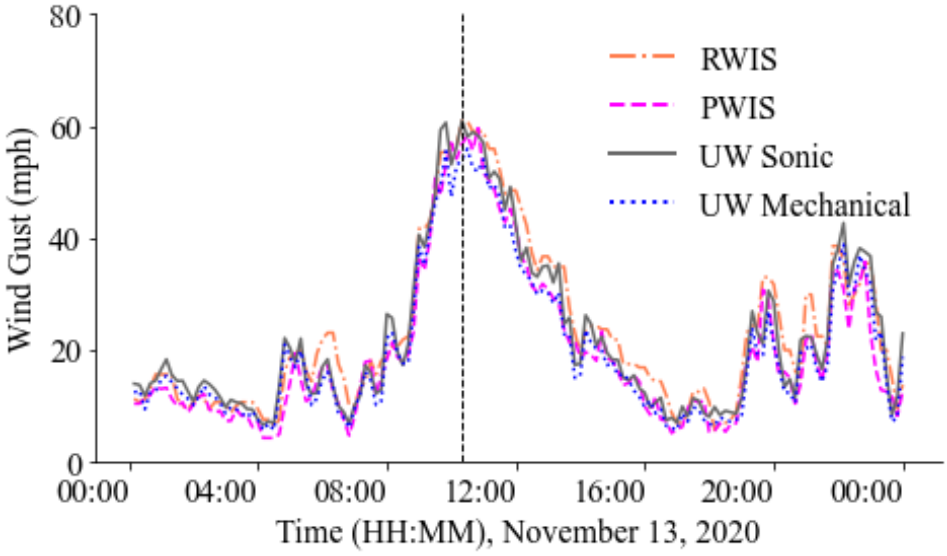

Subfigure B

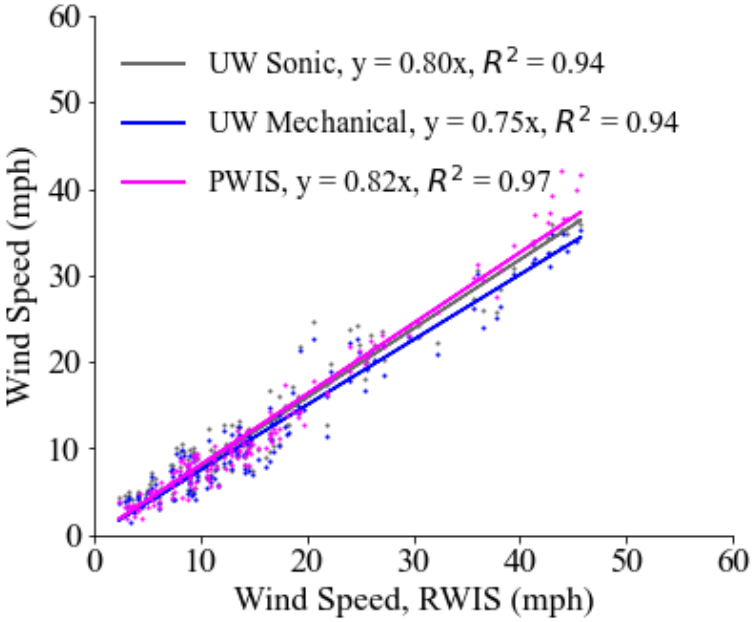

Subfigure C

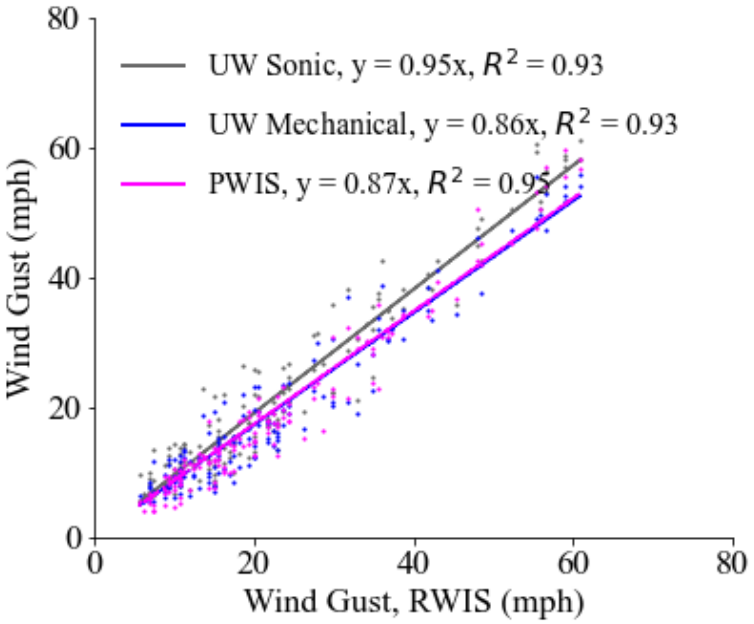

Subfigure D

Figure 12: Time series of the observed 10-minute average and maximum wind speeds on November 13, 2020 (Subfigure A,B), and their linear relation to the winds from RWIS station (Subfigure C,D)

The vertical dashed line shown in Figure 12 (Subfigure A,B) denotes the time of a specific blow over crash, and all the stations recorded high wind speeds at that time. This observation confirms that local wind measurements by weather stations, such as RWIS stations, can successfully predict blow over crashes (Young and Liesman, 2007a).

Furthermore, a strong correlation ($R^2 > 0.93$) in average and gust wind speeds measured between the RWIS ESS and other roadside stations was found for the day of the blow over (Figure 12 Subfigure C,D). Accordingly, these strong linear correlations between wind sensors suggest that the wind speeds recorded on the RWIS ESS nearby are a reasonable predictor of roadside wind in practice, at least for this study area.

Chapter 3 - Blow Over Risk Analysis

3.1 Vehicle Stability Model

3.1.1 Forces Acting on Vehicle

Because vehicle blow over conditions are influenced by many factors, such as wind speed, wind field, road geometry, vehicle speed, and vehicle weight, a vehicle stability model is needed to integrate these numerous variables. Currently, there are comprehensive numerical vehicle stability models available commercially (e.g., TruckSim®) despite considerable uncertainties in variable factors. However, to implement the model repeatedly throughout Wyoming at a very small time increment (e.g. 1 second), such a detailed vehicle stability model is unfeasible. In this study, a simple, high efficiency, static vehicle stability model was developed for state-wide implementation.

Blow over crashes occur when the resistance force of gravity is exceeded by the moment of wind-induced forces around the point of blow over. A static stability analysis (Kunieda, 1972; Baker, 1986; Hibino and Ishida, 2003) is customized for the blow over crash in this study. The lift forces by the headwind and the crosswind can be computed as,

$$L_x = \frac{1}{2} C_{Lx} \rho A_x (V + U_x)^2 \quad (1)$$

and

$$L_y = \frac{1}{2} C_{Ly} \rho A_y U_y^2, \quad (2)$$

respectively.

C_{Lx}= Lift coefficient for headwind
C_{Ly} = Lift coefficient for crosswind
ρ = Density of air (kg/m^3)
A_x = Reference area from front (m^2)
A_y = Reference area from side (m^2)
V =Vehicle travel speed (m/s)
U_x =Headwind speed (m/s)
U_y =Crosswind speed (m/s)

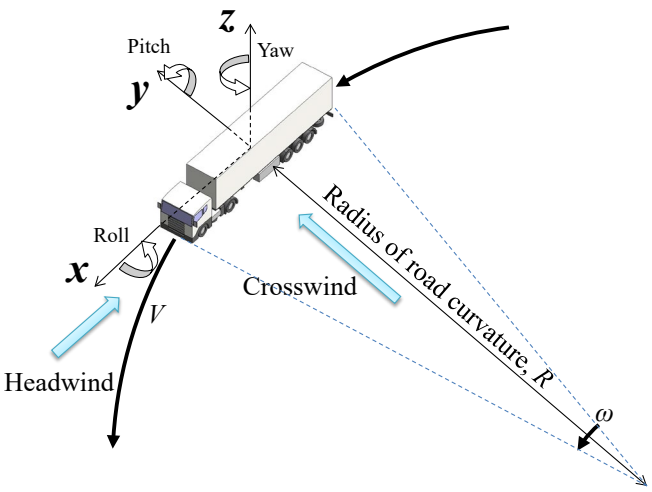

Figure 13: Definitions of axes for static blow over analysis

The drag force by the wind acts on the vehicle horizontally; therefore, only the crosswind component is effective. The drag force by of the crosswind, the centrifugal force due to road geometry, and the resisting gravitational force may, respectively, be written as:

$$D_y = \frac{1}{2} C_D \rho A_y U_y^2. \quad (3)$$

$$F_C = MR\omega^2 = \frac{MV^2}{R}. \quad (4)$$

$$W = Mg, \text{ respectively.} \quad (5)$$

C_D = Drag coefficient for crosswind

ω = Vehicle angular velocity
R = Radius of curve (m)
M = Mass of vehicle (kg)

V=Vehicle travel speed (m/s)

g = gravity (m/s^2)

3.1.2 Static Force Balance for Blow Over Condition

This project's blow over model has been developed through the consideration of three primary aspects: 1) installation of two blow over axes; 2) wind speed adjustment by road elevation for local terrain and bridges; 3) improved error management. The error management handles ineffective conditions of the road parameters, as well as invalid model outputs (e.g., negative and imaginary roots of the system equation). These model elements are crucial for a future spatially distributed statewide application. Figure 14 shows the definitions of aerodynamic forces and rollover axes. Note that the crosswind direction is assumed to be parallel to the local ground surface.

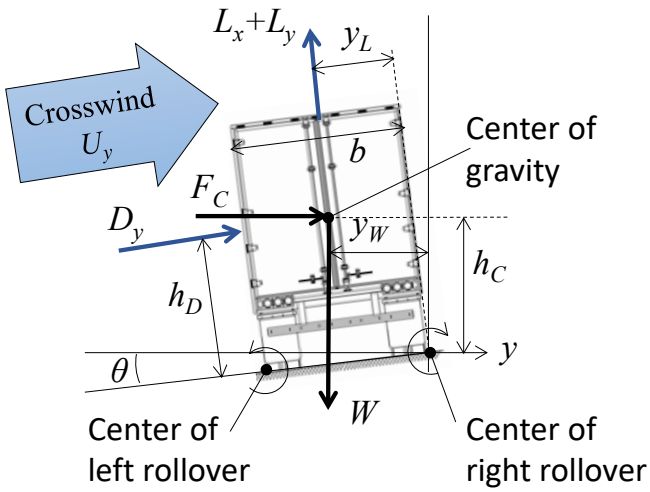

α = Safety factor

b = Width of vehicle (m)

h = Hight of vehicle (m)

h_D = Center height of drag force (m)

h_C = Center height of centrifugal force (m)

y_L = Center location of lift forces (m)

y_W = Center location of gravitational force (m)

L_x = Lift force due to headwind

L_y = Lift force due to crosswind

D_y = Drag force

F_c = Centrifugal force

W = Gravitational force

θ = cant angle or cross slope

Figure 14: Various forces acting on a vehicle.

It is important to consider both right and left side rollover axes when the drag force and the centrifugal force are acting in opposite directions. Therefore, there are two moment balance equations depending on the rollover axis selected. Both conditions shown below must be met to travel safely.

$$\begin{cases} \alpha\left[y_L(L_x+L_y)+h_D D_y \operatorname{sign}[U_y]\right]+h_{CR}F_C\operatorname{sign}(\theta)-y_{WR}W\le 0\,;right\ rollover\ axis \\ \alpha\left[y_L(L_x+L_y)-h_D D_y \operatorname{sign}[U_y]\right]-h_{CL}F_C\operatorname{sign}(\theta)-y_{WL}W\le 0\,;left\ rollover\ axis \end{cases} \quad (6)$$

The cross slope (also known as cant angle or angle of superelevation) of the road, *θ, must* be considered in the computation of the locations of the centrifugal and gravitational forces. The central heights of centrifugal force from the right and left rollover centers, therefore, are,

$$h_{CR} = \frac{1}{2}(h\cos\theta - b\sin\theta), \text{ and}$$

$$h_{CL} = \frac{1}{2}(h\cos\theta + b\sin\theta) \text{ , respectively.}$$

Similarly, center locations of gravitational force from the right and left rollover centers are,

$$y_{WR} = \frac{1}{2}(b\cos\theta + h\sin\theta), \text{ and}$$

$$y_{WL} = \frac{1}{2}(b\cos\theta - h\sin\theta) \text{ , respectively.}$$

The critical vehicle speed (V_C) for the right rollover axis is computed by solving the following quadratic equation derived by substituting Eq. (1) through Eq. (5) into Eq. (6):

$$A_R V_C^2 + B_R V_C + C_R = 0 \tag{7}$$

where,

$$A_R = \alpha y_L C_{Lx} \rho A_x + 2h_{CR}\frac{M}{R}\text{sign}(\theta)$$
$$B_R = 2\alpha y_L C_{Lx} \rho A_x U_x$$
$$C_R = \alpha y_L C_{Lx} \rho A_x U_x^2 + \alpha\rho A_y U_y^2\left[\alpha y_L C_{Lx} + h_D C_D \text{sign}\left(U_y\right)\right] - 2y_{WR} Mg$$

Similarly, the equation for the left rollover axis is,

$$A_L V_C^2 + B_L V_C + C_L = 0 \tag{8}$$

where,

$$A_L = \alpha y_L C_{Lx} \rho A_x - 2h_{CL}\frac{M}{R}\text{sign}(\theta)$$
$$B_L = 2\alpha y_L C_{Lx} \rho A_x U_x$$
$$C_L = \alpha y_L C_{Lx} \rho A_x U_x^2 + \alpha\rho A_y U_y^2\left[\alpha y_L C_{Lx} - h_D C_D \text{sign}\left(U_y\right)\right] - 2y_{WL} Mg$$

The smallest positive real root of Eq. (7) and Eq. (8) is taken as V_C. This method integrates many factors affecting the vehicle stability on the road and provides a single critical vehicle speed, which will be used for blow over risk quantification. It should be emphasized that this analytical solution takes very minimal computational resource, which is a key requirement for the stochastic treatment presented in later sections.

3.1.3 Roadside Wind Field Estimation

Figure 15 shows the schematic of the wind profile assumed by this model. A simple logarithmic wind profile was adopted to adjust the observation height as well as the relative road elevation to the mean surrounding ground elevation. The crosswind was adjusted by the relative road elevation (*h'*) especially

for bridges because many blow over crashes occur on the BNSF (Burlington Northern Santa Fe railroad) bridge (MP4) and nearby elevated sections of the road. This adjustment is only applicable to the crosswind component since the elevation transition along the driving course (headwind direction) is assumed to be smooth and continuous.

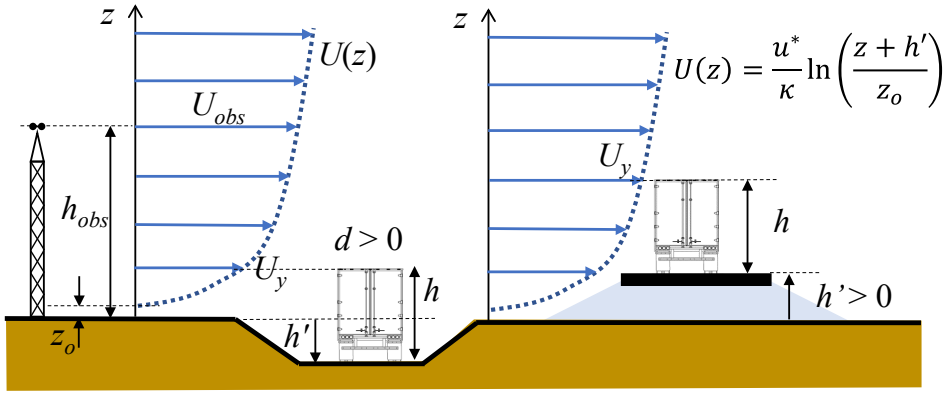

Figure 15: Wind profile, wind height adjustment, and road elevation adjustment

h = vehicle height (m)

z_o = roughness height (m)

h' = relative road elevation (m)

h_{obs} = the anemometer height

Relative headwind and crosswind speeds can be computed from wind and vehicle azimuth angles. Definitions of such angles are illustrated in Figure 16.

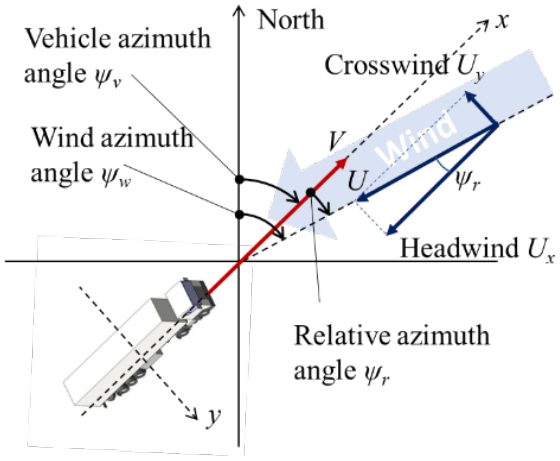

Figure 16: Computation of headwind and crosswind components from wind and vehicle azimuth angles

As previously discussed, stations in the Wyoming Hill study area measure wind speeds at different heights. Thus, a simple logarithmic wind profile model was adopted to find components of wind speeds

acting at the top of the vehicle, specifically. The crosswind component was further adjusted to account for the higher winds a vehicle may experience at elevated sections of the road, as demonstrated in Figure 15. The relative elevation (h') of the road was calculated as the difference between the elevation of the road surface and the average elevation of both sides of the road. The elevation data was computed using the digital elevation model (DEM) maps from the United States Geological Survey (USGS) at 10 m spatial resolution (National Elevation Dataset (NED), USGS, 1999). The headwind and the crosswind on the road were then computed by,

$$U_x = U_{obs}\cos(\psi_r)\cdot\frac{\ln\left(\frac{h}{z_o}\right)}{\ln\left(\frac{h_{obs}}{z_o}\right)};\ U_y = -U_{obs}\sin(\psi_r)\cdot\frac{\ln\left(\frac{h+h'}{z_o}\right)}{\ln\left(\frac{h_{obs}}{z_o}\right)} \quad (9)$$

where h is vehicle height; $z_o$is the average roughness length; h_{obs} is the anemometer height; U_{obs} is the observed wind speed; and ψ_r is the relative azimuth angle that can be computed as a difference between wind azimuth angle (ψ_w) and vehicle azimuth angle (ψ_v). The elevation difference in the transverse direction (crosswind direction) tended to be considerably larger than the longitudinal direction (headwind direction) because the longitudinal grades for the highway are highly regulated.

The robustness of the model herein developed was tested through sensitivity analyses of various parameter combinations. Figure 17 shows the critical vehicle speed at November 13, 2020, crash site (vehicle azimuth angle of 218°) for various wind azimuth angles at the wind speed of 60 mph. The critical vehicle speed V_c was defined as the fastest travel speed without a blow over crash. Therefore, the smaller the V_c, the more susceptible the vehicle may be to blow over.

In the models below, the straight road assumption showed a symmetric pattern to the vehicle orientation in the blow over threshold, while the road curvature provoked asymmetry. This analysis demonstrates that the azimuth angle of 280°-300° is one of the worst wind directions on the straight section of I-25 southbound around MP 4.0. The critical vehicle speed reaches the minimum at wind azimuth angles of 138° and 298°, respectively, which are different from the crosswind directions of 128° and 308° (right angles to the vehicle), respectively. This indicates that the lift force by headwind somewhat contributes to the blow over condition in addition to the drag force caused by the crosswind.

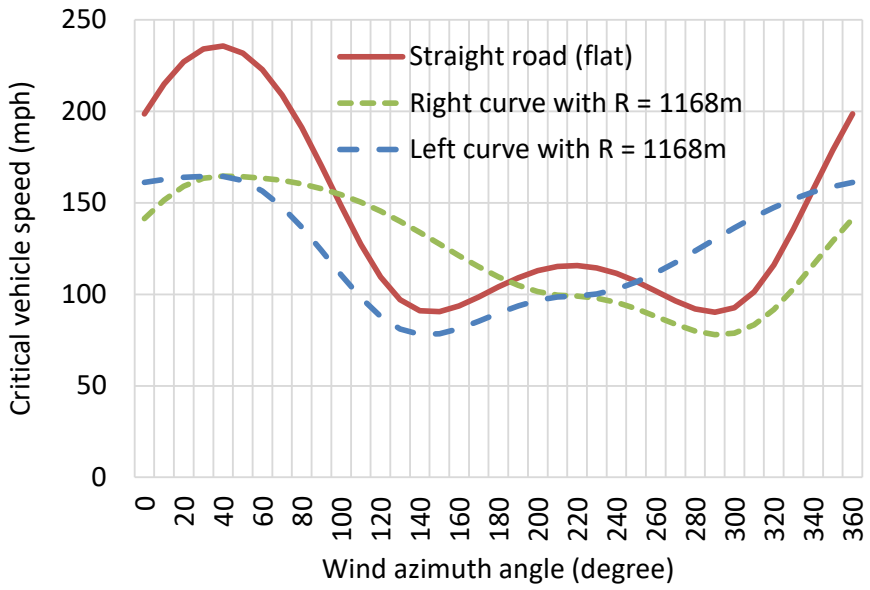

Figure 17: Sensitivity analysis of wind azimuth angle to the critical vehicle speed with a gust wind speed of 60 mph and the definitions of the angles as shown

Figure 18 shows the modelled effects of vehicle weight on the critical vehicle speed during the November 13, 2020, blow over crash event with wind speed measured at 60 mph. As may be seen, a vehicle lighter than 35,000 lbs is vulnerable to blow over even when traveling under the posted speed limit of 75 mph. Although this is a site and time specific result, this analysis may be useful in visualizing the universal characteristics of the blow over mechanism for truck operators on I-25.

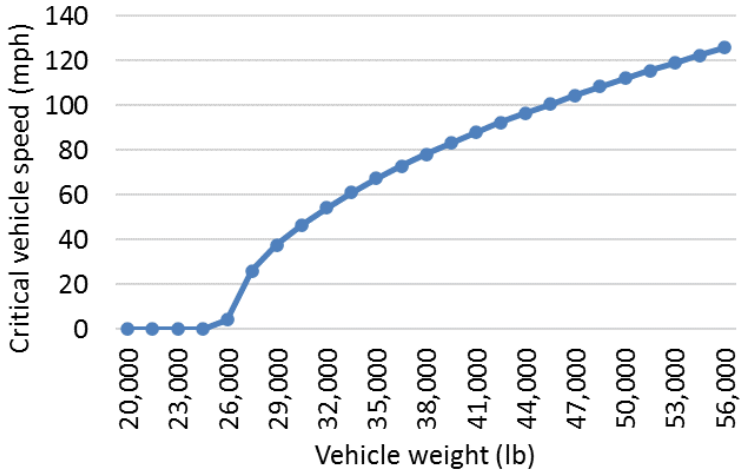

Figure 18: Sensitivity analysis of vehicle weight to the critical vehicle speed with a gust wind speed of 60 mph

In sum, the wind model established herein generally verifies the following known facts through experience:

- A traveler with a high-profile, light-weight vehicle will likely experience a blow over crash when the critical vehicle travel speed is exceeded.
- The lighter the vehicle, the higher the blow over risk.
- The critical vehicle travel speed (V_c) is dependent on the gust wind field, the road geometry, and the vehicle weight.

Thanks to these verifications, the blow over model herein developed can effectively integrate major factors into a single variable, the critical vehicle speed.

3.2 Stochastic Model for Blow over Crash

3.2.1 Probability of Blow Over Crash

From previous research, it is obvious that increasing vehicular speed increases the likelihood of blow over crash occurrence. Theoretically, if the speed at which a vehicle is traveling is higher than critical vehicle speed (V_c), the vehicle is at risk of a blow over. Because vehicles on the roadway are generally expected to follow posted speed limits, the blow over risk probability for any duration can be quantified from the length of time during which V_c equal to or less than the posted speed limit. Therefore, if a suitable distribution of the V_c data can be identified, then a blow over risk can be calculated as the probability of having a V_c value less than the posted speed limit, based on a cumulative density function of the posted speed limit. In this study, the V_c at every second was computed by the blow over model using the high-frequency wind measurements at the UW station. Then, frequency histograms of V_c were fitted by theoretical probability distributions for every time interval of the most convenient conventional wind monitoring system, such as RWIS, which reports every 2-15 minutes.

In general, a blow over crash requires two conditions: very strong winds and a light-weight, high-profile vehicle on the road. When the independence between these conditions can be assumed, the probability of blow over crash occurrence can then be computed as P[blow over crash] =P[A]·P[B] where A = excess vehicle speed over the critical vehicle speed ($V_c < V$); and B = light-weight, high-profile vehicle on the road section. An example probability density function (PDF) of the critical vehicle speed derived from wind observations in the ultrasonic sensor is shown in Figure 19. Once the distribution of the PDF is estimated from the observed mean and maximum wind speed values at the coarse temporal resolution, the blow over risk in terms of probability can be estimated every 15 minutes as a p-value of the fitted PDF. Note that the “blow over risk” in this report denotes the probability of blow over, P[A] or P[$V_c < V$], instead of the probability of blow over crash, P[blow over crash], which is influenced by an additional factor, P[B] (presence of light-weight high-profile, reckless drivers, road closure, etc.). If the road is closed then the blow over risk still exists but the probability of a vehicle being present to be blown over in a crash event (P[Blow over crash]) is very low.

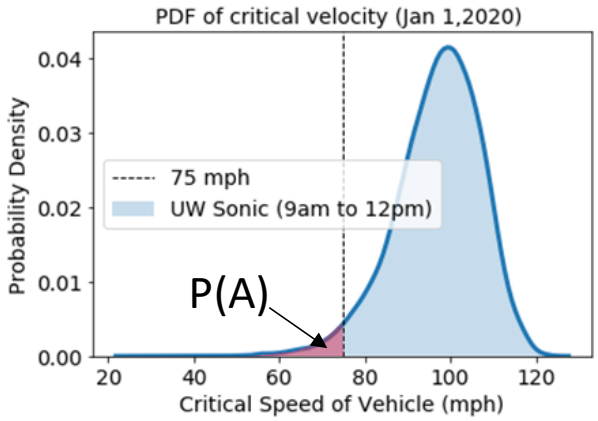

Figure 19: Example PDF of the critical vehicle speed during Jan 1, 2020, at the I-25 study section

As will be described in detail later, several distributions usually associated with the distribution of maximum winds were selected for fitting 2 to 15-minute V_c data. To find the best fitting distribution, root mean square error (RMSE) between the observed frequency histogram and the fitted PDF of the 15-minute V_c data was used.

3.2.2 Statistical Distributions for Extreme Value

It is important to characterize the time-evolution of the critical vehicle speed for the blow over risk quantification as it rapidly changes within a wind measurement and recording interval (typically between 2 to 15 minutes). However, the variation of the critical vehicle speed in a 2 to 15-minute interval has not been studied in past literature. This section provides a general background of statistical modeling of extreme values as well as the practical estimation procedure for risk quantification.

Table 1 lists the statistical distributions commonly used in modeling the extreme values found in nature. In this table, the parameters α, θ, and μ are typically referred to as shape parameter, scale parameter, and location parameter, respectively, although they may be different for each distribution. Also, Γ is the gamma function, ψ is the digamma function and ψ_1 is the trigamma function.

Extreme value theory is used to model the maximum or minimum of the collection of random observations. The theory consists of three distributions, Gumbel, Fréchet, and Weibull distributions, which are effective in describing a stochastic process that has a highly skewed distribution. The three distributions are combined as the general extreme value (GEV) distribution although it is one of three distributions; therefore, the type must be prescribed before fitting exercise. Strictly speaking, this combined distribution is a quasi-three-parameter distribution. Therefore, Gumbel, the extended Fréchet, and Weibull distributions with three parameters, shown in Table 1, will be discussed in this study because they are equivalent to the GEV.

English mathematician Karl Pearson organized all statistical distributions into seven types. Among these types, a Pearson Type III distribution generalizes the normal distribution, the gamma distribution, the exponential distribution, and the Weibull distribution. Pearson Type III distribution is effective to describe skewed (asymmetric) distribution that appears in survival analysis and hydrological analysis. This distribution consists of three parameters (location, shape, and scale parameters) that can define the distribution. The three parameters can be uniquely determined by three moments of the distribution (mean, variance, and skew). This distribution is sometimes referred to as a generalized gamma

distribution associated with the sum of squares of the independent unit normal variables. Although the original Pearson categorization has not been very popular, the re-parameterized version of Pearson Type III distribution shown in Table 1 has been extensively used in extreme value modeling, including that of aviation loads (e.g., Hovey and DeFiore, 2003).

Another generalization may be performed by logarithmic transformation. For example, the log-normal and the log-Pearson Type III distributions are the most common distributions for flood frequency analysis. Also, the log-gamma distribution can be used as an approximation to determine the independence of two sets of normally distributed random variables as well as to test linear hypotheses regarding matrix regression coefficients. However, the exp-gamma distribution (exponential transformed gamma distribution) is more suitable for general extreme value modeling. The extreme value theorem states that the maximum or minimum of a sample of independent and identically distributed (ibid) random variables converges to one of three possible distributions: Gumbel Distribution, Fréchet Distribution, and Weibull Distribution, as stated above. All three of these latter distributions are, indeed, special cases of the exp-gamma distribution. As such, the exp-gamma distribution is one of the most general and flexible distributions for extreme value modeling with three parameters.

Table 1: Common statistical distributions for extreme value modeling

Probability Density Function (PDF of x)	$\mathrm{E}(X)$ and $\mathrm{Var}(X)$
Gumbel Distribution $f(x;\mu,\theta)=\frac{\exp\left[-\frac{x-\mu}{\theta}-\exp\left(-\frac{x-\mu}{\theta}\right)\right]}{\theta}$	$\mathrm{E}(X)=\mu+\theta\cdot\gamma$ $\mathrm{Var}(X)=\pi^2\theta^2/6$
Fréchet Distribution $f(x;\alpha,\theta,\mu)=\frac{\alpha}{\theta}\left(\frac{x-\mu}{\theta}\right)^{-\alpha-1}\exp\left(-\left[\frac{x-\mu}{\theta}\right]^{-\alpha}\right)$	$\mathrm{E}(X)=\mu+\theta\cdot\Gamma\left(1-\frac{1}{\alpha}\right)$ $\mathrm{Var}(X)=\left[\Gamma\left(1-\frac{1}{\alpha}\right)-\left\{\Gamma\left(1-\frac{1}{\alpha}\right)^2\right\}\right]\theta^2$
Weibull Distribution $f(x;\alpha,\theta,\mu)=\frac{\alpha}{\theta}\left(\frac{x-\mu}{\theta}\right)^{\alpha-1}\exp\left(-\left[\frac{x-\mu}{\theta}\right]^{\alpha}\right)$	$\mathrm{E}(X)=\mu+\theta\cdot\Gamma\left(1+\frac{1}{\alpha}\right)$ $\mathrm{Var}(X)=\left[\Gamma\left(1+\frac{1}{\alpha}\right)-\left\{\Gamma\left(1+\frac{1}{\alpha}\right)^2\right\}\right]\theta^2$
Gamma Distribution $f(x;\alpha,\theta)=\frac{\cdot x^{\alpha-1}\theta^{-\alpha}}{\Gamma(\alpha)}\exp\left(-\frac{x}{\theta}\right)$	$\mathrm{E}(X)=\alpha\theta$ $\mathrm{Var}(X)=\alpha\theta^2$
Pearson Type III distribution (Generalized Gamma Distribution) $f(x;\alpha,\theta,\mu)=\frac{(x-\mu)^{\alpha-1}\theta^{-\alpha}}{\Gamma(\alpha)}\exp\left[-\frac{(x-\mu)}{\theta}\right]$	$\mathrm{E}(X)=\alpha\theta+\mu$ $\mathrm{Var}(X)=\alpha\theta^2$
Log-Normal Distribution $f(x;\mu,\theta)=\frac{1}{x\theta\sqrt{2\pi}}\exp\left[-\frac{\{ln\ (x-\mu)\}^2}{2\theta^2}\right]$	$\mathrm{E}(X)=\exp\left(\mu+\frac{\theta^2}{2}\right)$ $\mathrm{Var}(X)=[\exp(\theta^2)-1]\exp(2\mu+\theta^2)$
Log-logistic distribution $f(x;\mu,\theta)=\frac{(\alpha/\theta)(x/\theta)^{\alpha-1}}{\{1+(x/\theta)\}^2}$	$\mathrm{E}(X)=\frac{\theta\pi/\alpha}{\sin(\pi/\alpha)}$ $\mathrm{Var}(X)=\theta^2\left[\frac{2\pi/\alpha}{\sin(2\pi/\alpha)}-\frac{(\pi/\alpha)^2}{\sin^2(\pi/\alpha)}\right]$
Log-Gamma Distribution $f(x;\ \alpha,\theta,\mu)=\frac{\theta^{-\alpha}(1+x-\mu)^{-\frac{1+\theta}{\theta}}}{\Gamma(\alpha)}(log[1+x-\mu])^{-1+\alpha}$	$\mathrm{E}(X)=-1+(1-\theta)^{-\alpha}+\mu$ $\mathrm{Var}(X)=(1-2\theta)^{-\alpha}-(1-\theta)^{-2\alpha}$
Exp-Gamma Distribution $f(x;\alpha,\mu,\theta)=\frac{\exp\left[\alpha\frac{x-\mu}{\theta}-\exp\left(\frac{x-\mu}{\theta}\right)\right]}{\theta\cdot\Gamma(\alpha)}$	$\mathrm{E}(X)=\mu+\theta\cdot\psi(\alpha)$ $\mathrm{Var}(X)=\psi_1(\alpha)\cdot\theta^2$

As presented in the next section, the exponential gamma (exp-gamma) distribution was found to be the best fitting distribution for the estimated critical vehicle speed V_c based on the high-frequency data acquired. The exp-gamma distribution has three parameters. For the two-parameter distributions, standard deviation (SD), and mean were sufficient for finding the two parameters that define the distributions. However, for a three-parameter distribution, like the exp-gamma distribution, an additional regression relationship needed to be used to find the third parameter. This report shows that the exp-gamma distribution, even using the additional regression relationship, is the best fitting distribution with the lowest annual average RMSE value. The blow over risk, therefore, will be calculated as the cumulative distribution function (CDF) of the posted speed limit since it is the best fitting distribution.

3.2.3 Distribution of the Critical Vehicle Speed

Blow over risk assessment was computed as the exceedance probability of the frequency histogram of the critical vehicle speed (V_c) using the high-frequency wind monitoring system, as described previously. The frequency histograms at every time window, which correspond to the RWIS data frequency, can be modeled by fitted theoretical distributions. The root mean squar error (RMSE) of the critical vehicle speed was calculated for each distribution for the performance measure. The distribution with the lowest RMSE error was the distribution closest to the actual distribution of critical vehicle speeds. The distributions were compared and ranked based on their average annual RMSE values.

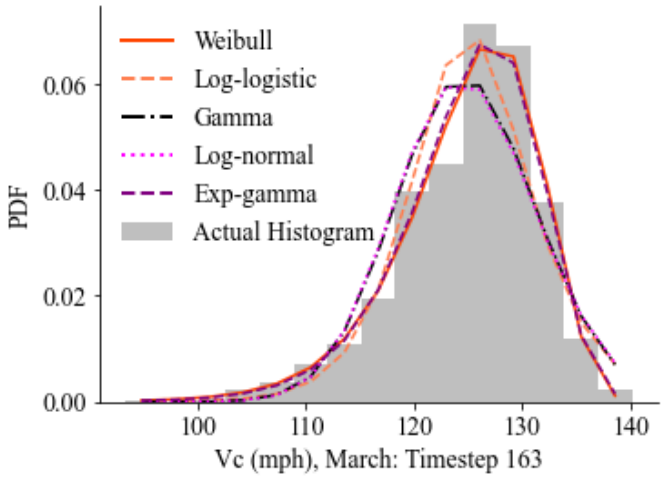

Subfigure A

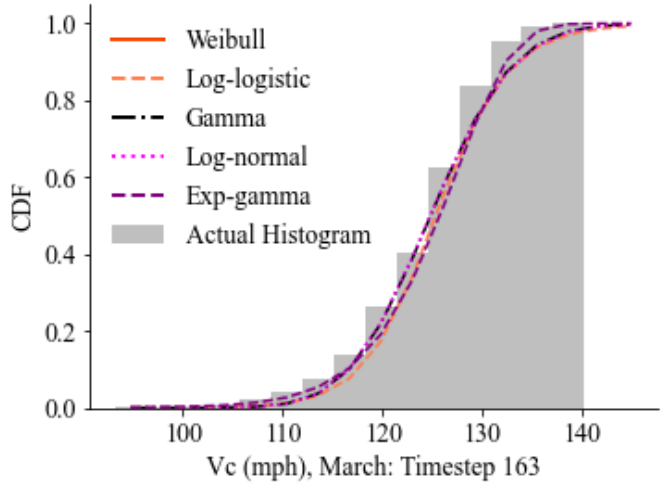

Subfigure B

Figure 20: Example of fitted distribution and actual data of critical vehicle speed (Time step 163 of 15-minute data for March)

High-frequency estimates of critical vehicle speed provided an opportunity for the temporal statistical analysis of the blow over risk. A representative example of the fitted PDF and CDF for different

distributions is shown in Figure 20. The grey shading in this figure represents the observed data of the critical vehicle speed derived from wind records from the ultrasonic sensor.

Figure 21 shows the average values of the RMSE of 15-minute histograms for different distributions computed based on the collected data during the project period (mainly in the calendar year 2020). Note that the fitting parameters for each distribution were estimated by the maximum likelihood estimation (MLE) method. The exponential-gamma distribution (Wolfram, 2010), having the least value of RMSE on average, was therefore found to be the best fit for the 15-minute datasets in 2020.

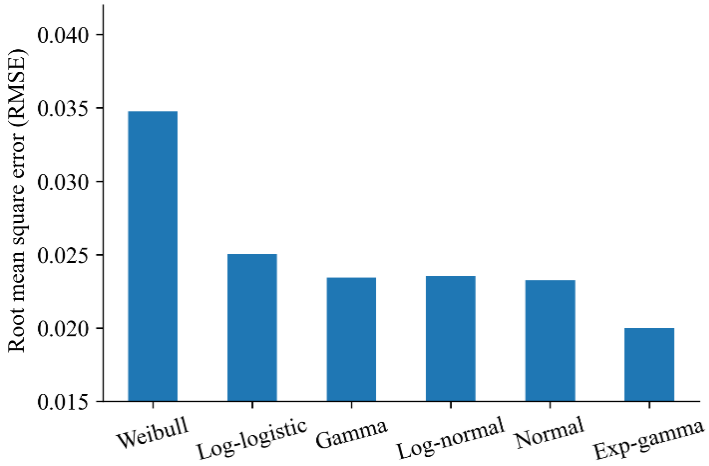

Figure 21: Annual average RMSE values, 2020

The estimated exp-gamma distribution exceeded the significance level of 5 percent ($p \geq 0.05$) for the χ^2 test 60.6 percent of the time in 2020 based on the 15-minute interval. These statistics are generally considered satisfactory as the wind record includes windless calm periods as well as windy periods and wind field transitions.

3.2.4 Parametric Exp-gamma Distribution

To estimate the blow over risk from the conventional wind monitoring system (i.e., RWIS), the PDF of the critical vehicle speed must be estimated from average and maximum (gust) wind speed observations in the time interval (typically 2 to 3 minutes in raw data and 10 minutes in historical processed records). Therefore, researchers must estimate the three parameters (location, scale, and shape) for the exp-gamma distribution from the two observable variables (mean and standard deviation).

The best distribution, exp-gamma distribution is one of the most general and flexible distributions for extreme value modeling with three parameters, as discussed in the previous sections. In fact, the exp-gamma distribution is used in modeling various phenomena like the speed of wind in meteorology or the speed of currents in ocean engineering (Wolfram, 2010). The PDF of the exp-gamma distribution can be written as follows,

$$f(x;\kappa,\mu,\theta) = \frac{\exp\left[\kappa\frac{x-\mu}{\theta} - \exp\left(\frac{x-\mu}{\theta}\right)\right]}{\theta\cdot\Gamma(\kappa)} \tag{10}$$

where μ is a location parameter, κ is a shape parameter, and θ is a scale parameter. The mean and variance may be expressed as

$$\mathrm{E}(X) = \mu + \theta\cdot\psi(\kappa), \text{ and} \tag{11}$$

$$\mathrm{Var}(X) = \psi_1(\kappa)\cdot\theta^2, \text{ respectively.} \tag{12}$$

ψ is the digamma function and ψ_1 is the trigamma function. These special functions can be evaluated by a function called polyfunction in the common math library of Python. The PDF formulation of the exp-gamma distribution is a double exponential function (Equation (10)).

The three parameters (location, scale, and shape) must be estimated from the two commonly observed/recorded variables (mean and standard deviation). Among these variables, the correlation between the location parameter and mean was found to be most significant, as discussed below.

3.2.5 Estimation of the Mean Critical Vehicle Speed from the Mean Wind Speed

The mean V_c for parametric distribution is calculated from the blow over model using average wind direction and average wind speed. Figure 22 shows a good linear relationship between the mean of every 15-minute V_c datapoint from 1 sec-frequency (Mean V_c on y-axis) to V_c calculated from average wind and average wind direction (x-axis). Therefore, the mean of V_c may be calculated from the average wind without further consideration.

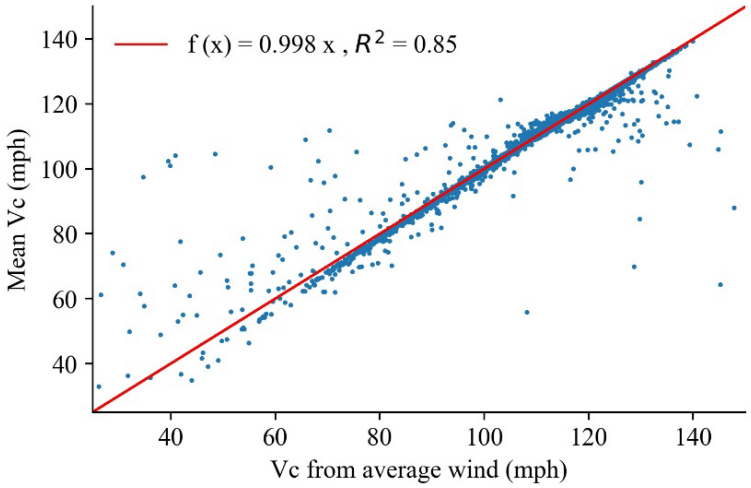

Figure 22: The relation between the mean of V_c by statistical analysis of high-frequency wind data within 15-minute and the V_c calculated from average wind and average wind direction during the corresponding periods.

3.2.6 Estimation of the SD from the Gust Wind Speed and Average Wind Speed

The risk of blow over can be quantified by calculating the parametric exp-gamma distribution of the critical vehicle speed from average wind and the standard deviation (SD) of critical vehicle speed. However, the SD of critical vehicle speed (V_c) cannot be found using standard wind measurements from RWIS ESS. Hence, the SD value of critical vehicle speed needs to be estimated from the regression related to the corresponding value based on the gust (maximum) wind by the mechanical anemometer.

For finding the SD of V_c, the SD of every 15-minute V_c data from 1 sec-frequency was compared to the V_c generated from the maximum wind and the average wind direction. The relationship, after removing some outliers denoted by red dots, showed the R-squared value to be 0.79 (Figure 23). Secondly, SD was calculated based on the difference between the V_c calculated from the average wind and gust wind. This relationship was much stronger, boasting an R^2 value of 0.85 (Figure 24). Consequently, the SD of V_c was more effectively estimated from the second correlation at times when the SD of wind speed was not available.

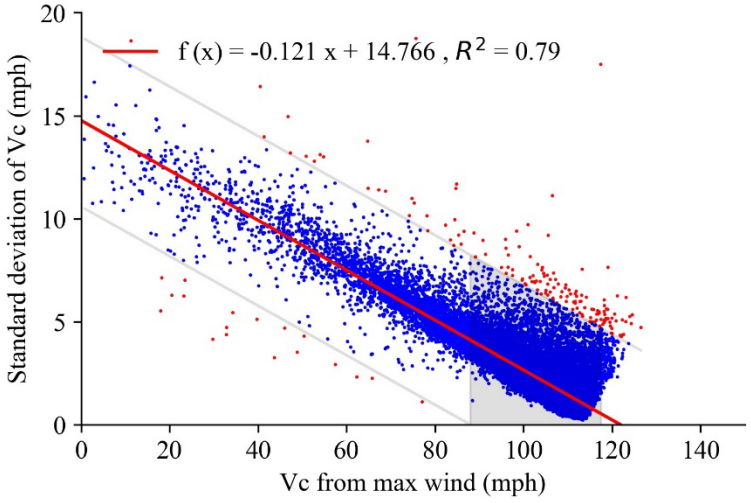

Figure 23: The relationship between the standard deviation of V_c and Vc computed from the wind gust. Red dots are the outliers.

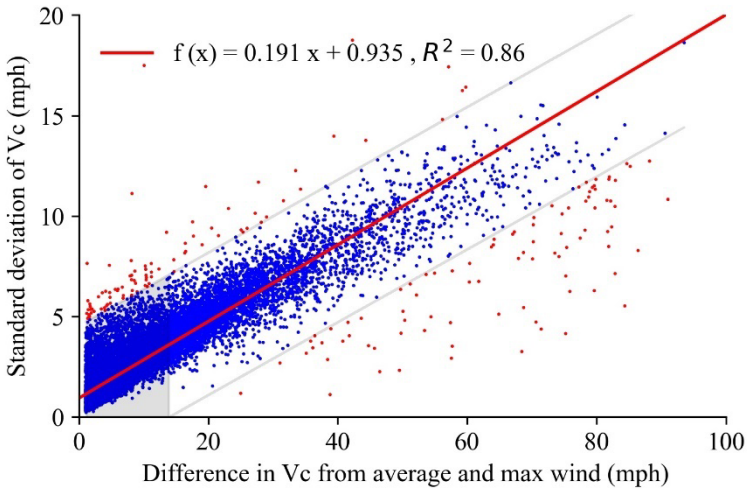

Figure 24: The relationship between the difference in V_c from 15-minute average and gust speed and standard deviation of V_c. Red dots are the outliers.

3.2.7 Parameter Estimation Algorithm for the Critical Wind Speed Distribution

Once the location parameter was estimated by a regression related to the sample mean value $\mathrm{E}(X)$, the other two parameters were then determined by Equations (11) and (12). Rearranging Equation (12) yields,

$$\theta = \sqrt{\frac{\mathrm{Var}\,(X)}{\psi_1(\kappa)}} = \frac{SD}{\sqrt{\psi_1(\kappa)}} \tag{13}$$

where *SD* is the sample SD, which may be estimated from the regression described above if it is unavailable. Then, substituting Equation (13) into Equation (11) yields,

$$0 = \hat{\mu} - \mathrm{E}(X) + SD \cdot \frac{\psi(\kappa)}{\sqrt{\psi_1(\kappa)}}, \tag{14}$$

were $\mathrm{E}(X)$ is the sample mean and $\hat{\mu}$ is the estimated location parameter by the regression relationship. Equation (14) is solved by a numerical solver for the shape parameter κ. Then, the scale parameter is determined by Equation (13) using the estimated location and shape parameters. The parametric distribution for the critical wind speed can be determined by this procedure.

3.2.8 Validation of the Parametric Distribution

This section presents the performance evaluation of fitted distribution based on the mean and maximum wind speed rather than the maximum likelihood method (which would involve an overly simplistic pure fitting technique).

The three parameters of exp-gamma distribution, along with the other two-parameter distributions, defined by their relationships to the SD and average value of V_c, are used for finding the best fitting distribution. The high-frequency wind data PDFs were used as true distributions to test the PDFs determined from the average and gust wind values.

Figure 25 shows the comparison of the RMSE value of each distribution to the actual data PDF. From this figure, the exp-gamma distribution was again deemed to be the best fitting distribution among the selected distributions since it boasted the lowest annual average value of RMSE for the selected 15-minute V_c values. This result also attested to the validity of the regression relations for the parameters in the exp-gamma distribution.

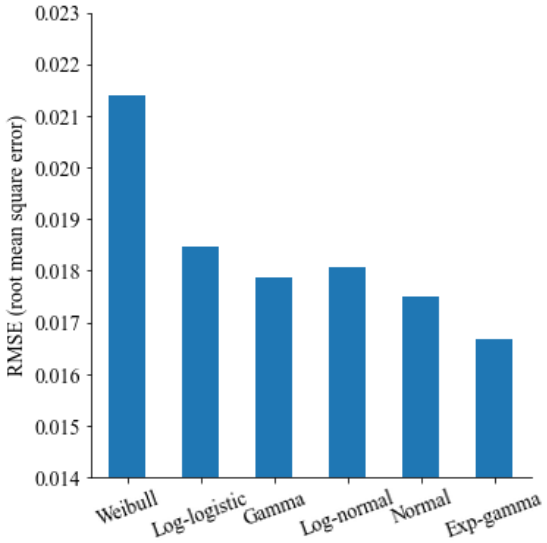

Figure 25: The annual average RMSE value of the parametric distributions for those 15-minute instances with an average V_c less than 105 mph.

A randomly chosen representative parametric distribution with the regression estimated SD value and the corresponding measurement-based histogram are shown in Figure 26 and Figure 27.

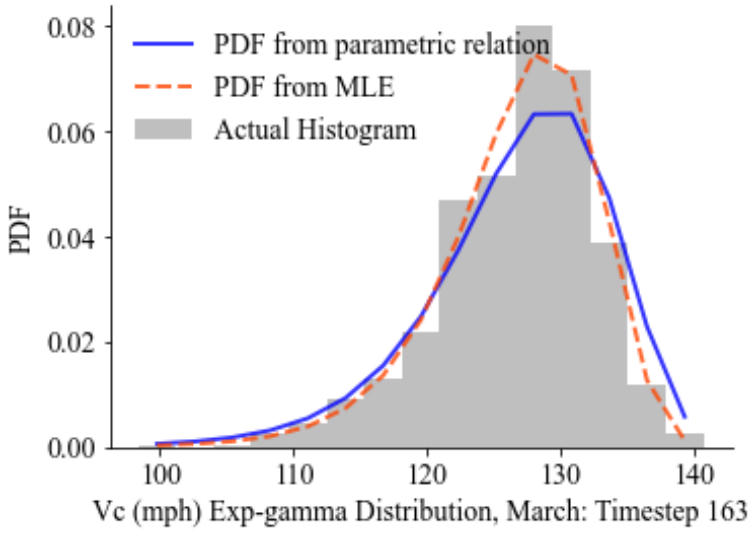

Figure 26: The PDF of the actual data with their associated parametric distributions.

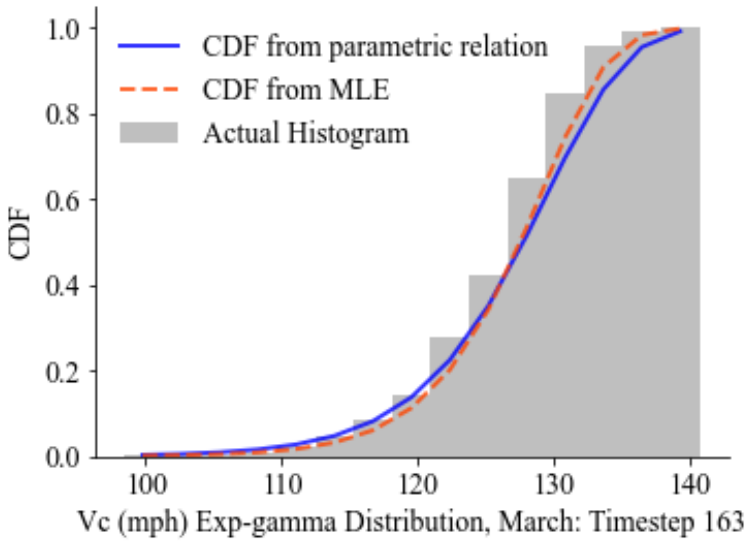

Figure 27: The CDF of the actual data with their associated parametric distributions.

3.3 Model Performance Demonstration

3.3.1 Baseline Vehicle Type and the Model Parameters

To demonstrate blow over risk characteristics, sensitivity analyses were performed using the configured model. Table 2 shows the baseline model parameters that are used in this section (unless specified otherwise for model sensitivity). This corresponds to a typical tractor-trailer truck traveling in the study area of I-25.

Table 2: Baseline parameter values for sensitivity analysis.

Variable name	*Letter*	Values
Width of the vehicle	b	2.6 (m)
Height of vehicle	H_v	4.15 (m)
Overall length of vehicle	L_v	23.5 (m)
Lift coefficient x (headwind)	C_{Lx}	1.5
Lift coefficient y (crosswind)	C_{Ly}	0.3
Drag coefficient (crosswind)	C_D	0.3
Mass of vehicle	M	15000 (kg)
Speed limit or vehicle travel speed	SL or V	75 (mph)
Radius of road curve	R	1168 (m)
Cant angle (cross slope or superelevation) of road surface	θ	4.59 (%)
Relative height of road surface	h'	5 (m)
Wind azimuth angle	ψ_W	270 (degree) = west
Vehicle orientation	ψ_V	0 (degree) = heading north
Factor of safety (FOS)	α	5.5

Figure 28 shows the sensitivity of the average wind speed (WS_ave) and the maximum wind speed (WS_max) on blow over risk. For this scenario, the blow over risk increases when the average overall wind speed is around 45 mph, which is unlikely (it is too fast) even for Wyoming. Still, a larger gust wind speed causes a decent blow over risk even at smaller overall wind speeds. For example, when gust wind is 150 percent of average wind speed (gust factor = 1.5), the blow over risk may become perceptible at 36 mph of average wind speed and above.

Determination of the associated FOS will be further discussed in later chapters.

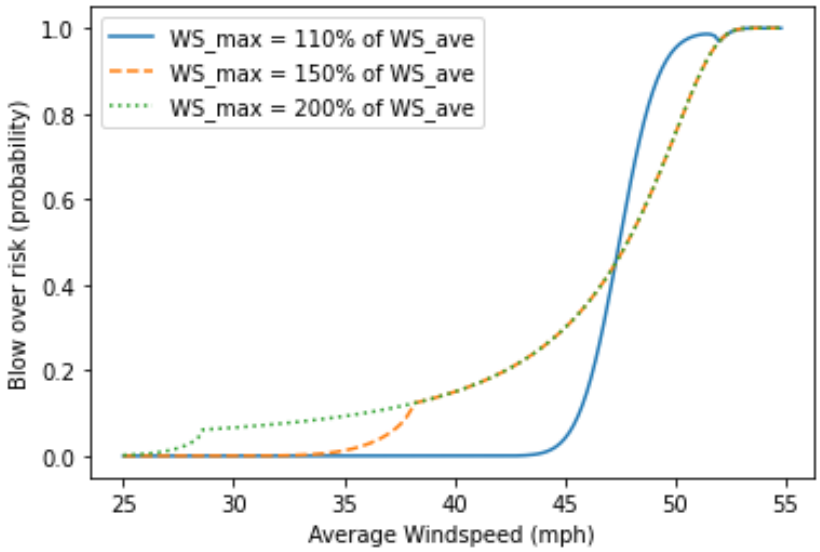

Figure 28: Sensitivity analysis of the blow over risk model with respect to wind speed. Both average and maximum speeds influence the blow over risk.

Figure 29 presents the sensitivity of the wind direction (azimuth angle) for curved and straight roads for a relatively heavy vehicle (e.g., partially loaded tractor-trailer truck). The blow over risk roses (polar plots of risks) visualize the crash probabilities for various wind directions for northbound and southbound vehicle orientations with conditions listed in Table 2. The direction of each rose corresponds to the wind azimuth angle. It is shown that wind directions slightly frontward from crosswind will effectively blow over the vehicle due to the headwind lift force (L_x, Figure 14), in addition to the crosswind lift and drag forces. The road curvature and cant angle bring about asymmetry in the polar plot of the crash risk. While no road is built without a cross slope (cant angle of 0 percent) due to drainage concerns, this scenario is used to illustrate the effects of the angle direction on blow over risk.

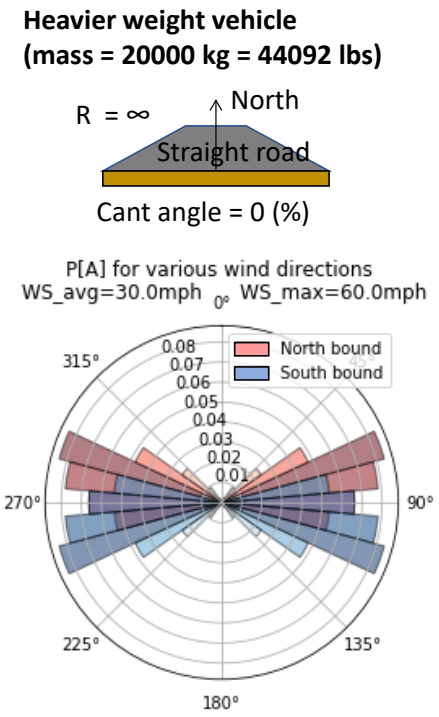

Subfigure A

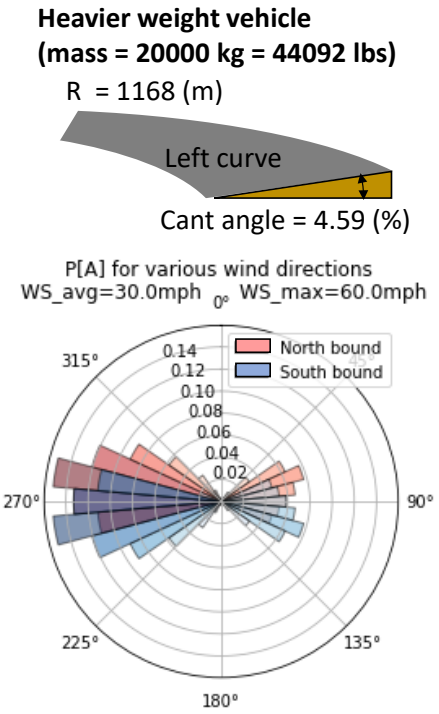

Subfigure B

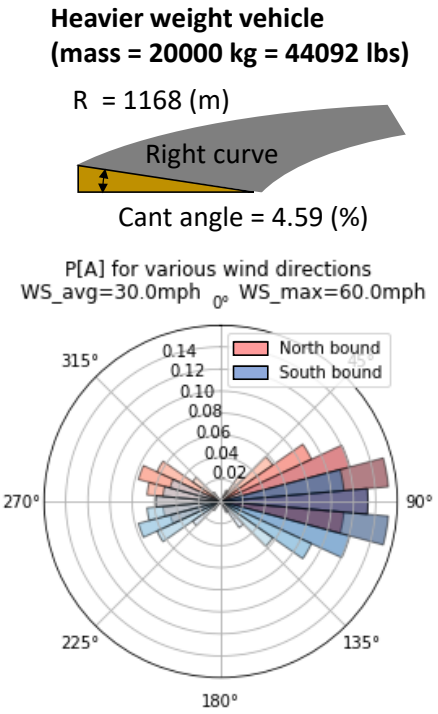

Subfigure C

Figure 29: Sensitivity analysis of the blow over risk model with respect to wind direction for the heavier vehicle (20000 kg).

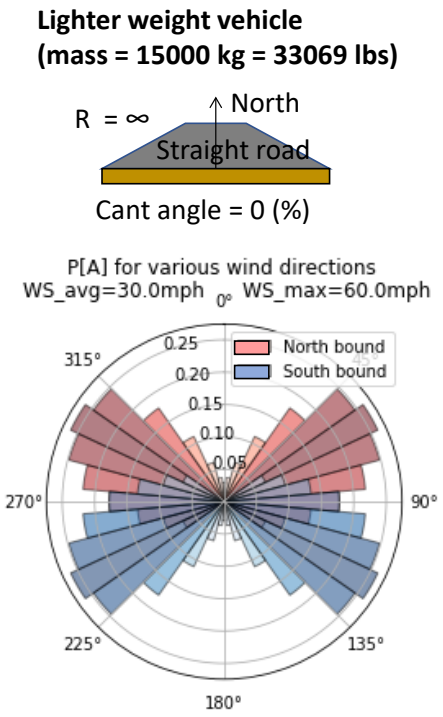

Subfigure A

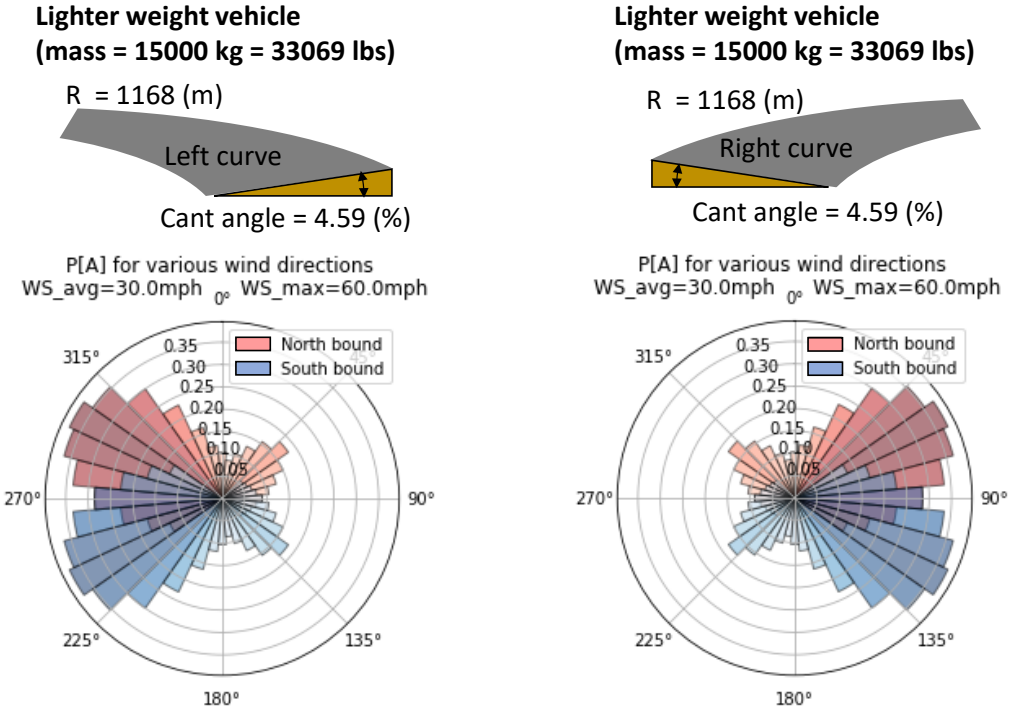

Subfigure B

Subfigure C

Figure 30: Sensitivity analysis of the blow over risk model with respect to wind direction for a lighter vehicle (15000 kg).

Figure 30 presents the same analysis with a lighter-weight vehicle (e.g., a nearly empty tractor-trailer truck). The lighter vehicle is much more vulnerable to the blow over crash condition since the magnitude

of the crash probability is generally greater for it than for the heavier vehicle. Interestingly, the risk for the lighter vehicle is broadly distributed in wind directions because the aerodynamic forces become larger than the centrifugal and gravitational forces in vehicle stability analysis.

If winds are generally crosswinds, even with small deviations in the wind direction, the blow over risk can reach a maximum in either of the two directions of travel. For example, for a vehicle traveling north on a road orientated north, with the wind blowing from 260°, the critical vehicle speed is below the speed limit for the northbound vehicle but above the speed limit for the southbound vehicle. However, if the winds deviate by 20° to the south (240°), the risk switches. Additionally, if the road section is predominantly affected by crosswinds, the traffic in all lanes must be stopped because even a small deviation in wind direction can alter the severity of risk in either or both directions of travel.

Figure 31 shows the model sensitivity of vehicle weight and travel speed to blow over risk. As may be seen, the vehicle weight is very sensitive, while reduction of travel speed is effective to reduce the blow over risk. Horizontal road geometry (the plane curvature of the road) is more important for heavier vehicles. Although there are too many variables that affect the blow over condition for each unique condition, this vehicle stability model, shown in this diagram, can provide useful advice to travelers and road management personnel.

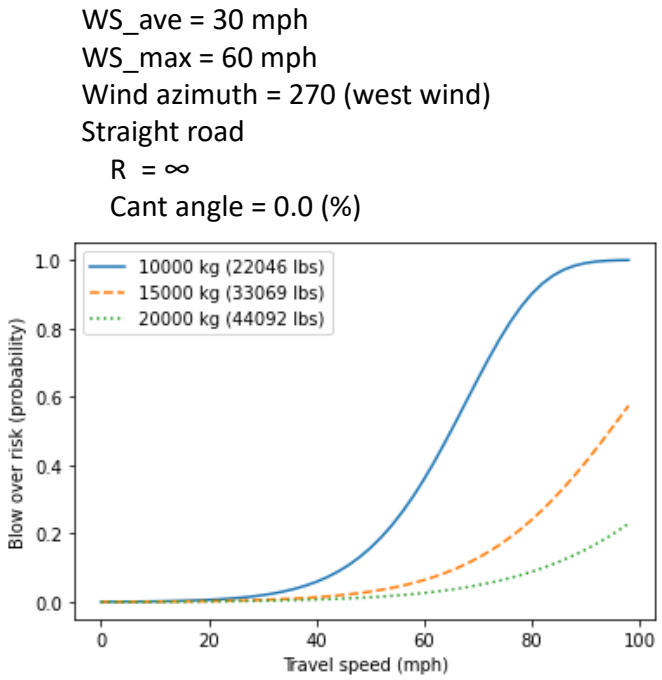

Figure 31: Sensitivity analysis of the blow over risk model with respect to vehicle weight and travel speed on a straight road.

WS_ave = 30 mph
WS_max = 60 mph
Wind azimuth = 270 (west wind)
Curved road
R = 1168 (m)
Cant angle = 4.59 (%)

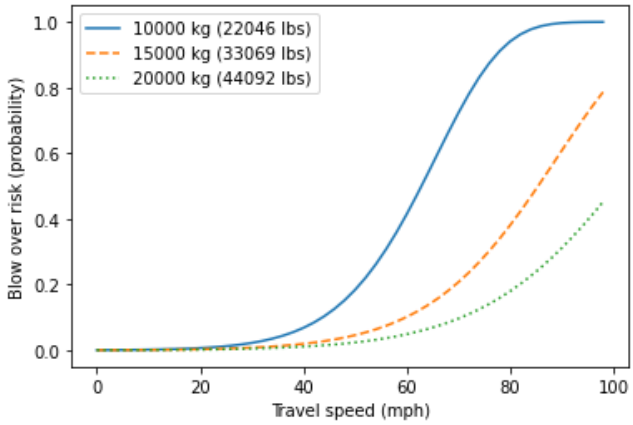

Figure 32: Sensitivity analysis of the blow over risk model with respect to vehicle weight and travel speed on a curved road.

3.3.2 Computational Efficiency of the Blow over Model

It is important to ensure rapid blow over risk quantification for successful and useful model implementation. The static vehicle stability model developed in this project is advantageous for potential nowcasting and forecasting of the blow over risk in a large area such as the State of Wyoming. The benchmark statistics of the computational efficiency shown below use a desktop computer at a UW laboratory. This program is written in the Python programing language with and without the multi-thread parallelization (with 4 cores), using the Concurrent module, which appears to be very effective. Further rapidity can be achieved by region-by-region or road-by-road parallelization using multiple computers. Also, the visualization of the results requires more processing time and power than only the computation of risk values.

Processor: Intel Core i7-4791K @ 4 GHz, 4 cores

Installed Physical Ram: 32 GB

Number of points equal 53,529 (One tenth of a mile data) times 2 (two lanes) = 107058 point locations

Wind Stations from which data are taken = 90 stations

Time taken for calculation = 1 minute: 55 seconds (without parallelization)

Time taken for calculation = 40 seconds (with parallelization)

Time taken to plot HTML map = 50 seconds

3.3.3 Case Studies: Three Observed Blow Over Crashes in the Wyoming Hill Study Area

3.3.3.1 2020 New Year's Day Blow over Crash

One blow over crash on January 1, 2020, near the wind monitoring network, was analysed in depth using the vehicle blow over model. Figure 33 shows the estimated blow over risk evolution and the corresponding PDF of critical vehicle speed, during the January 1, 2020 event. The high-frequency wind data from the UW station were used to estimate the PDFs of the V_c. These PDFs were computed from the fitted Vc data based on the high-frequency wind data. The blow over crash took place when the tails of PDFs reached below the speed limit of 75 mph. This figure illustrates that the stochastic model can effectively evaluate the blow over risk during a windy day at the crash site.

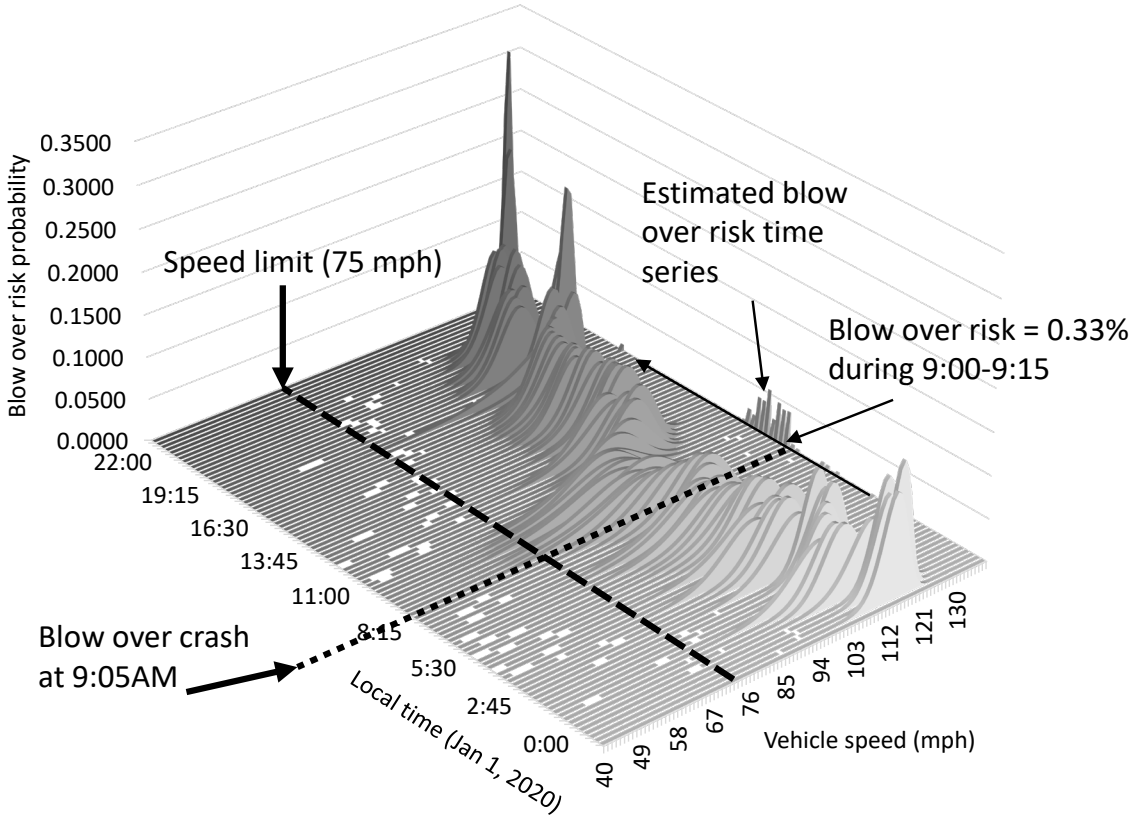

Figure 33: Estimated blow over risk evolution and the corresponding PDF of critical vehicle speed V_c during January 1st, 2020

3.3.3.2 November 13, 2020 Crash

On November 13, 2020, a tractor-trailer was involved in a blow over crash on southbound I-25 close to MP 4. The timing of the crash was before 10:34 a.m. (MST) as the crash was captured by the webcam on the Wyoming Hill RWIS ESS. There was another blow over crash around the same location on November 15, 2020. These incidents caused I-25 closure for several hours on both days. Figure 34 shows a map of the area around both crash sites. Both crashes were initiated near the elevated straight section for the railroad bridge during west-southwest wind events (wind azimuth angle of 218°).

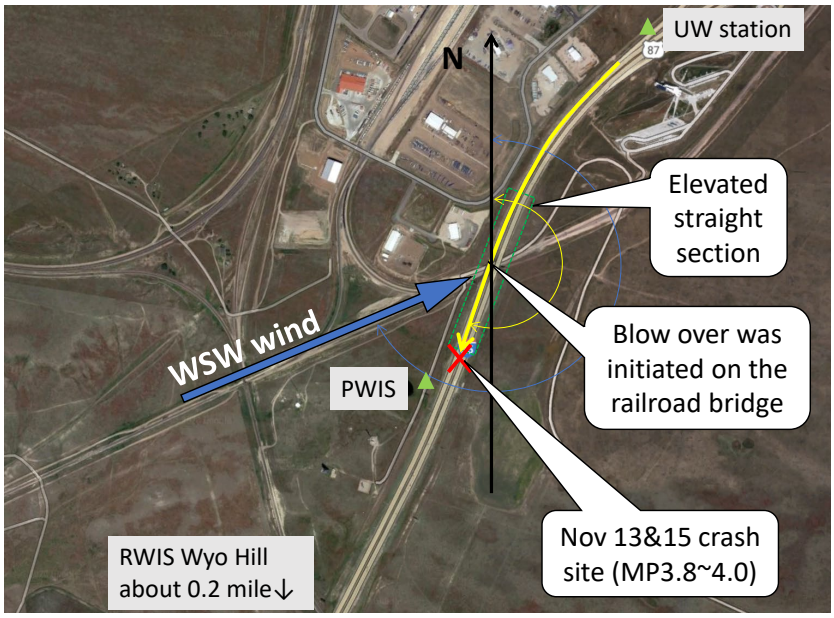

Source: Adapted from Google Map

Figure 34: Photographs of the Nov 13 blow over crash from the webcam at the Wyoming Hill RWIS ESS and the map of the incident

Figure 35 shows the evolutions of the estimated critical vehicle speeds at the locations of the blow over crash on the three days when the crashes occurred. The vertical dashed lines denote the time of crash whereas the horizontal dashed line is the posted speed limit (75 mph) for the road stretch. The place of blow over crash had a relative elevation (h') of 8.9 m. The wind measurements were adjusted for the road surface elevation using the logarithmic wind profile. The values for the UW sonic sensor show high fluctuations as they were plotted every second. All three blow overs were in the southbound direction. The time series for the southbound traffic showed a significant lowering of the critical speed of the vehicle at the time of blow over on all three days. For the northbound traffic, the critical vehicle speed values throughout these days were comparatively higher, indicating lower chances of blow over.

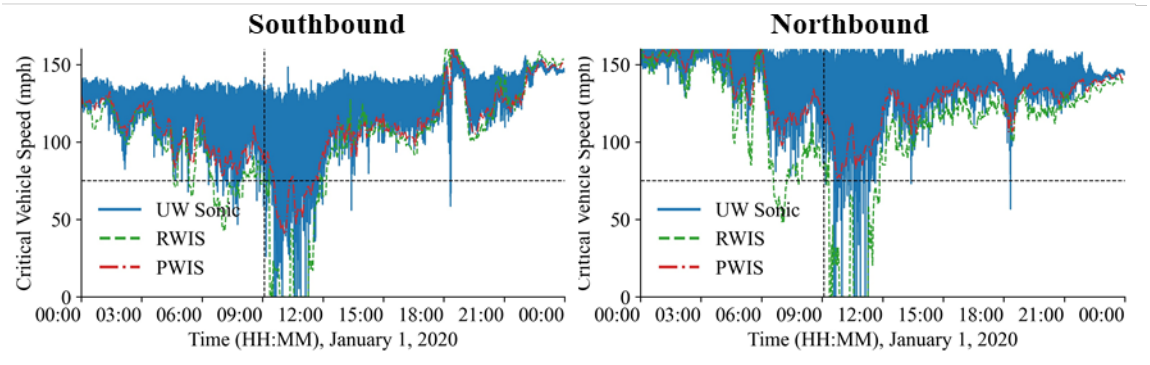

Subfigure A

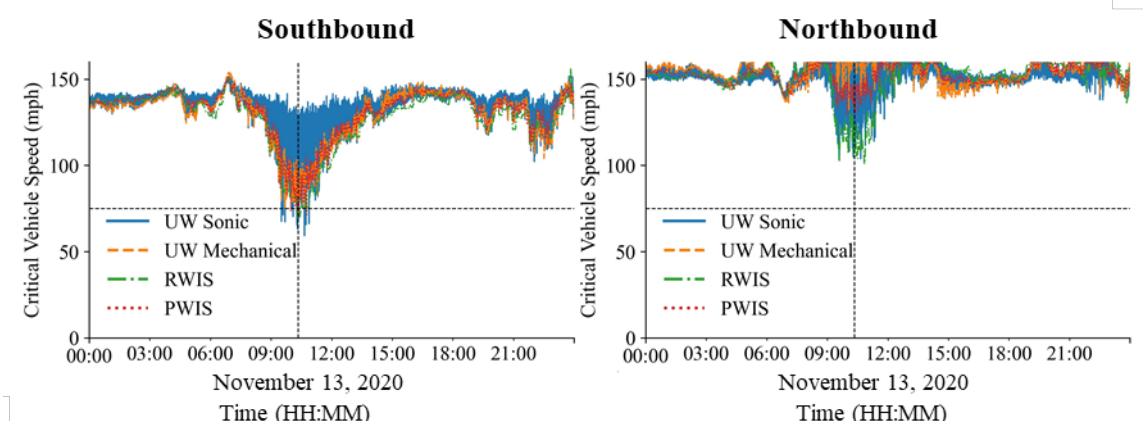

Subfigure B

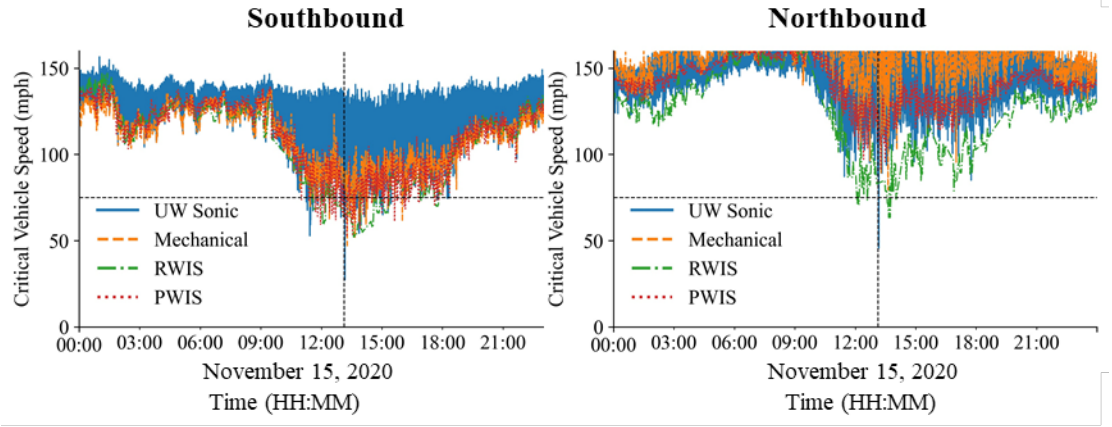

Subfigure C

Figure 35: The critical vehicle speed on the day of reported blow over crash at the crash site

There were also instances when the critical vehicle speed was below the posted speed limit without the occurrence of an actual crash. This could have occurred due to several factors, including the traffic being halted after the initial crash, a lack of vulnerable vehicles, variability in vehicle weight, variability in vehicle speed, variability in driver experience, and other unmeasurable uncertainties in wind and road conditions. For example, the trailers passing through that point at those instances might have been heavier than the mass of the model truck 15,000 kg (33,000 lb). It is also possible that vehicles passing through that point were driving at a speed below the critical vehicle speed, which was already below the posted speed limit. Given all these factors, the risk-based analysis or stochastic interpretation is as important as the physical vehicle stability model.

Figure 36 (left panels of Subfigures A,B, and C) shows the evolving probability of a blow over crash calculated every fifteen minutes based on the fitted probability distribution for the three high-wind days when blow over crashes were reported. The risk model was based on a lightly loaded semi-trailer with a weight of 33,000 lbs. (15,000 kg) traveling at the speed limit of 75 mph. The time of each crash is denoted by the dashed vertical lines. All three crashes were in the southbound lane. It may be seen that the blow over crash risk increased significantly when there was an actual blow over crash. Obviously, a blow over crash requires high-profile lightweight vehicle presence on the road as well as high wind

conditions. Moreover, when one blow over crash is reported, the road is usually closed. Therefore, the actual frequency of blow over crashes must be much smaller than the estimated blow over risk. Additionally, there were risks of blow over crashes in the northbound lane (opposite direction) during high winds on January 1 and November 15, 2020, so it was advisable to shut down both directions of travel.

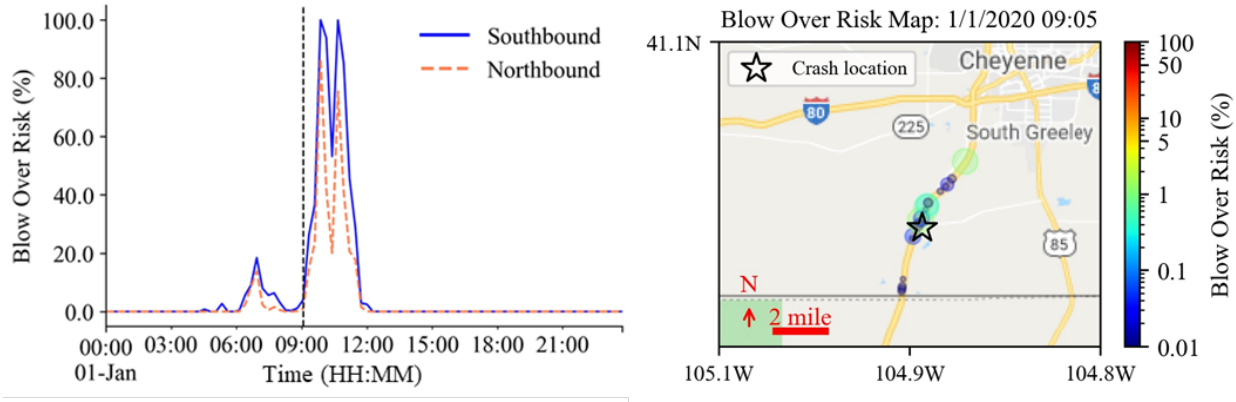

Subfigure A

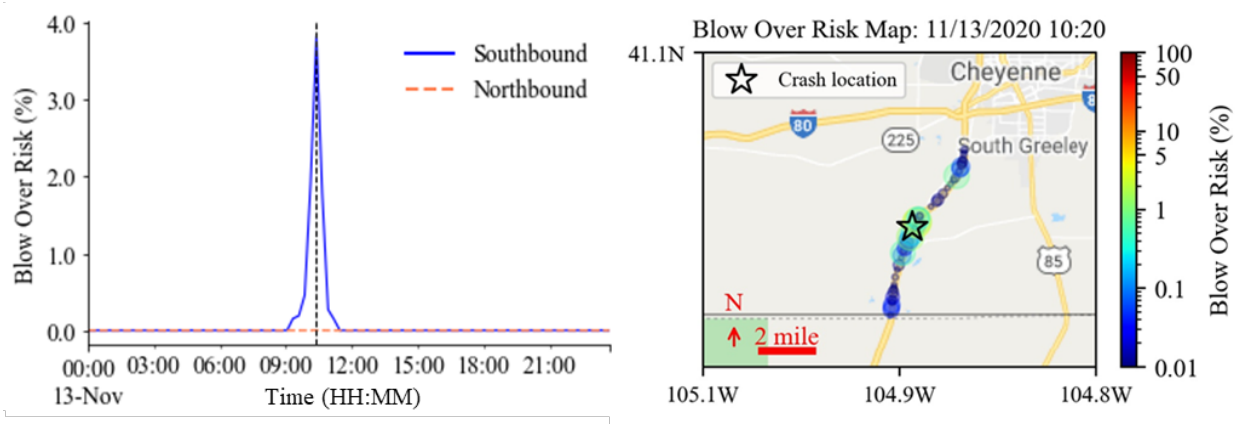

Subfigure B

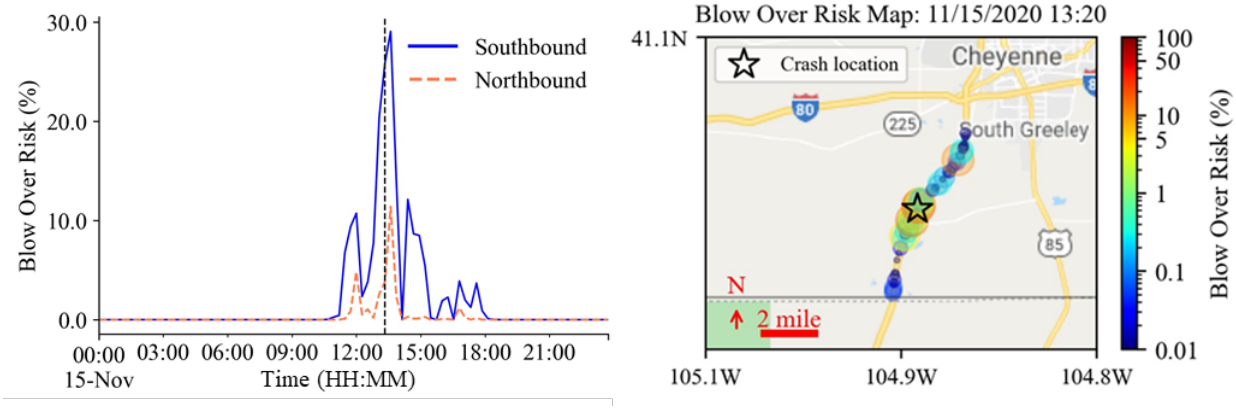

Subfigure C

Figure 36: The blow over risk probability calculated based on the fitted distribution

In Figure 36, the right panels of Subfigures A, B, and C illustrate the spatial risk distribution in MP 1-10, I-25, calculated at each tenth of a mile using the blow over risk evaluation system. The blow over risk is computed every tenth of a mile with wind records taken from the RWIS station and road point properties required by the blow over model taken from the point database created for this study. For each point**,** the figure shows the highest value of blow over risk among the two directions of travel. The blow over risk is shown using both the log scale color as well as size of the point for a better representation of blow over risk. For example, any point with blow over risk below 0.1 percent does not appear on the map. For the crashes plotted on the map, the points on the road closest to the crashes have a high value of blow over.

Chapter 4 – Blow Over Risk Assessment in Wyoming

4.1 Blow Over Risk Assessment System

The blow over risk assessment system will eventually use the wind data from existing wind monitoring stations or an external wind prediction system (e.g., weather forecasts) to calculate the blow over risk for roads statewide. Figure 37 shows a flowchart of the blow over risk assessment system using wind measurements from mechanical anemometers used in the RWIS ESS. The RWIS ESS already spans the state, recording wind data at a frequency of two minutes. Typical statistical distribution fits using the maximum likelihood estimation (MLE) cannot be performed because the frequency of the data collection typically occurs at only a 15-minute interval in the historical record. Therefore, the parameters of the distribution must be estimated from the relationship to the mean and SD of the data, as described in Sections 3.2.5 through 3.2.7. This estimated distribution is called the "parametric distribution" hereafter.

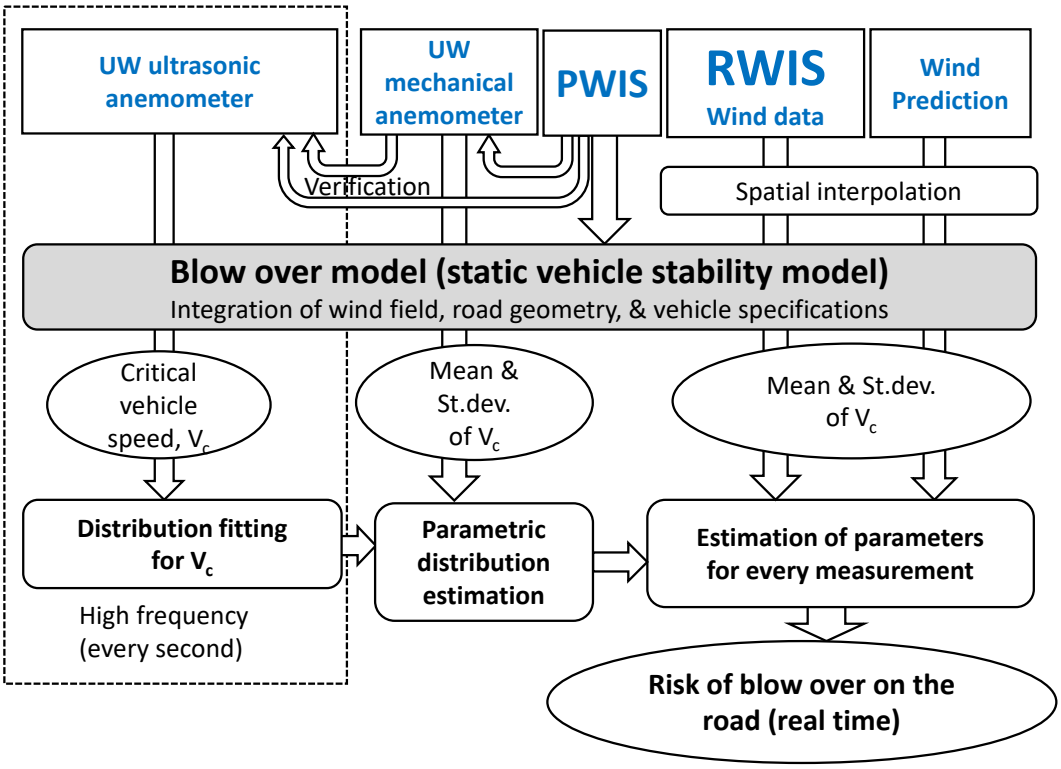

Figure 37: Flowchart for blow over risk (BO risk or P(A)) assessment system

The prevalent mechanical sensors that are already in place statewide provide wind measurements, which include average wind speed, average gust speed, and average wind direction. From these three input values, steps are taken to find the value of the mean and SD of V_c. To perform this task, the high-frequency V_c values are divided into 15-minute groups. The mean and SD of V_c are calculated along with mean wind, mean direction, and maximum wind for each 15-minute interval data for the year 2020. It was found that the average wind speed, maximum wind speed (gust speed), and average wind direction calculated for every 15-minute interval from the high-frequency anemometer were comparable to their

counterparts from the mechanical anemometer. The average wind direction was used with both the mean wind and maximum wind in the vehicle stability model to calculate V_c.

4.2 Road Geometry Parameter Database

A shapefile of the WYDOT highway system was obtained from an open data service hosting the data provided by WYDOT. The roads in this shapefile were polylines with associated lengths, starting and ending mileposts (MPs), and posted speed limits stored as attributes. The locations of MPs were received from WYDOT in the form of a Google Earth file (KMZ file). The road polylines were then split into mile-long segments based on the MPs using ArcMap tools. These lines were further divided into ten equal parts and points were generated from the vertices of these lines in order to effectively establish points at each tenth of a mile throughout the Wyoming road system. Through this process, a total of 53,540 points were generated on the WYDOT highway system. (Figure 38).

Figure 38: Road points established at each tenth of a mile in the Wyoming highway system.

Each of these points would need road geometry parameters, such as radius of the road, orientation, cross slope angles, etc. to be used as inputs in the wind blow over model. To attain this necessary information, the radii of curves were calculated using an ESRI ArcGIS toolbox called Road Curvature Analyst (ROCA) (Bíl et al. 2018). Next, the relative elevation of these points was determined as the difference between the elevation of the road to the average elevation of either side of the road, a calculation which is shown in a subsequent section (Figure 39). Additionally, the points were also associated with the nearest RWIS ESS and their distances were noted.

The elevation data was then computed using the DEM maps from the USGS website with 10 m spatial resolution. The elevation of points on the roads and their either side at a given instant were taken from the DEM using the “extract values to points” toolbox in ArcGIS at every tenth of a mile. The computed values were added to the existing state-wide road geometry file, which included several other road parameters, such as radius and orientation, which were also required inputs for the blow over model.

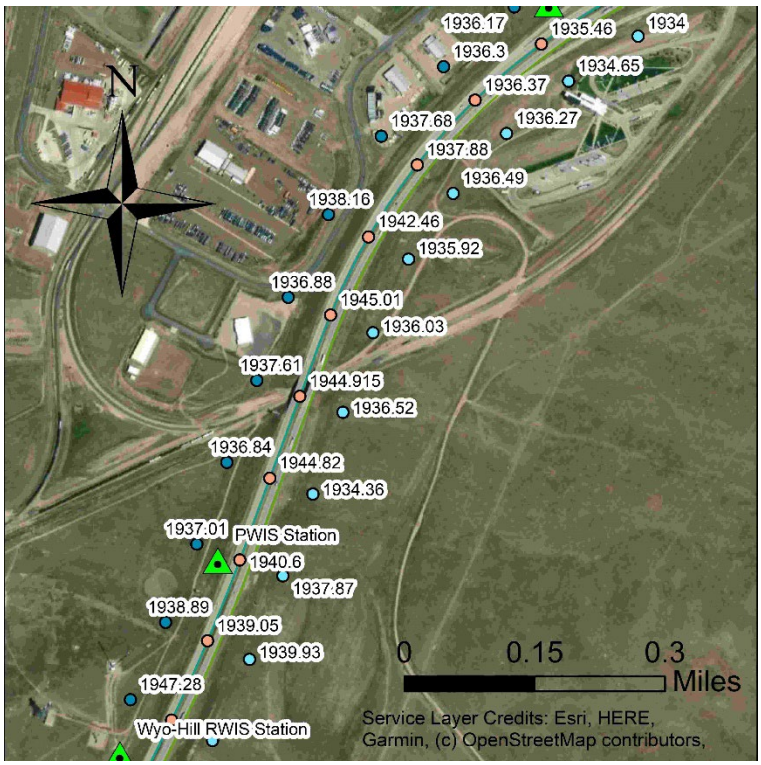

Basemap source: ESRI

Figure 39: Computed elevation in meters above sea level (MASL) around the study area (MP 3-5) of I-25

Figure 39 shows the elevation of the road points and roadsides around the hotspot in the Wyoming Hill study area around I-25 at MP 4. The elevation difference on the transverse direction (crosswind direction) is considerably larger than the longitudinal direction (headwind direction) because the longitudinal grades for the highway are generally kept at 5 percent or lower. Accordingly, this dataset suggests that only the crosswind component that uses the relative elevation of the road surface evaluated for modeling.

Figure 40 shows the estimated relative road surface elevation along the interstates around Cheyenne, Wyoming. This figure also includes the historical blow over crash sites during 2012-2017. Most of the historical crashes took place at the elevated sections ($h' > 0$) denoted by the orange and red (darker) colors in the figure. However, this map also shows a few crashes in valleys and depressions, so the crosswind reduction by the local terrain might underestimate blow over risks in low lying areas. Therefore, the magnitude of the elevation effect may need to be adjusted based on the crash record.

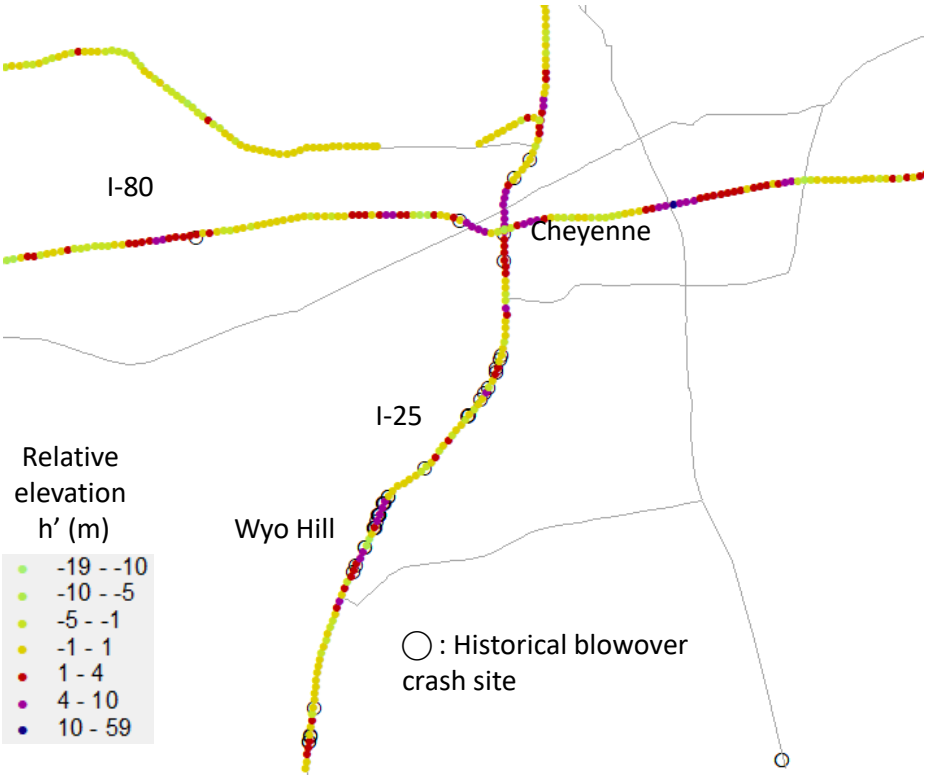

Source: Wyoming Geolibrary and WYDOT

Figure 40: Estimated relative road surface elevation in the study area and the historical blow over crash sites.

To calculate the V_c of the vehicle at curved sections of the road, the cant angle (cross slope angle, or superelevation) of the road is required. The cant angle or superelevation is calculated using the equation below from the American Association of State Highway and Transportation Officials (AASHTO) *Policy on the Geometric Design of Highway and Street,* known by transportation professionals as the "Green Book" (2018).

$$0.01e + f = \frac{V^2}{15\,R} \tag{15}$$

e = Superelevation or cant angle, percent

f = Side friction factor

V = Design speed, mph

R = Radius, ft

The value of design speed (V) is taken as the posted speed limit and is already available along with the value of radius (R) from interstate points data prepared for this study. The side friction factor (f) is calculated from its relationship to different values of design speed (V), as shown in the Green Book. This formula was used to estimate the cant angle (superelevation) for every road point without missing although this is known to be less conservative than the actual road geometry.

Additional road geometry parameters were derived at an accuracy of every tenth of a mile to quantify the blow over risk based on the observed wind speed and wind direction. Figure 41 shows an example of the derived road geometry parameters associated with the road point database. The headwind and crosswind components of wind can be computed by this database using the time-dependent wind angle. Complete specifications concerning the developed database are presented in Section 6.2.

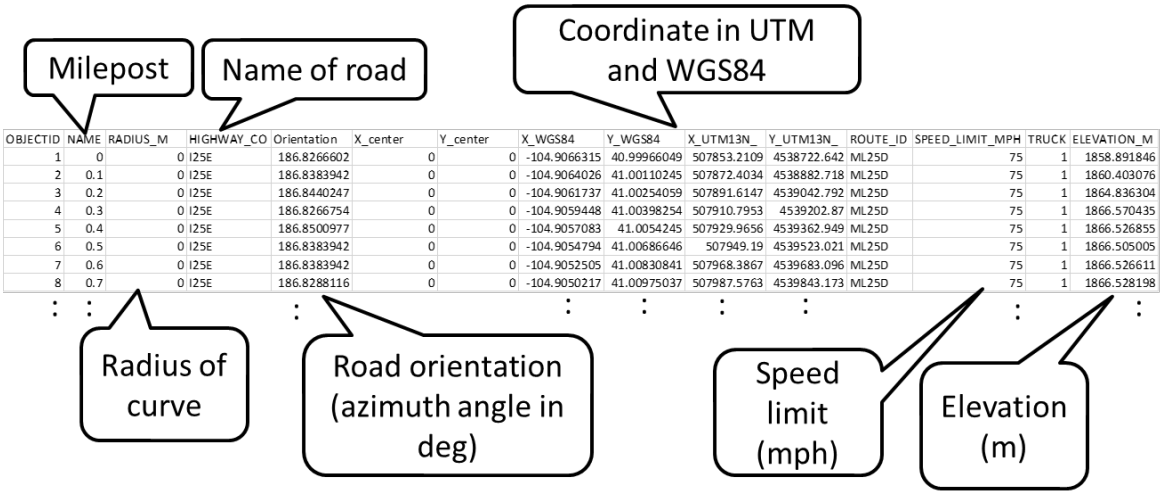

OBJECTID	NAME	RADIUS_M	HIGHWAY_CO	Orientation	X_center	Y_center	X_WGS84	Y_WGS84	X_UTM13N_	Y_UTM13N_	ROUTE_ID	SPEED_LIMIT_MPH	TRUCK	ELEVATION_M
1	0	0	I25E	186.8266602	0	0	-104.9066315	40.99966049	507853.2109	4538722.642	ML25D	75	1	1858.891846
2	0.1	0	I25E	186.8383942	0	0	-104.9064026	41.00110245	507872.4034	4538882.718	ML25D	75	1	1860.403076
3	0.2	0	I25E	186.8440247	0	0	-104.9061737	41.00254059	507891.6147	4539042.792	ML25D	75	1	1864.836304
4	0.3	0	I25E	186.8266754	0	0	-104.9059448	41.00398254	507910.7953	4539202.87	ML25D	75	1	1866.570435
5	0.4	0	I25E	186.8500977	0	0	-104.9057083	41.0054245	507929.9656	4539362.949	ML25D	75	1	1866.526855
6	0.5	0	I25E	186.8383942	0	0	-104.9054794	41.00686646	507949.19	4539523.021	ML25D	75	1	1866.505005
7	0.6	0	I25E	186.8383942	0	0	-104.9052505	41.00830841	507968.3867	4539683.096	ML25D	75	1	1866.526611
8	0.7	0	I25E	186.8288116	0	0	-104.9050217	41.00975037	507987.5763	4539843.173	ML25D	75	1	1866.528198

Figure 41: Example parameters associated with the road point database.

4.3 Implementation of the Blow Over Risk Assessment System

4.3.1 Ground-Based Wind Data

RWIS is the most reliable source of roadside, real time wind data. Figure 42 shows the map of the RWIS ESS in Wyoming. The real time and historical wind data (wind direction, mean and maximum wind speeds) can be downloaded from the WYDOT Statewide Weather Sensors and the Iowa Environmental Mesonet (IEM) archives.

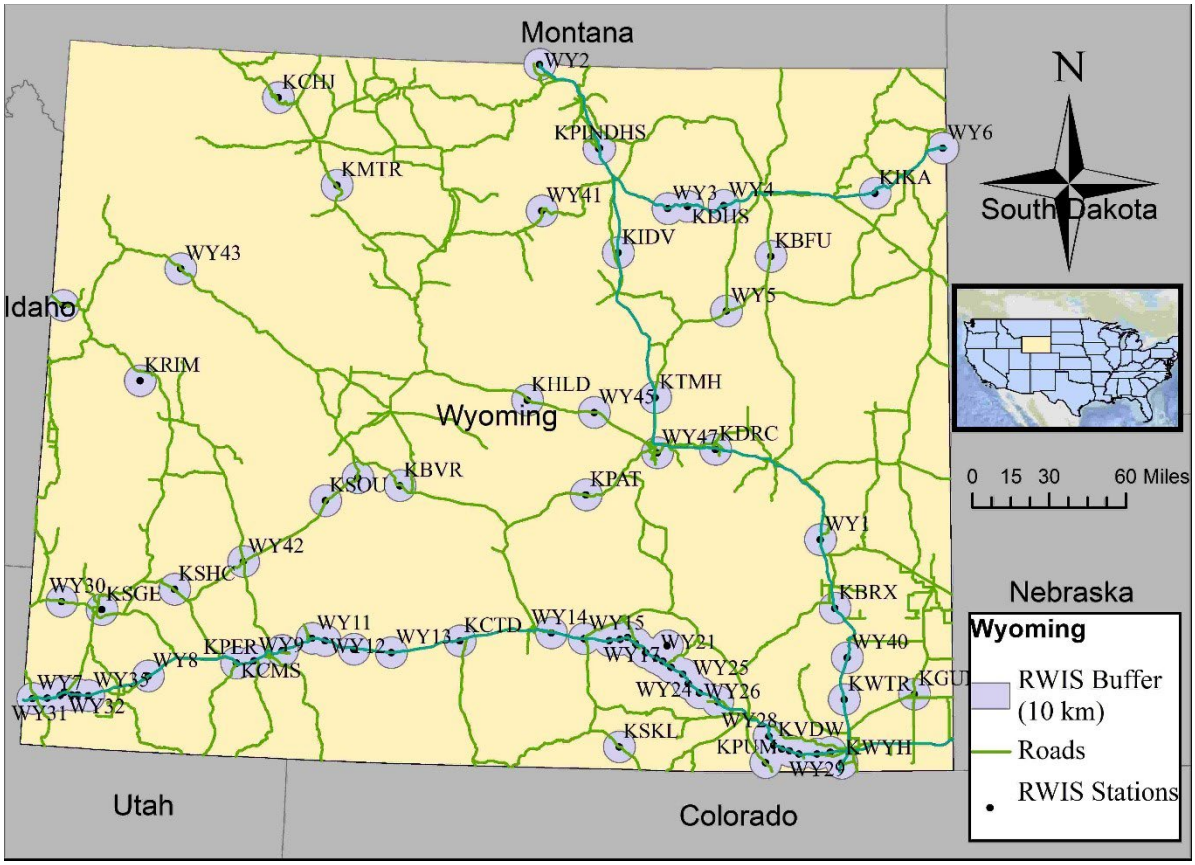

Source: IEM, US Census Bureau, ESRI, and WYDOT

Figure 42: RWIS Stations with Buffer of 10 km Around them in Wyoming

4.3.2 Spatial Distribution of Blow Over Risk During November 13, 2020 Crash Period

The series of blow over crash incidents that occurred on November 13, 2020, was selected because thirteen crashes were reported on the interstates of the southwestern part of Wyoming. November 13, 2020 was in the middle of a winter storm with a high wind warning in effect for central and western Wyoming throughout the day (LaChance, 2020). Figure 43 visualizes the blow over risk (colored dots) with the corresponding blow over crash sites (stars) at four example time slices on the Wyoming highways.

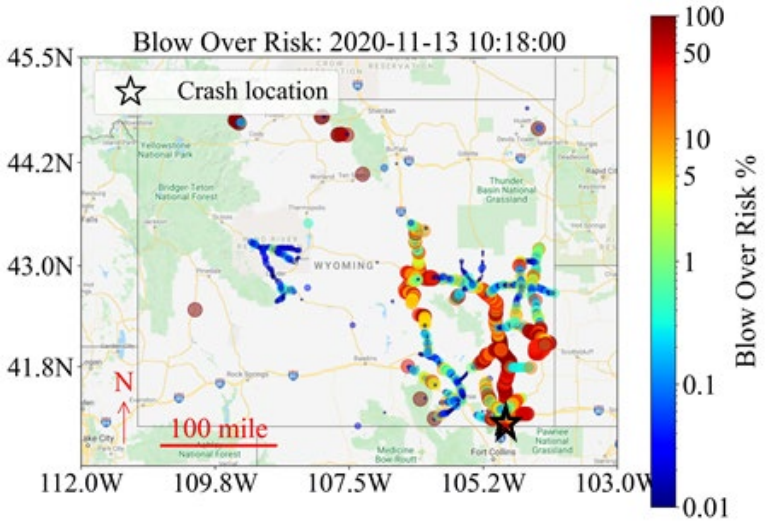

Subfigure A

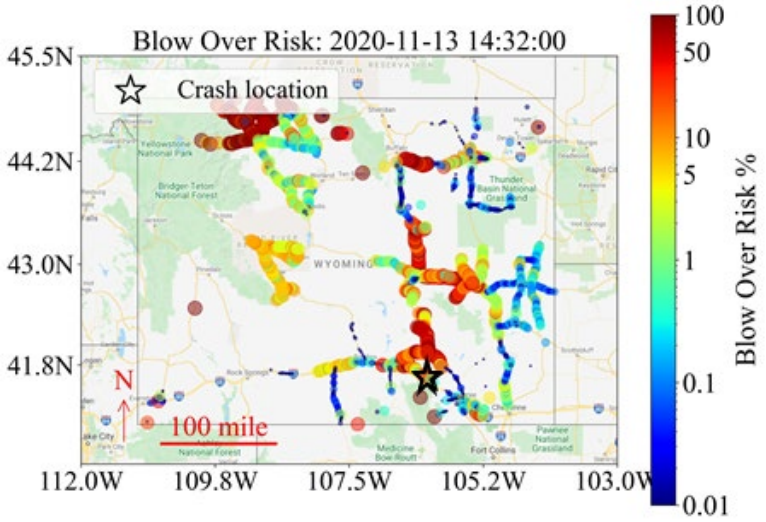

Subfigure B

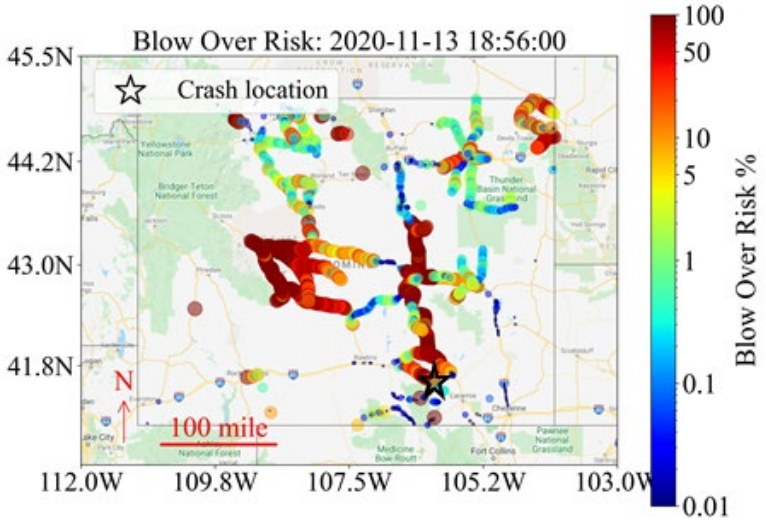

Subfigure C

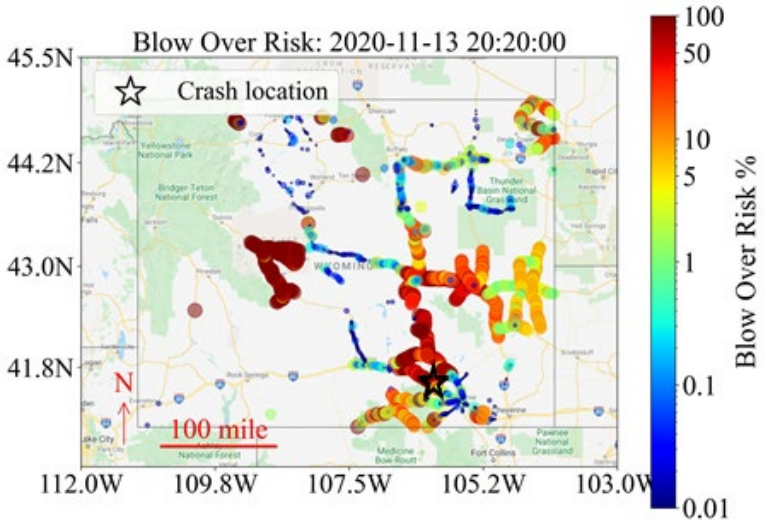

Subfigure D

Figure 43: Blow over risk map at four different times on November 13, 2020. Size of dots, as well as color, reflects blow over risk severity.

The computed risk levels shown in Figure 43 assumed an empty semi-trailer with a weight of 30,000 lbs. (13,600 kg). The blow over risk was computed at every MP with wind records taken from the nearest RWIS ESS and road point properties taken from the point database created for this study. For each MP**,** the figure shows the highest value of blow over risk among the two directions of travel. The threshold of the blow over risk is 0.1 percent, so a log scale color bar is used for better differentiation of blow over risk levels. The size of the point is also proportional to the level of risk while any point with blow over risk below 0.1 percent does not appear on the map.

The location of each crash is denoted by a hollow star marker on each map, as demonstrated in each map's key. For the four crashes plotted on the maps above, the points on the road closest to the crashes

have a high value of blow over risk represented by darkening shades of red. Figure 43 (Subfigure A) shows the crash also analyzed in Figure 35. If the wind data was replaced by real time measurement, this modeling system could be used to assess the real time risk of blow over on Wyoming roads. Additionally, such blow over risk maps could be created for different weights of vehicles, and advisories could be placed on DMS targeting specific vehicle classes.

4.3.3 Other Historical Blow Over Crashes

Historical blow over risk analysis for this report was performed based on dates that possessed the largest frequencies of blow over crashes for the years 2012-2020. The frequency of the crashes was calculated only considering those crashes that had wind records within the ±10-minute time period from the recorded time of the crash. The results of the dates with the highest occurrence of crashes in order are shown in Table 3. The download for the historical wind records from the RWIS stations was automated using the Synoptic Data API Service (Synoptic Data, 2021). Finally, the blow over risk was calculated for each historic crash using the framework for all the 5726 MPs in the Wyoming roads with wind records from the nearest RWIS station.

Table 3: The historical days with high frequencies of blow over crashes

S.no	Date	Crashes
1	12/19/2016	12
2	2/22/2012	10
3	11/13/2020	10
4	12/20/2020	8
5	1/18/2012	8
6	12/21/2018	7
7	11/15/2020	6
8	2/10/2017	6

Once blow over risk was calculated for each point for the entire day, the data was reorganized to store the blow over risk associated with every MP for a given time step. The geometric parameters required for the model were based on the database created for points at every tenth of a mile in the Wyoming roads system, as previously discussed. The crash record information was also added to the wind data frame for the time closest to the recorded time of the crash. Therefore, each time step in the day shows the associated blow over risk for every MP as well as the location of any blow over(s) that occurred during that time step.

Because recognizing past patterns is often the key to predicting future events, risk evaluations during historical wind events can effectively test the efficacy of new modeling systems like this one. Such visualizations can also help by assessing the strength of the model for future instances of high winds.

One windy 10-minute period from January 18, 2012, used for testing, is shown in Figure 44. The windy period saw two blow over crashes in a zone where there was a relatively high blow over risk as calculated by the new blow over model. All the RWIS winds may not record the wind at the same time, so the blow over risk at all the MPs may not be visible for every timestamp. Nevertheless, it is encouraging to see the blow overs take place in the zones of higher risks in a small period.

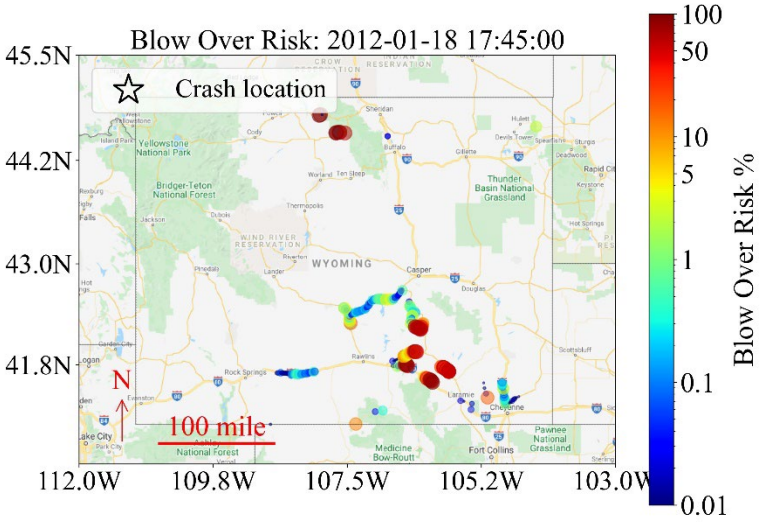

Subfigure A

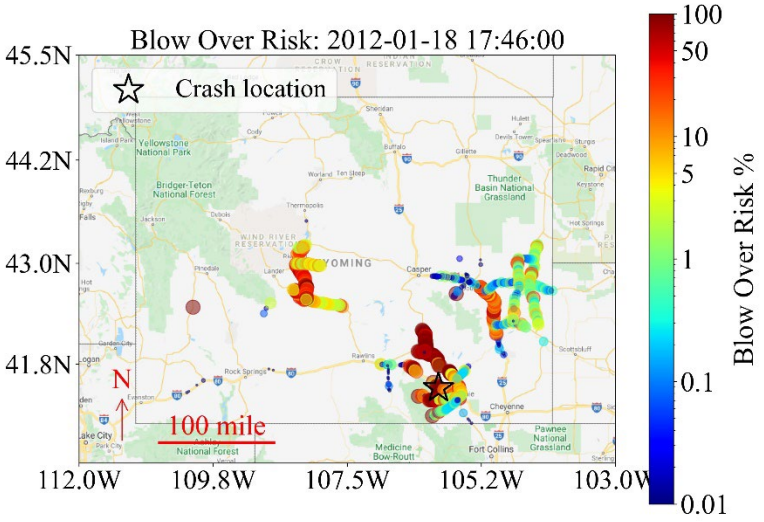

Subfigure B

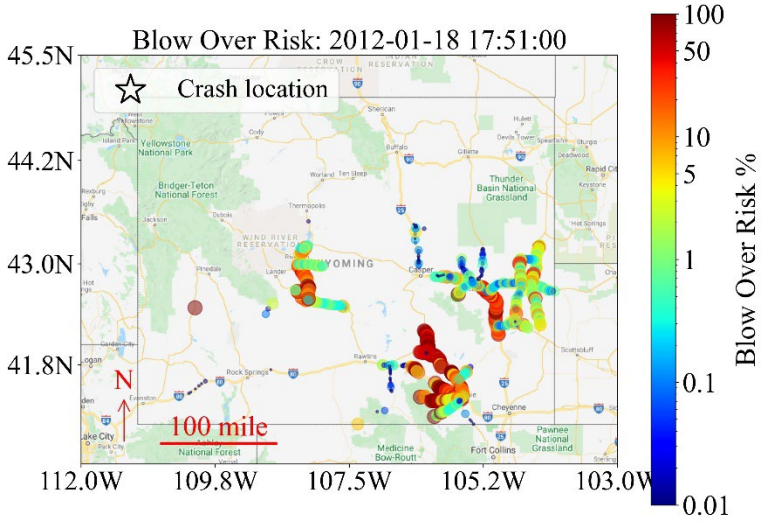

Subfigure C

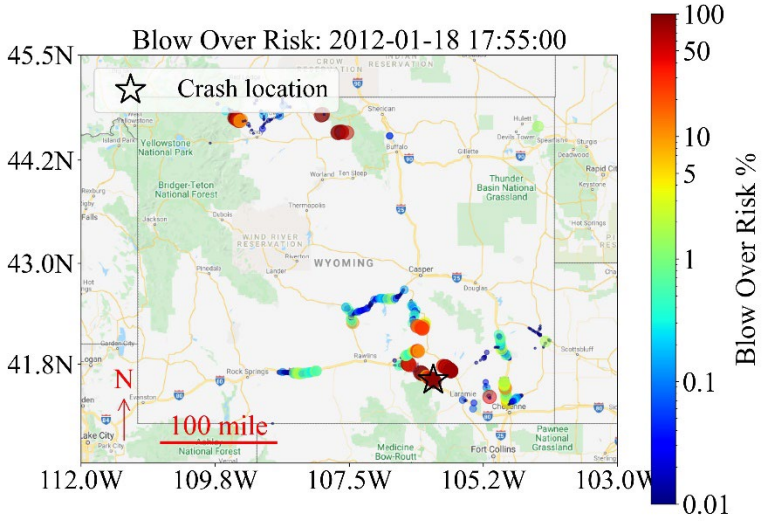

Subfigure D

Figure 44: Model Analysis of windy period from January 18, 2012. Size of dots, as well as color, reflects blow over risk.

4.3.4 Factor of Safety (FOS) Selection

In a project such as this, FOS selection is crucial for incorporating the uncertainties of wind parameters and vehicle parameters used in a physical system into a model of that system. The FOS value for this project was determined through sensitivity analysis associated with historical blow over crashes.

The framework used for calculating the blow over risk was then used to find the risk at the time of a blow over crash between 2012 and 2020. This analysis used the highest wind speed observed, within a time window of 10-60 minutes, around the blow over crashes at the nearest RWIS station. Also, crashes for

which the lane of crash, direction of travel, or actual location could not be identified, were not chosen for analysis. From 323 crashes, only 268 crashes were considered usable in complete analysis.

Each one-tenth of a mile was associated with the nearest RWIS wind station and other parameters required in the model to calculate blow over risk. Each of the RWIS stations was also assumed to be recording winds at 30 ft (10 m) above the ground. The download of the daily wind records for all the dates in which the blow over crashes took place was automated by the IEM. The time interval between the successive wind recordings varied from 2 to 15 minutes based on the year and season of data collection.

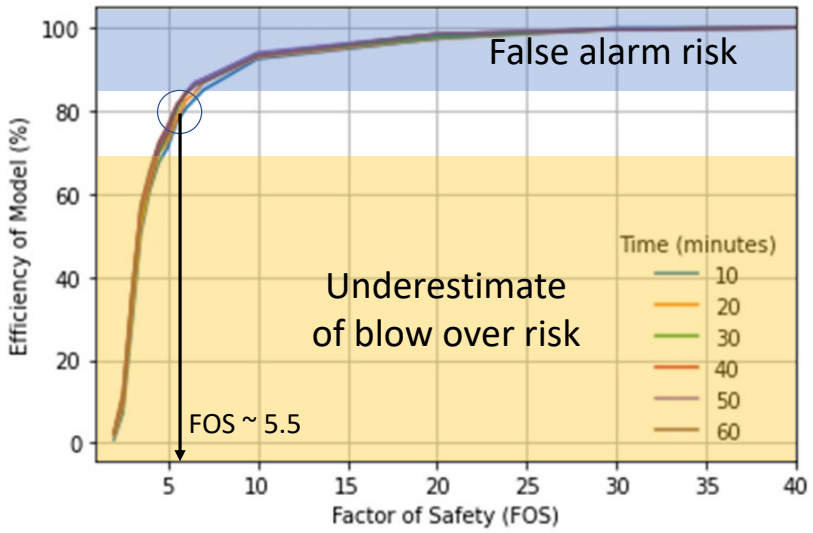

Figure 45: The FOS used in the model vs the efficiency of the model at different time intervals.

To visualize the sensitivity of the FOS, a wide range of FOSs between 1 through 50 was considered for this analysis. The time window sizes before and after the recorded time of the crash for the blow over risk computation were also varied to accommodate differences between the blow over crash times and their reporting times. The maximum gust wind data within the time window was used for the calculation of blow over risk. For example, the efficiency of the model in predicting an actual crash that follows the blue line (Figure 45) would use a wind record corresponding to the time of maximum gust within 10 minutes of the crash report time. The efficiency of the model can be measured as a percentage of the number of predicted crashes over the number of total actual blow over crashes (267 crashes). The predicted crash by the model was judged as correctly predicted if the computed risk is more than 0.1 percent for the reported blow over crash.

Considering the significant uncertainties associated with wind measurements, driver behaviors, and vehicle type variabilities, the greater model efficiency did not always indicate accurate predictions, and it also showed the possibility of resulting in false alarms (i.e. overpredicting risk), which could lead travelers to disregard severe warnings. The model was run numerous times varying the FOSs between 1 and 50, and the efficiency of the model was determined at each FOS (Figure 45). From this repetition, an inflection point in the model efficiency was seen around an FOS of 5.5. Based on engineering judgment, the FOS of 5.5 was therefore considered advisable for the system operation. However, the FOS value

should be adjusted if the road managers and travelers find that it is too sensitive (overpredicting risk) or insensitive (underpredicting risk).

4.3.5 Performance Evaluation of the Blow Over Risk Assessment System

The developed blow over risk model was applied to the historical blow over crashes that occurred on the interstates of Wyoming between 2012 and 2020. The wind measurements were always taken from the closest RWIS ESS. The blow over risk was calculated based on the wind measurements closest to the time of the crash. Table 4 demonstrates the overall crash analysis of the model. It can be seen that the performance of the model decreases as the distance from the crash site to the nearest RWIS ESS increases. It is recommended, therefore, that the RWIS ESS sites be placed within at least 10,000 m (6.2 miles) from blow over hotspots for an accurate risk evaluation. Referring to the map of the RWIS stations with buffer of 10 km (6.2 miles) around them in Wyoming (Figure 42), considerable sections of the highways cannot currently be covered by the existing stations. It is noted that the known hot spots for blow over crashes are reasonably covered by RWIS but if a statewide risk model is desired, additional instrumentation may be necessary.

Table 4: Results based on the distance to the nearest RWIS ESS.

Distance to nearest RWIS ESS (m)	Number of crashes within RWIS range	Efficiency of model Percent of blow over crashes correctly predicted (>0.01 risk)
0 -1000	110	76.4%
1000 -2000	64	68.7%
2000 -5000	74	67.5%
5000-10000	25	68.0%
10,000-20000	33	48.5%
> 20000	17	29.4%
Total	323	

Additional analysis was conducted on those instances where the wind data was measured less than 10 km (6.2 miles) from the point of the crash. Also, only crashes with gust wind of greater than 40 mph at the time of the crash were selected. The resulting efficiency of the model with the selected crashes is shown in Table 5. The tabulated results indicate that the direction of travel is not that important for blow over risk, likely due to substantial wind angle variability. Overall, the model appears to be an effective tool for blow over hotspot identification or traffic management at least within 10 km from the nearest RWIS ESS sites (Figure 42).

Table 5: Efficiency of the model based on the crashes within 10 km (6.2 miles) of RWIS.

Condition	Nos	Efficiency of model Percentage of blow over probability > 0.1%
With direction considered	249	77.9%
Without direction consideration (Taking largest risk of two lanes)	249	92.4%

4.3.6 Real time Implementation of the Configured Blow Over Risk Evaluation System

One of this blow over risk model's applications is to become a real time decision support tool for the WYDOT TMC. One of the advantages of this model is that this model can extract the geometric and other parameters of individual points on the road, and then use them to calculate the blow over risks quickly and efficiently.

The real time blow over risk evaluation system was implemented using the configured model for demonstration. A link to the demonstration website can be found in Chapter 6. The website hosted by WYDOT (2021b) provides the wind conditions for RWIS locations in Wyoming, with the RWIS locations identified by route and milepost information. These locations were then associated with this project's RWIS map. The RWIS wind data are then entered into the model and displayed on a map. The map is updated every 2 minutes using Python programs. An example map from this process is shown in Figure 46.

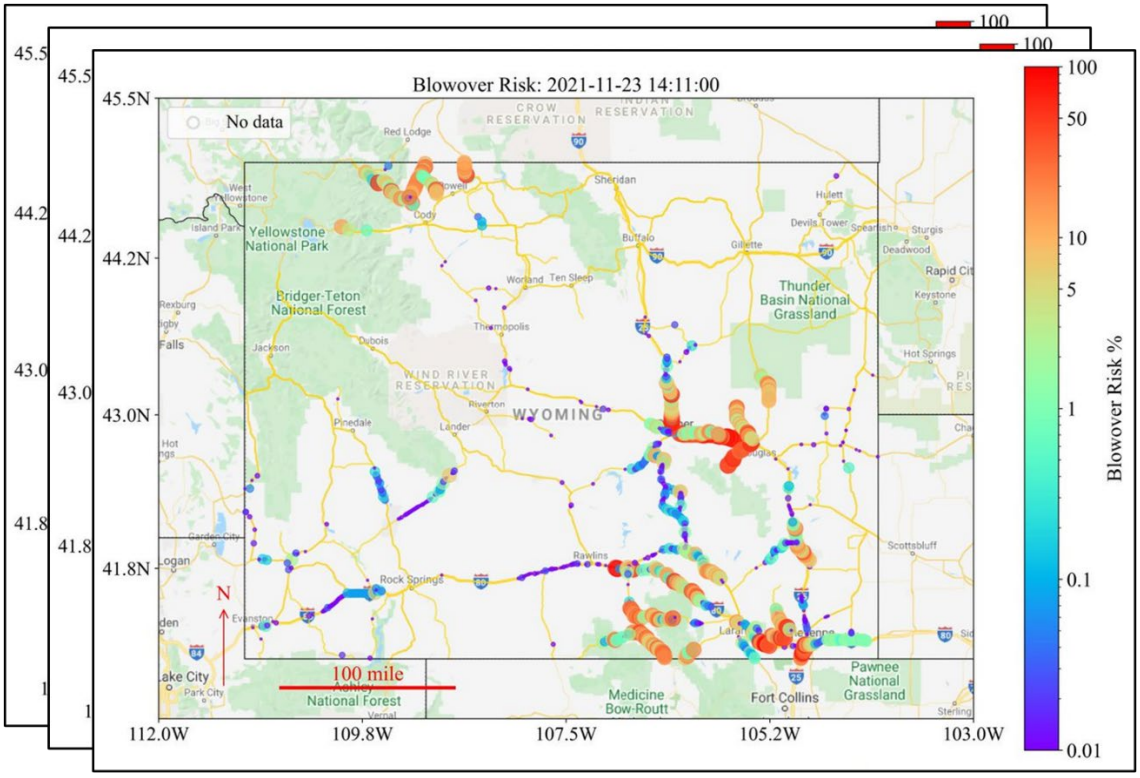

Figure 46: Statewide real time blow over risk maps

4.4 Blow Over Hazard Maps based on Simulated Wind Data

A blow over hazard map that identifies the road sections with significant blow over risk is useful to optimize the Department of Transportation's transportation resource distribution (e.g. wind monitoring stations). For this purpose, researchers used the climatological historical wind field reconstructed by the WRF model using the historical atmospheric reanalysis because that model offered uniform accuracy even in the areas without the RWIS ESS service. This study began by using the WRF simulated wind fields prepared in the previous study (Ohara, 2017). The WRF wind speed and direction data were then converted into component forms (u & v components) at every WRF data point. The winds at road points were next computed by 4-point inverse distance interpolations. The historical mean wind direction was evaluated by the Yamartino method (Yamartino, 1984; Ohara, 2017). For this analysis, mean and maximum magnitudes of wind speed were dynamically computed at every road point. The computed mean and maximum wind data points were then used to calculate the critical vehicle speed at every individual road point. The vehicle stability model parameters, shown in Table 2, were all used as variables except for the vehicle weight, which was kept constant at 15,000 kg (33069 lbs).

4.4.1 Model-Based Historical Wind Data

Reconstructed historical climatological wind data were used for the blow over hazard maps, which could identify the road sections with significant blow over risk. The WRF model simulated the climatological historical wind fields based on the historical atmospheric reanalysis.

This study uses the WRF simulated wind fields prepared in the previous study (Ohara, 2017). The WRF model was configured with double nesting domains, as shown in Figure 47. The outer domain (Domain 1) had a 12 km (7.5 mi) resolution, and the inner domain (Domain 2) had a 4 km (2.5 mi) resolution. Data from the National Centers for Environmental Prediction (NCEP) North American Regional Reanalysis (NARR) were used for preparing the initial and boundary conditions of the WRF model. The NARR is the atmospheric reanalysis dataset that includes 29 levels of atmospheric state variables at a 3-hour time increment for the North American Region at a 32 km (20 mi) resolution.

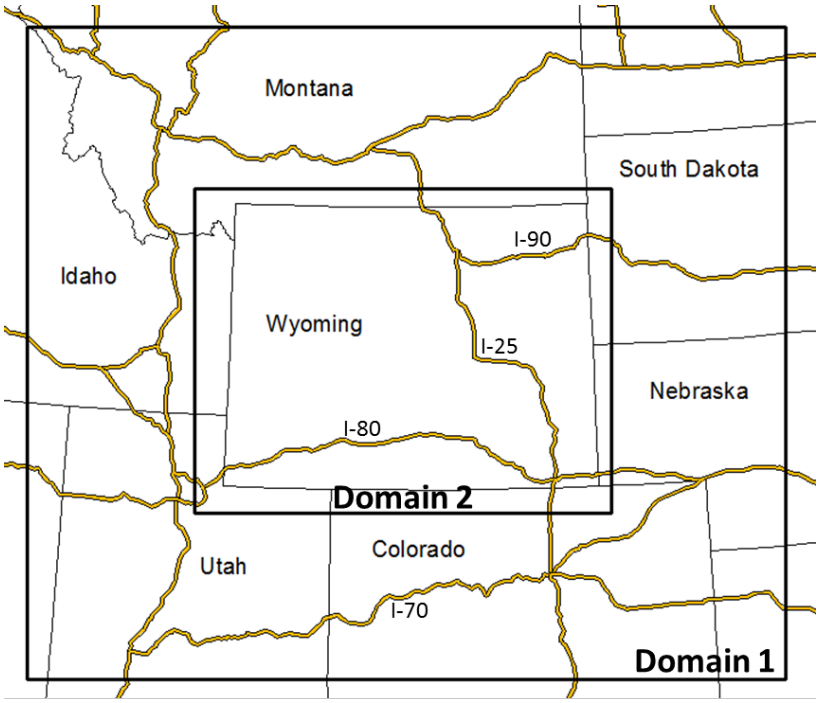

Sources: ESRI

Figure 47: The nesting domains of the WRF model for wind field reconstruction (Ohara, 2017)

For the configured WRF model, the Morrison Double Moment scheme (Morrison et al., 2008), the Noah Land Surface model (Kusaka et al., 2001), and the Yonsei University scheme (Hong et al., 2006) were selected for the cloud microphysics, land surface modeling, and the planetary boundary layer (PBL) options, respectively.

The fine resolution WRF simulation at 4 km (2.5 mi) resolution was implemented during 500 historical windy periods (Ohara, 2017). The WRF wind speed and direction data were converted into component form (u & v components) at every WRF data point. Note that u is the east-west component of wind speed (m/s, east positive), and v is the north-south component of wind speed (m/s, north positive). The wind azimuth was related to the x and y components of wind speed by an arctangent function. The two-argument arctangent function, atan2(y, x) was used because it is commonly available to obtain the arctangent of y/x in the range $-\pi$ to π radians (-180 to 180 degrees). However, this placed the zero azimuth of the geographic wind on the north (y-axis) instead of the east (x-axis). Since the azimuth of geographic wind corresponds to the direction from which the wind came, therefore, the geographical wind direction and wind speed had to be computed from westerly and southerly wind components, *u* and *v*, to produce the WRF simulation,

$$\psi_w = \text{atan2}(-u, -v) \tag{16}$$

$$Spd = \sqrt{u^2 + v^2} \tag{17}$$

where

ψ_w = wind azimuth (rad)

u = East-west component of wind speed (m/s, east positive)

v = North-south component of wind speed (m/s, north positive)

Spd = wind speed (m/s).

Note that radians may be converted to degrees by multiplying by 57.29578 (= 180/π). The reverse conversion can be performed by,

$$u = -Spd \ \sin(\psi_w) \tag{18}$$

$$v = -Spd \ \cos(\psi_w) \tag{19}$$

Meanwhile, the Yamartino Method (Yamartino, 1984) is an algorithm for calculating an approximation to the statistics of wind fields including the mean ψ_{w_a} and the deviation σ_θ of wind direction during the simulation period. The average values of sin ψ_w and cos ψ_w were first computed as,

$$s_a = \frac{1}{n}\sum_{i=1}^{n} \sin \psi_{w_i} \tag{20}$$

$$c_a = \frac{1}{n}\sum_{i=1}^{n} \cos \psi_{w_i} \tag{21}$$

where i denotes the time step, and n is the sample size or the number of the total time steps. Then, the average azimuth angle and the standard deviation of the angle were computed as follows:

$$\psi_{w_a} = \text{atan2}(s_a, c_a) \tag{22}$$

$$\sigma_\theta = \arcsin(\varepsilon)\left[1 + \left(\frac{2}{\sqrt{3}} - 1\right)\varepsilon^3\right] \tag{23}$$

where,

$$\varepsilon = \sqrt{1 - (s_a^2 + c_a^2)} \tag{24}$$

The winds at the road points could then be computed by the 4-point inverse distance interpolation. The mean and maximum magnitudes of wind speeds were computed at every road point throughout the simulated windy periods. The common Beaufort wind classification with various wind speed units is shown in Figure 48 for convenience.

BEAUFORT SCALE

Force		Anemometer reading mph	kmh	m/s	knts	Description		Effect on kite
0	○	0-1	<1	<0.3	0-1	Calm; smoke rises vertically.	Calm	Launch frustration
1		1-3	1-5	0.3-1.5	1-3	**Direction of wind shown by smoke drift, but not by wind vane.**	**Light air**	Very large lightweight deltas, Rokkaku etc, may fly on a light line
2		4-7	6-11	1.5-3.3	4-6	**Wind felt on face; leaves rustle; ordinary vanes moved.**	**Light Breeze**	Sutton ff30 lofts 650g at 3.5mph
3		8-12	12-19	3.3-5.5	7-10	**Leaves and small twigs in constant motion; wind extends light flag.**	**Gentle Breeze**	Drogue needed on Flowform kites
4		13-18	20-28	5.5-8.0	11-16	**Raises dust and loose paper; small branches are moved.**	**Moderate Breeze**	
5		19-24	29-38	8.0-10.8	17-21	**Small trees in leaf begin to sway; crested wavelets form on inland waters.**	**Fresh Breeze**	Reduce kite size increase line weight & drogue size
6		25-31	39-49	10.8-13.9	22-27	Large branches in motion; whistling heard in telegraph.	Strong Breeze	
7		32-38	50-61	13.9-17.2	28-33	Whole trees in motion; inconvenience felt when walking.	Near Gale	KAP not possible without severe risk of injury to operator and equipment.
8		39-46	62-74	17.2-20.7	34-40	Breaks twigs off trees; generally impedes progress.	Gale	
9		47-54	75-88	20.7-24.5	41-47	Slight structural damage occurs (chimney-pots and slates removed).	Severe Gale	
10		55-63	89-102	24.5-28.4	48-55	Seldom experienced inland; trees uprooted; considerable structural damage occurs.	Storm	
11		64-72	103-117	28.4-32.6	56-63	Very rarely experienced; accompanied by wide-spread damage.	Violent Storm	
12		73-83	≥118	≥32.6	64-71		Hurricane	

Source: adapted from the website: [Billyboyheritagesurvey's Blog]

Figure 48: Beaufort scale for various wind speed units

4.4.2 Historical Mean Wind Records and Blow Over Risk

Although it may be obvious that the annual mean wind field is too small to demonstrate a conclusive blow over risk, the historical mean wind was also included in the analysis for verification purposes, in addition to the historical maximum wind. Average wind speed in the historical period ranges between Beaufort force categories of 3 – 5 (8 – 24 mph) in Wyoming, while gust wind speed in the historical period ranges in the Beaufort category 3 – 6 (8 – 31 mph) in Wyoming.

Figure 49 displays the blow over hazard map from the WRF simulated historical average wind condition. It is confirmed that the average wind field does not cause any perceptible blow over risk.

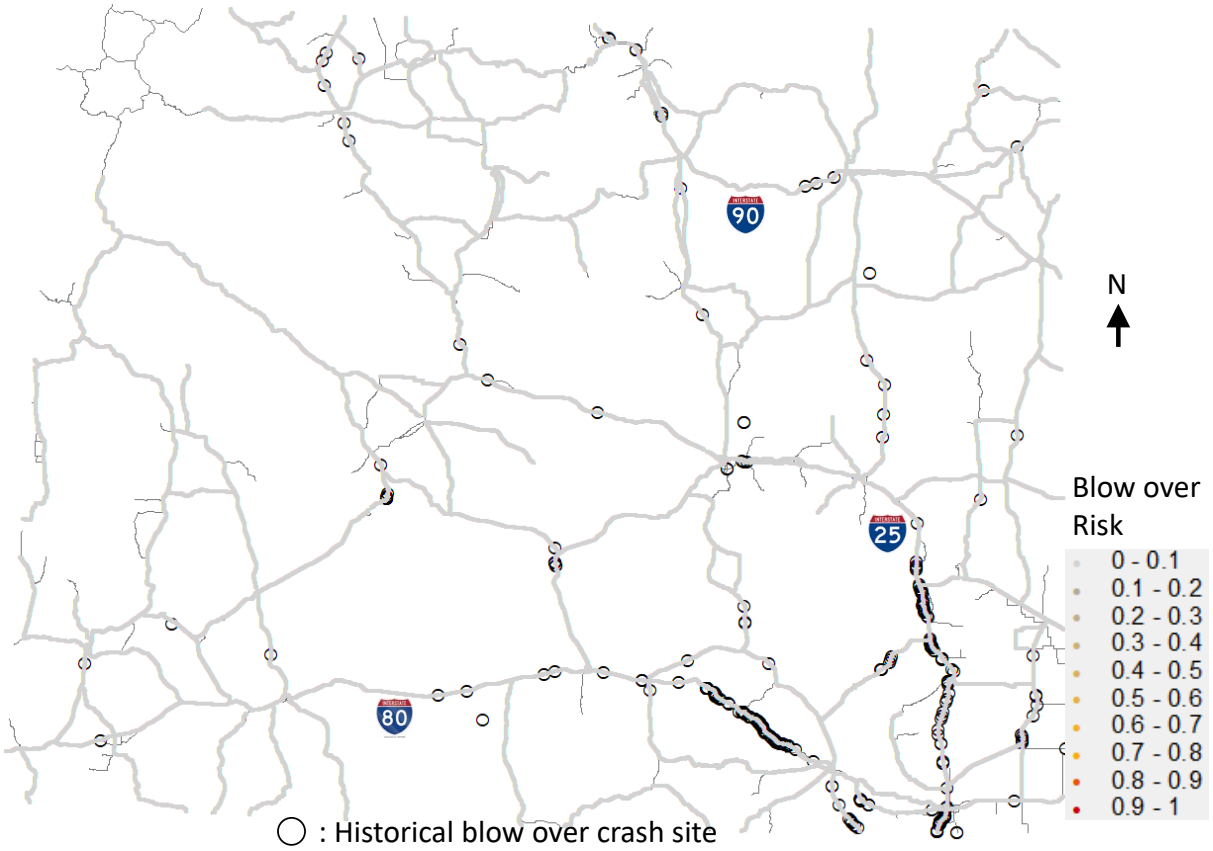

Source: Wyoming Geolibrary and WYDOT

Figure 49: Estimated blow over risk using the historical average wind on the highway network of Wyoming based on the WRF simulation.

4.4.3 Historical Maximum Wind and Blow Over Risk

Maximum average wind speed in the historical period ranges in the Beaufort scale of 6 – 11 (25 – 72mph) in Wyoming, while gust wind speed in the historical period ranges in the Beaufort scale from 7 – 12 (32 mph or above) in Wyoming.

Figure 50 shows the blow over hazard map derived from the WRF simulated historical maximum wind condition. Approximately 42.6 percent of the highways in Wyoming have considerable blow over risk using the historical maximum wind speed. The crash incidents in the red-colored section imply either vehicle speed above the speed limit or a vehicle weight of 15,000 kg (33069 lbs) or lighter. It is clear that the developed blow over risk model can explain the distribution of blow over risk crash, while the historical wind field alone does not.

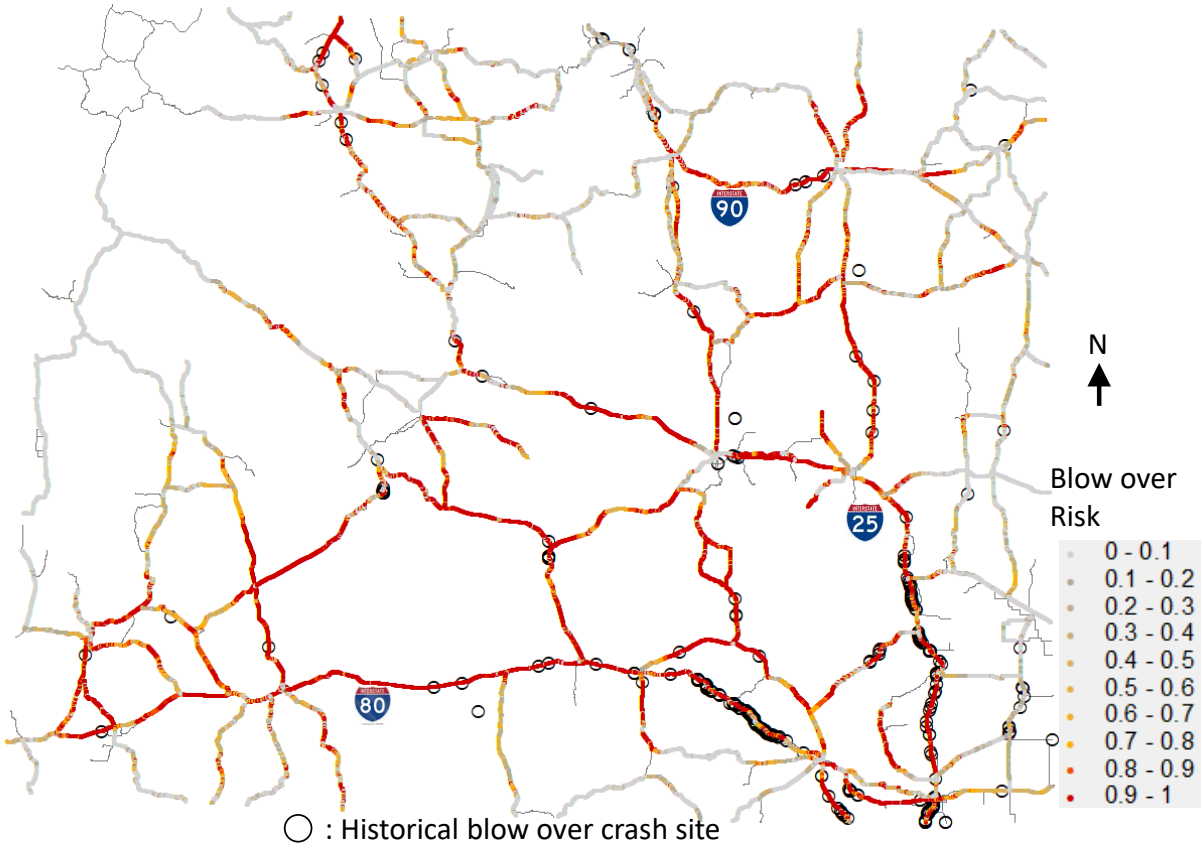

Source: Wyoming Geolibrary and WYDOT

Figure 50: Estimated blow over risk at the historical maximum wind on the highway network of Wyoming based on the WRF simulation.

Source: Wyoming Geolibrary and WYDOT

Figure 51: Estimated blow over risk at the historical maximum wind on the highway network of southeast Wyoming based on the WRF simulation. Black circles denote historical blow over crash sites.

Figure 52 illustrates the spatial coverage of the RWIS ESS with 10 km (6.2 mile) radii, in Wyoming. As discussed in Section 4.3.5, the accuracy of the blow over risk largely depends on the distance from the nearest wind monitoring station. Table 4 indicates that the predictability of the model significantly drops where the distance is greater than 10 km. Numerous road segments with blow over risk lie outside of RWIS ESS coverage. It is therefore recommended, based on these layered observations, to install additional roadside wind monitoring stations, especially for road sections with high traffic volume for high-profile light-weight vehicles.

Since it is unfeasible to cover the entire State of Wyoming with ground-based wind monitoring network instruments, the numerical weather prediction (NWP) model products must be effective at overcoming this shortcoming for the foreseeable future.

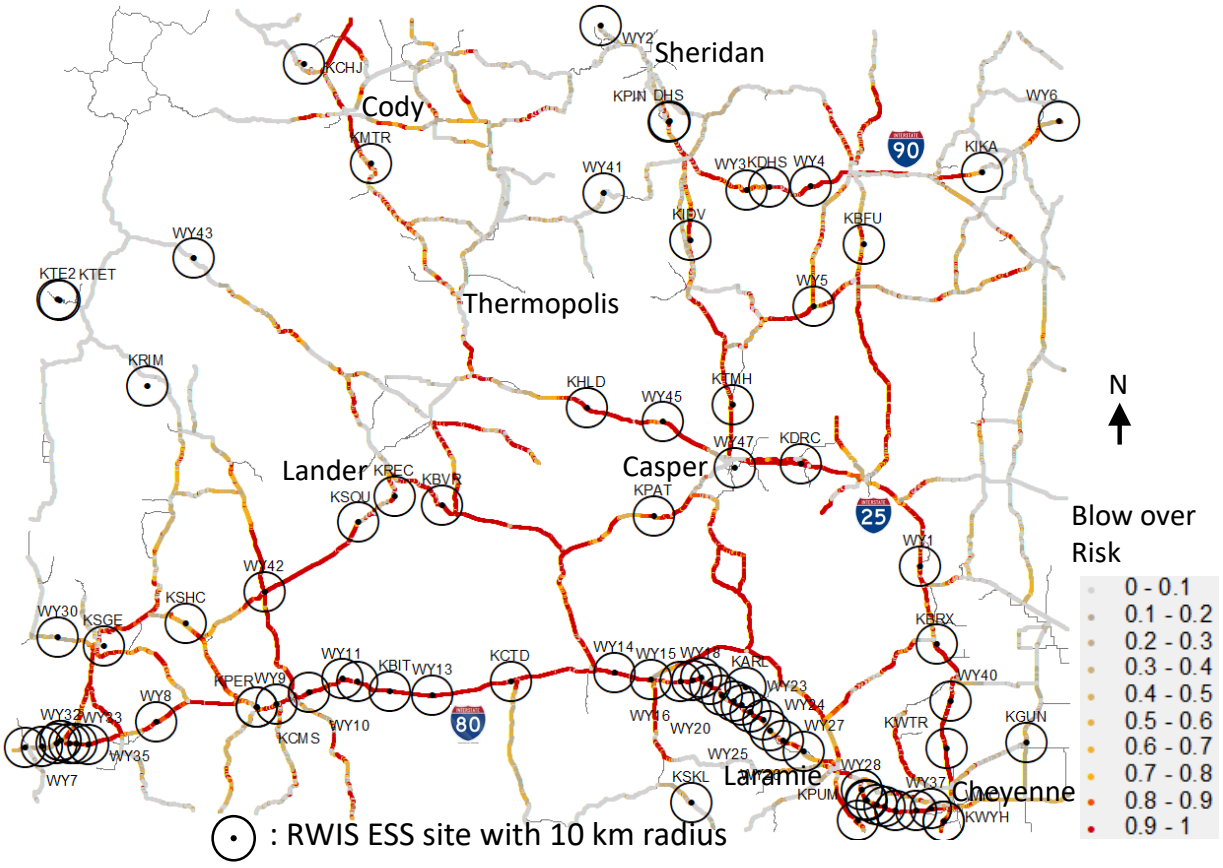

Source: Wyoming Geolibrary and WYDOT

Figure 52: Estimated blow over risk at the historical maximum wind and the 10 km coverage of the RWIS ESS network in Wyoming

Chapter 5 – Integration of Results into WYDOT Traveler Information Systems and Recommendations

Road weather management is a transportation field that aims to improve the resiliency of a given transportation network by reducing the impacts of weather on the safety and mobility of the network, and its users (FHWA, 2021). A comprehensive road weather management system includes weather monitoring and prediction; traveler information systems to convey information and recommendations to system users; and development and deployment of weather-responsive management strategies, such as setting regulatory or advisory speeds and implementing full or partial road closures. WYDOT has a long history of road weather management given the high elevations, challenging weather patterns, and remote areas that exist throughout the state. Managing high wind events has become an important feature of WYDOT's road weather management system given the prevalence and severity of these weather patterns. WYDOT has deployed an extensive system of field technologies, system monitors, back-office data systems, and, more recently, in-vehicle technologies to support these management activities.

This chapter describes the existing technologies, systems, and protocols deployed by WYDOT for the management of high wind events, and it explores how the results of the improved blow over risk model could be leveraged to improve the safety and efficiency of the system during high wind conditions. This chapter first describes the methods available for disseminating road weather information to motorists. Then, it explains how road weather information is obtained and hazardous conditions are identified. Finally, this chapter examines how the results from this project could be incorporated to improve the accuracy and timeliness of road weather information to help motorists better quantify their individual risks. Many of the systems and processes described in this chapter are utilized for a range of road weather events; however, the focus of the work in this report remains specific to high wind conditions.

5.1 Road Weather Information Dissemination

Road weather information can be an effective tool for improving the safety of a system by providing timely and actionable information to motorists that can affect their travel decisions about whether to make a particular trip or what is an appropriate driving speed. Road weather information can also help motorists to make moment-to-moment in-route decisions, such as whether to continue traveling, whether to find a safe place to park and wait out a weather event, whether to select an alternative route, or whether to simply turn around. The challenges of providing useful and timely information are compounded by the fast-moving weather events and the long distances between services in Wyoming, both of which combine to limit the points at which drivers can reasonably make "go/no go" decisions. Given these challenges, WYDOT has successfully developed a sophisticated system for providing road weather information to road users through a variety of platforms.

At the heart of the traveler information system is the TMC, in Cheyenne, Wyoming (Figure 53). The TMC is a 24/7/365 operation where TMC operators monitor the statewide roadway system, make decisions about the information that is sent out, and the methods used to reach motorists.

Photograph: Rhonda Young

Figure 53: WYDOT Cheyenne Traffic Management Center (TMC)

Some TMC information dissemination methods require action from the driver to either self-monitor, such as the WYDOT Traveler Information Service website, or to subscribe in advance to receive automatic notifications, such as the Wyoming 511 smartphone application that is GPS enabled to provide notifications specific to certain locations (Figure 54). Other methods are more directly available to all drivers on the highway, classic technology of Highway Advisory Radio (HAR), and, for specially equipped vehicles, new in-vehicle devices that are part of WYDOT's CV Pilot Deployment Project (WYDOT, 2021c).

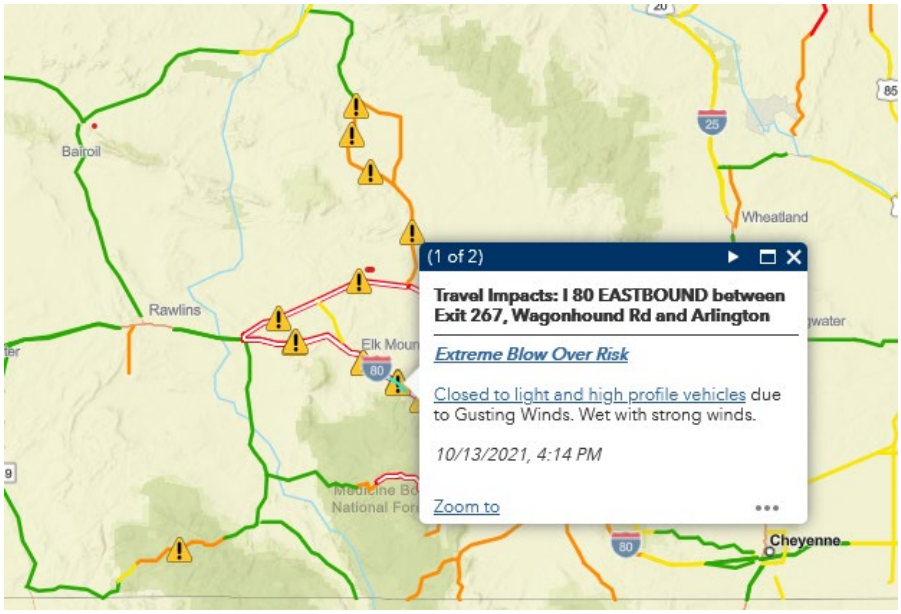

Source: Wyoroad.info

Figure 54: Example of an extreme blow over risk traveler message from Wyoroad.info

A specialized information source for travelers is the WYDOT Commercial Vehicle Operator Portal (CVOP), which is a free service provided to commercial vehicle operators that recognizes the unique challenges that larger and high-profile vehicles inevitably face during road weather events (WYDOT,

2021a). CVOP information is provided for travelers on the Wyoming interstates (I-25, I-80, and I-90) and other state routes frequented by freight traffic.

5.2 Generating Road Weather Information

TMC operators have a variety of information sources from which to generate road weather information for current and future conditions. Current weather information sources include a statewide system of RWIS outfitted with a host of environmental sensors, reports from maintenance and field personnel and in-house meteorologists, citizen reports through the 511 application, weather radar maps, and the Pikalert software program, which was deployed in recent years as part of USDOT's CV Pilot Deployment Program. Pikalert® also provides forecasted road weather information to the TMC along with regional and national weather forecasts and in-house meteorologists. This ensures that travelers and CVOP users are provided with 72-hour forecasts in 12-hour increments that concern visibility and road surface conditions. In addition, Pikalert® also provides three-hour incremental wind condition forecasts. An important component of generating road weather information is to recognize the difference between atmospheric weather (typically 30' and above) and road weather (<30'), and to translate information as necessary to predict what conditions the driver will experience. Therefore, these forecasts provide estimated road weather impact levels (low, moderate, or high) for different road segments for each of these weather conditions.

The most common types of high wind information provided to travelers are high wind warning messages that include the approximate wind speed or wind gust speed. As a more direct safety control, TMC operators can also lower the regulatory speed limit within variable speed limit corridors, which include about 150 miles of the 400-mile Wyoming Interstate 80 corridor. Advisory speed limits can be displayed in specially equipped vehicles enlisted in the CV Pilot in any part of the state. If conditions warrant, TMC operators can ultimately call for a wind-related closure for high-profile vehicles, which is communicated through DMS signs. For the most serious wind events or after high wind crashes occur, roadway segments can be closed to all vehicles through roadway closure gates.

The standard process for identifying high wind events is for TMC operators to monitor RWIS wind readings and to receive reports from field personnel. Messages are posted on DMSs stating that there is a blow over risk when wind gusts exceed 50 mph. An extreme blow over risk is posted when wind gusts exceed 60 mph. Current protocol calls for TMC operators to enable a wind-related road closure, if there are observed gust speeds above 60 mph or if there is a blow over crash. Once the road is closed due to wind gust speed, the wind gusts must be observed to be less than 50 mph for more than 30 minutes before the roads are re-opened. Closures can be partial in that they are limited to light, high-profile vehicles, such as moving vans, campers, recreational vehicles, small trailers, and empty or lightly-loaded commercial trucks. Partial closures require self-compliance, as there are no automatic enforcement measures in place, and it can be difficult to tell if a vehicle is lightly or fully loaded. If a driver is found to have ignored these messages, then he or she could be subject to fines and would be expected to pay the costs associated with any damage due to a crash that resulted from his or her decision to proceed along the roadway. Additional fines are up to $750 and 30 days in jail, subject to Wyo. Stat. §24-1-109.

At the Wyoming Hill investigation site, on I-25 specifically, another process has recently been deployed that WYDOT refers to as "sorting potatoes," which is a form of partial closure that does not rely on self-compliance alone. When wind conditions become high, but do not rise to the criteria of closing I-25 completely, the Wyoming Highway Patrol (WHP) will route all vehicles to the off ramps and separate the

vehicles into two groups. The first group consists of passenger vehicles and other low vulnerability vehicles, such as tanker trucks. The second group consists of the vehicle configurations most likely to overturn under high wind conditions—all high-profile vehicles and trucks with trailers. The WHP will allow the first group to pass through the Wyoming Hill corridor, while the second group is required to exit and is unable to proceed until the road is re-opened.

5.2.1 Pikalert® System

WYDOT was selected by the USDOT in 2015 as one of three sites to pilot connected vehicle technology. Part of the proposed system was to deploy a software technology called Pikalert®. The Pikalert® System was developed by the National Center for Atmospheric Research (NCAR) and is a collection of analysis modules comprised of the Vehicle Data Translator, Road Weather Hazard Module, Road Weather Forecasting System, Road Weather Alert Module, and the Motorist Advisory and Warning System (Young et al., 2018). The Pikalert® System is designed to retrieve weather data from vehicles and then combine this mobile data with RWIS and radar weather data to provide more accurate reporting of road surface weather conditions. A new component to Pikalert® with the Wyoming CV Pilot project is the Blow Over Hazard Module.

To communicate weather and environmental updates to vehicles, Pikalert® uses a Vehicle Data Translator module to log roadway conditions along the route. For this system, conditions are recorded every one mile along a WYDOT administrated road as well as every five minutes (see Figure 55).

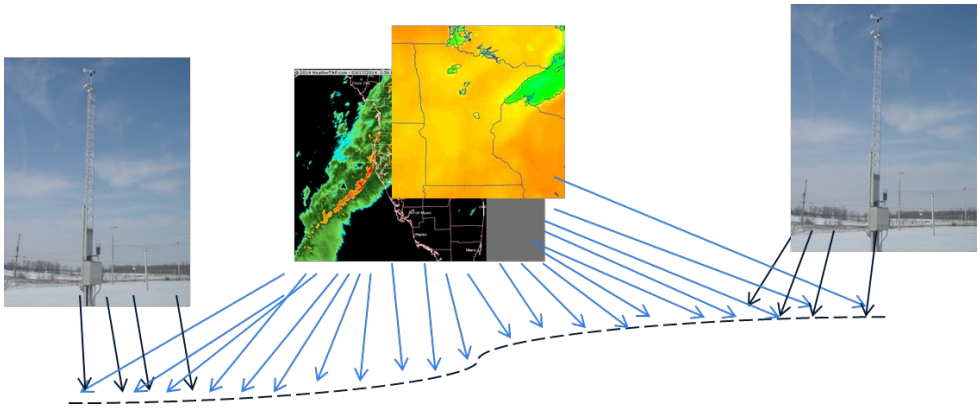

Source: Young, et al., 2018

Figure 55: Diagram of weather data feeding into vehicle data translator module's line of communication

Each connected vehicle that is part of the pilot program is equipped, as available, with the Weather Cloud system. This system tracks real time data relative to the vehicle (e.g., wiper frequency, GPS coordinates, ground temperature, ambient temperature, barometric pressure, relative humidity) on top of basic safety messages (BSMs) that the vehicle already carries (e.g., GPS coordinates, timestamp, ambient air pressure, exterior light, wiper status and rate, brake status, coefficient of friction of tires against the pavement, ABS/traction/stability control, etc.). Weather Cloud data is communicated to the RWIS and other vehicles through the connected vehicle modules (see Figure 56).

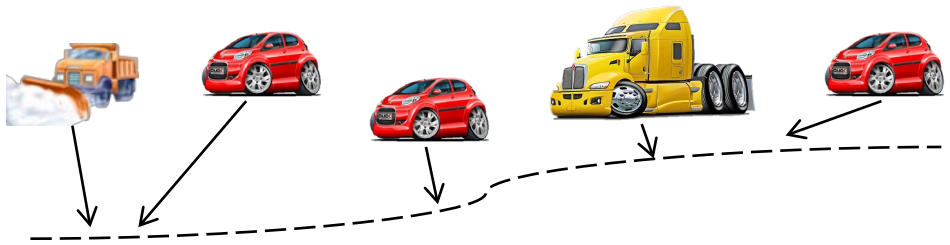

Source: Young, et al., 2018

Figure 56: Diagram of connected vehicles communicating road conditions and changes in road maintenance

The traditional weather observations from RWIS, Automated Surface Observing System (ASOS) stations, radar data, and background model analysis are mapped to road segments to provide details on the atmospheric and above-ground conditions (Figure 57).

Along with the Vehicle Data Translator is the Road Weather Hazard module that assesses the road segments for precipitation, visibility, and blow over hazards (Young, et al., 2019) using the collective road surface conditions, mobile data, and atmospheric weather data. Pikalert® then puts these parameters into a blow over algorithm based on fuzzy logic utilizing the road weather conditions and truck stability, and weight parameters to output driver alerts to three different truck types– heavy, light, and high-profile trucks, (Figure 57).

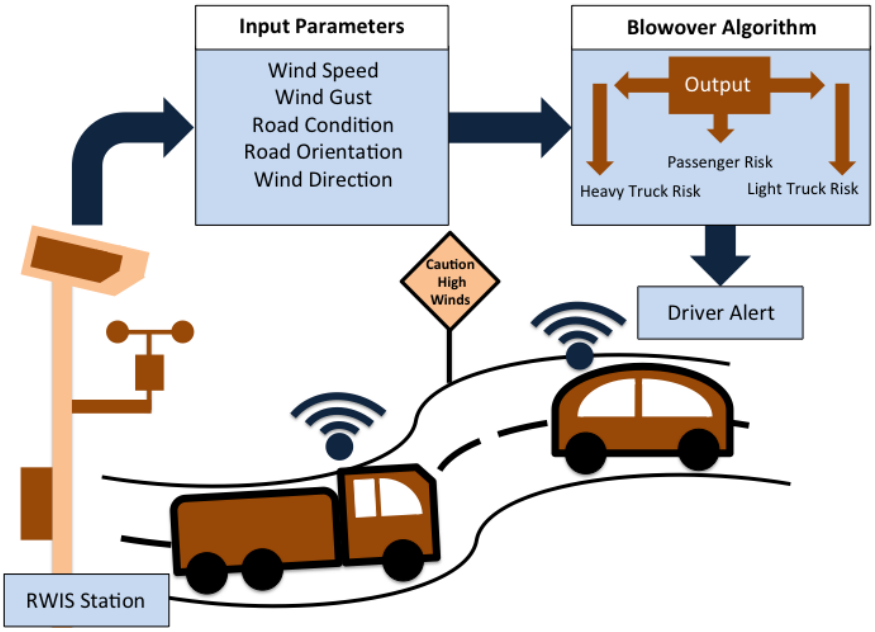

Source: Brittany Welch, 2018

Figure 57: Pikalert® Blow over Algorithm

Early versions of this algorithm were partially based on WYDOT high wind research in the Bordeaux area of I-25 (Young et al., 2010), along with research by Baker et al. (2008). The initial algorithm was tested on a dataset of crashes from 2010 to 2017. Refinements to the algorithm have since been implemented in the current phase of the CV Pilot project to provide more efficient alerts to drivers since the 2017-2018 algorithm testing resulted in an over-alerting of drivers, as well as missing wind differentials, directions, and functional information (Young, et. Al, 2018). Evaluation of the updated algorithm is currently ongoing and the Wyoming TMC is still using the previous version of the Pikalert algorithm and collecting data on the effectiveness of the alerts to drivers.

The current blow over hazard algorithm uses four sets of fuzzy logic weights and functions using wind gust speed, wind speed, wind direction relative to road segment, and whether or not there are slick road surface conditions. Sustained wind speed is used to compute the differential between sustained wind and wind gusts. The measured or estimated wind direction is compared to the road segment orientation to determine the direction of the wind relative to the road. The road surface slickness is based on the precipitation and pavement algorithms within Pikalert®. The precipitation algorithm generates precipitation type and intensity from air temperature and weather radar. Vehicle-based data, such as wiper status and blade speed, headlight status, and vehicle speed relative to speed limits, supplement the algorithm where available. The pavement algorithm uses the precipitation type and output from the precipitation algorithm along with road surface temperature and RWIS-reported surface condition to determine, if the pavement surface is impacted or dry. Vehicle-based anti-lock braking system (ABS) and traction system data can supplement the algorithm where available. The pavement algorithm output conditions are dry, wet, snowy, icy, or hydroplaning risk, along with a yes/no slickness flag. This slickness flag is the input to the blow over risk algorithm surface condition.

Wind hazard conditions are analyzed for four types of vehicles, including passenger cars, pickups with a trailer, high-profile light vehicles, and high-profile heavy vehicles. High-profile, heavy vehicles are taken to include semi freight trucks greater than 26,000 pounds, while light semi-trucks are considered to be between 10,000 and 26,000 pounds. For each of these vehicle types, an interest value between 0 and 1 is generated with 0 being no risk and 1 being the highest risk. If the interest value is calculated to be greater than 0.6, the algorithm produces a blow over risk for that vehicle type.

The Road Weather Alert (RWA) module in Pikalert® takes the hazard module output described above and generates traveler information alerts. The RWA provides segment-based assessments for road conditions at three alert levels: clear, advisory, and warning, and it also generates alert message text. This process avoids alerting drivers excessively (i.e., every mile) for conditions that remain constant for several miles. Further integration of Pikalert® in the road weather system occurs through the Motorist Advisory and Warning System (MAW) that takes the alerts from the RWA and pushes them to traditional systems, like the road weather web page, wyoroad.info, HAR, or the Wyoming 511 smartphone application.

During the deployment and evaluation phases of the Wyoming CV Pilot, the Pikalert messages were sent to the TMC operators for verification, and part of the system evaluation was to monitor the number of messages accepted or rejected by the TMC operators. This evaluation process has led to continuous improvement of the entire Pikalert® system over the last several years, as the software program has adapted to more complex weather patterns.

5.2.2 CV Pilot Spot Weather Impact Warning

The Spot Weather Impact Warning (SWIW) is part of the Wyoming CV Pilot project. This is the application that pushes weather alerts, including those generated by Pikalert®, into CV equipped vehicles (Figure 58). Each CV is equipped with both an onboard unit that sends and receives messages through short range and satellite communication technology, and an onboard tablet called the Human-Machine Interface (HMI) that displays received alerts. An example from the driver-training module of how this tablet is configured, is shown in Figure 59. During the Pilot deployment phase, the onboard unit (OBU) and HMI were after-market devices; however, they are expected to be fully integrated into vehicles at the factory as this technology becomes fully deployed over the next decade. Currently, there are some high-end vehicles sold that are already compatible with CV technology.

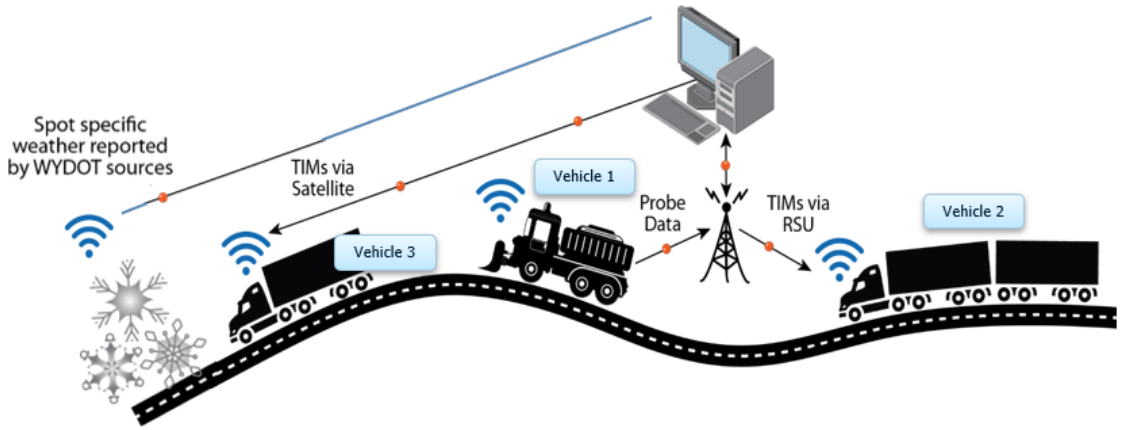

***Spot Weather Impact Warning**: Localized road weather information (fog, wind, ice, etc.)

Source: Gopalakrishna et al.,2016

Figure 58: CV Pilot spot weather impact warning application (SWIW)

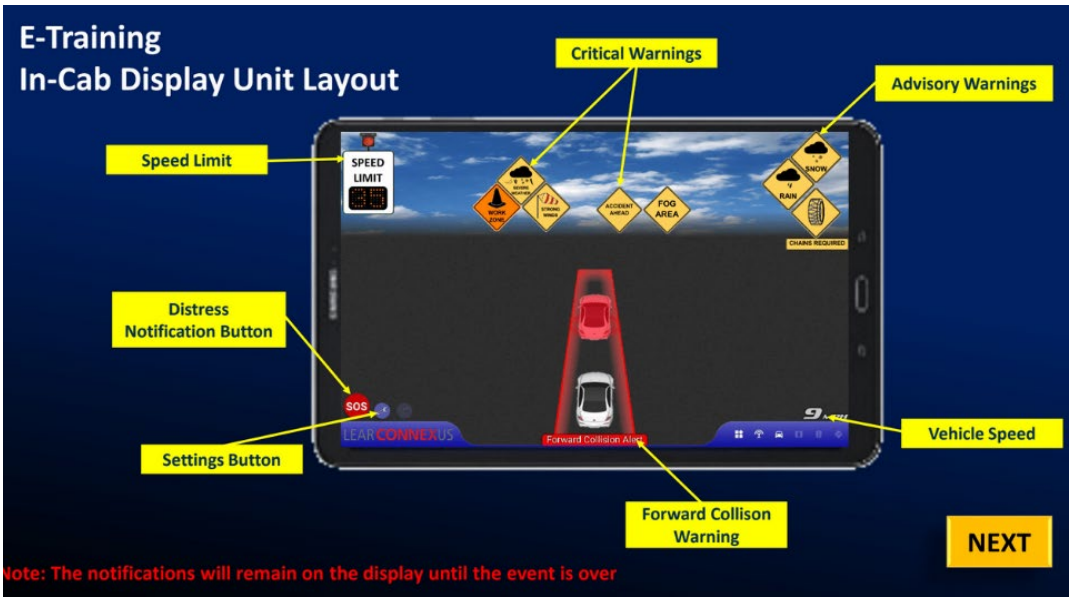

Source: Ahmed et al., 2019

Figure 59: CV Pilot Project HMI for traveler information messages

The CV Pilot system's warnings are derived from Traveler Information Messages (TIMs) that are generated in the TMC, either by TMC operators or automated through the Pikalert® system. As the Pikalert® system is still being calibrated, all messages generated are required to be verified by a TMC operator before being sent out as TIMs. TIM messages are sent to the vehicles and held until the vehicle enters a specified location (known as a geofence) associated with that message. The message is presented as text on the HMI, and an audible alert is broadcasted in the vehicle, if the vehicle operator opted for sound alerts.

5.3 Incorporating Findings into Road Weather Systems

For the results of this research to be fully leveraged toward improving the safety and mobility of the transportation system, the developed model should be integrated into the Road Weather Management systems at WYDOT. This can be done in the back-office systems that generate and manage road information for the TMC operators, similar to how the Pikalert® system is integrated. Alternatively, this research can also be applied through a more manual approach by influencing the wind thresholds used for setting different alert levels, such as blow over risk or extreme blow over messaging.

Current protocols, as explained in earlier sections, are dependent only on wind and wind gust speeds, and not on current speed limits, whether static or dynamic. Given the work done in this research regarding establishing the blow over risk relative to vehicle speeds, it is possible to use this methodology for setting variable speed limits, during high wind events to reduce risks. Advisory speed limits using this same methodology could be incorporated into vehicle-based solutions, such as the CV Pilot program and the Wyoming 511 smartphone application.

Another enhancement this model brings to the management system for high wind events is risk guidance measures that are more vehicle specific. If the weight and vehicle configuration details are provided to the system, a much more specific and useful risk could be calculated. This is similar to the Pikalert®

system's use of four vehicle configurations. This feature could be managed through the CVOP for freight travelers specifically.

Finally, another foreseeable enhancement would be the integration of the vehicle risk calculations with predicted weather. As discussed above, WYDOT is currently providing forecasts in 72-hour increments for general weather and in 3-hour increments for wind events (or 12-hour forecast windows for visibility and surface conditions). The blow over hazard methodology is currently based on real time RWIS observations, but it could be modified to ingest forecasted wind data and turn it into predicted risk values.

Chapter 6- Products

This chapter provides an enumeration of major product deliverables from this research project.

6.1 Demonstrative Real Time Implementation of the Blow Over Risk Evaluation System

The configured blow over risk evaluation system was implemented in real time on the BO-Wyomig website.

This demonstration is described in Section 4.3.6. below are the listed specifications of the current real time blow over risk map script:

- Blow over risk is quantified at every MP point (not every 0.1 mile) because of the map resolution.
- Each road point is associated with its two nearest weather stations. If the nearest station does not have wind recordings, the script looks for the second nearest station. If the second nearest station does not have the effective data, it will display as 'data is not available'.
- The National Highway System (NHS) accounts for about 90 percent of the heavy traffic in Wyoming. Therefore, only the MPs that fall under these highways are considered.
- The script only generates maps when there is an update to the data.
- If the Internet connection is lost or if the server for the website is down, then the script will try to read the website every 30 seconds. The program will not be terminated even with connectivity failure.
- The size of each dot also reflects the blow over risk level.
- The color palette of the map can be adjusted.

6.2 GIS map of road geometry (shapefile and csv)

The estimated road geometry parameters presented in Section 4.2 are stored in ArcGIS shapefile (Esri vector data) and .csv file formats. The GIS shapefile was projected in the WGS 84 / UTM zone 13N coordinate system. These files contained the following variables:

OBJECTID	= Sequential number
NAME	= Milepost (real number)
HIGHWAY_CO	= Highway name (e.g., I-25 eastbound)
ROUTE_ID	= Route ID
ORIENTATION	= Road azimuth angle (degree)
RADIUS_M_1	= Radius of curve (meter, 0 = straight section)
X_CENTER	= X coordinate of curve center (meter, UTM13, 0 = straight section)
Y_CENTER	= Y coordinate of curve center (meter, UTM13, 0 = straight section)
X_WGS84	= X coordinate of road center = Longitude (degree, WGS84)
Y_WGS84	= Y coordinate of road center = Latitude (degree, WGS84)
X_UTM13N_	= X coordinate of road center (meter, UTM13)
Y_UTM13N_	= Y coordinate of road center (meter, UTM13)
SPEED_LIMIT_MPH	= Speed limit (mph)
CANT %	= Cant angle/superelevation/cross angle of road surface
SIDEWRTORIENT	= Road orientation
RWIS_ID	= Nearest RWIS station ID

RWIS_ELE = Elevation of the nearest RWIS station
XL = X coordinate of left side reference elevation point (meter, UTM13)
YL = Y coordinate of left side reference elevation point (meter, UTM13)
XR = X coordinate of right side reference elevation point (meter, UTM13)
YR = Y coordinate of right side reference elevation point (meter, UTM13)
LEFTELE = Left side reference elevation (meter)
ELEVATIONROAD = Elevation of the road center (meter)
RIGHTELE = Right side reference elevation (meter)
BRIDGE? = Estimated bridge identifier (0: not on bridge; 1: on bridge)
h' = Relative road elevation (meter)

6.3 Blow Over Hazard Map (shapefile and csv)

The data of the developed blow over hazard map presented in Section 4.4 are stored in ArcGIS shapefile (Esri vector data) and .csv file formats. The GIS shapefile was projected in the WGS 84 / UTM zone 13N coordinate system. These files contained the following variables.

N = Sequential number (starting at 0)
OBJECTID = Sequential number (natural numbers)
LON = X coordinate of road center = Longitude (degree, WGS84)
LAT = Y coordinate of road center = Latitude (degree, WGS84)
X_UTM13N = X coordinate of road center (meter, UTM13)
Y_UTM13N = Y coordinate of road center (meter, UTM13)
ELV = Elevation of the road center (meter)
HIGHWAY_CO = Highway name (e.g., I25E = I-25 eastbound)
MileMarker = Milepost or MP (real number)
P[A1_max] = Probability of blow over on positive direction lane at historical maximum wind
P[A0_max] = Probability of blow over on opposite direction lane at historical maximum wind
P[A1_avg] = Probability of blow over on positive direction lane at historical average wind
P[A0_avg] = Probability of blow over on opposite direction lane at historical average wind
P[A_max] = Probability of blow over at historical maximum wind (max of both directions)*
P[A_avg] = Probability of blow over at historical average wind (max of both directions)

* This variable was used for the final Blow Over Hazard Map

6.4 Blow Over Sensitivity Analysis Source Code for General Characterization for Practice (Python code)

The source code of the sensitivity analysis presented in the Section 3.10 uses the same sub-program as the real time implementation of the blow over risk evaluation system. The program was written in the Python computer coding language. The user can modify the parameters in the section entitled "user specified parameters" for different conditions.

Input file: None

Output file: None (graphics)

6.5 Blow Over Hazard Map Source Code (Python code)

The program demonstrated the spatial implementation of the blow over cash risk evaluation. This code was not optimized for maximum computational efficiency; therefore, it takes several minutes to run all 53,527 road points (every 0.1 mile) in the Wyoming highway system. The output was presented in Section 4.4. The program was written in the Python computer coding language.

Input files: Met_Stat.csv; Road_Param.csv

Output file: BO_risk_hist.csv

The input file, Met_Stat.csv, contains the following variables estimated from the WRF simulation (Ohara, 2017).

NUM = Sequential number
LON(DEG) = X coordinate of road center = Longitude (degree, WGS84)
LAT(DEG) = Y coordinate of road center = Latitude (degree, WGS84)
ELV(M) = Elevation of the road center (meter)
U10ALL(M/S) = U component mean wind speed at 10 m height
V10ALL(M/S) = V component mean wind speed at 10 m height
N_DATA = Number of effective samples
WSP10(M/S) = Mean wind speed at 10 m height
G10(M/S) = Gust (max) wind speed at 10 m height
WSP1L(M/S) = Mean wind speed of the lowest layer of the WRF model
AZIMUTH_ALL = Mean wind azimuth angle (degree)
SD_AZIMUTH = Standard deviation of wind azimuth angle (degree)
1ST_max(WSP10) = Greatest mean wind speed in the historical period
2ND_max(WSP10) = 2nd greatest mean wind speed in the historical period
3RD_max(WSP10) = 3rd greatest mean wind speed in the historical period
4TH_max(WSP10) = 4th greatest mean wind speed in the historical period
5TH_max(WSP10) = 5th greatest mean wind speed in the historical period
1ST_max(G10) = Greatest gust (max) wind speed in the historical period
2ND_max(G10) = 2nd greatest gust (max) wind speed in the historical period
3RD_max(G10) = 3rd greatest gust (max) wind speed in the historical period
4TH_max(G10) = 4th greatest gust (max) wind speed in the historical period
5TH_max(G10) = 5th greatest gust (max) wind speed in the historical period

6.6 Excel spreadsheet for critical vehicle velocity

This MS Excel spreadsheet was used to check the developed system. The critical vehicle speed can be computed using this simple spreadsheet.

6.7 Publications on the Blow Over Risk Evaluation Methodology

Methodological development in this project was submitted to the Transportation Research Record (TRR) journal. This publication included details about the study area, the field measurements, the vehicle stability modeling, the local wind field adjustment, and the risk evaluation methodology. The abstract of the draft manuscript is posted below:

> "Tractor-trailer blow over crashes caused by strong winds are a major concern for the safety of their operators and others sharing the road. These crashes also trigger highway closures resulting in considerable economic impact. This study presents a blow over model based on stability forces that

integrates the wind field, road geometry, and vehicle specifications to provide critical vehicle speeds. A high-frequency sonic anemometer was deployed at the study area which oversaw three blow over crashes after its installation. For quantifying the blow over risk, the values of critical vehicle speed generated from the high-frequency winds provided ample data to identify exponential-gamma distribution as the best fitting distribution among a list of possible distributions. The results showed critical vehicle speed from the model dipped to the levels of the posted speed limit or below at the time of blow overs for all three blow over crashes. Furthermore, the probability of blow over based on the exponential-gamma distribution showed spikes in blow over probability during the time of blow over. This demonstrates the ability of the framework to identify the instance of higher blow over risk and provides enough evidence to proceed with further studies on its application on a larger scale with wind measurement from the more prevalent mechanical anemometers."

6.8 Opportunities for Training and Professional Development

Graduate assistant Mr. Adarsha Neupane has contributed to this project through the field monitoring system by assembling, programming, adjusting, installing, and maintaining the UW weather station. He has also completed data analysis and calibration under the supervision of Dr. Noriaki Ohara at the University of Wyoming. Mr. Neupane also provided support to the Winter Research Services at WYDOT.

Undergraduate assistant Mr. Antonio Roman Campos contributed to this project and this report under the supervision of Dr. Rhonda Young at Gonzaga University. Mr. Campos completed the statistical analysis of historic wind data 2012-2017, and he served as an editor and co-author of this report. Mr. Campos also contributed to this project by applying the expertise he has gained from his work as a researcher on the team of the WYDOT CV Pilot.

Chapter 7 – Conclusions and Recommendations

The stochastic blow over model for a tractor-trailer truck developed herein was envisioned to become a decision support system for road managers in Wyoming, one of the windiest states in the Union.

Major influencing factors on a blow over crash, such as wind speed, gust speed, wind direction, travel speed, vehicle weight, and road geometry, were integrated by the developed static vehicle stability model. This computationally efficient model can transform a multivariate, highly complex problem into a univariate system, in terms of the critical vehicle speed. The critical vehicle speed, which changes every second and every road segment, is defined as the maximum travel speed without a blow over risk. The critical vehicle speed was chosen as a design feature because it is recognized as one of the most easily adjustable variables for travelers as well as for road managers, who can respond to it through speed limit adjustment.

Frequency histograms of computed critical vehicle speeds (V_c) using the high frequency wind data from Wyoming Hill were modeled by statistical distribution. The estimated distribution could quantify the probability of blow over risk for a high-profile light-weight vehicle at every time interval. However, it is important to note that the blow over risk in this system does not include the probability of an at-risk vehicle being present on the road. No crash should occur even when very high blow over risk exists if a high-profile light-vehicle is not present, such as during a full road closure. Therefore, the methodology separated the probability of blow over risk from the probability of a blow over crash.

Detailed analyses of the blow over incidents reported during the project period and in the study area verified that the deterministic model was insufficient to predict the blow over crash; therefore, the stochastic approach was required. Through testing various statistical distributions, the exp-gamma distribution was found to be the most effective to model the stochastic process of vehicle blow over risk. A practical method was developed to determine the three-parameter distribution from the commonly available measurements, such as mean and maximum (gust) wind speeds. The statistical model was found to be effective at quantifying the blow over risk in terms of temporal probability of blow over within a wind measurement time interval in the presence of a high-profile, light-weight vehicle on a road segment. However, the model efficiency significantly dropped on the road points where the distance from the wind monitoring station was greater than 10 km (6.2 miles).

The sensitivity analysis of the vehicle stability model characterized the blow over risk of the vehicle with various attributes. As anticipated, the analysis demonstrated that, in general, road curvature causes asymmetry in the blow over risk associated with wind direction while the weight of the vehicle is crucially important in blow over risk. Applications using the historical RWIS data demonstrated the predictive capability of the developed tool for the historical blow over crashes. Blow over hazard maps were produced based on the reconstructed historical maximum and mean wind fields using the WRF model outputs. The hazard map showed about 43 percent of the Wyoming highway network was vulnerable to blow over crash at least once in the historical period. Finally, the model was implemented for the real time blow over risk map now available through the Internet.

The final task accomplished was to review WYDOT's Road Weather Management System processes to explore how the results of this research could be incorporated into the system to improve the accuracy and timeliness of the high wind hazard information. Given the wide range of roadside infrastructure, in-

vehicle technology, and back-office systems at the WYDOT Traffic Management Center, there is substantial potential for integration. The blow over risk algorithm (Young et al., 2018) in the Wyoming CV Pilot Pikalert program was also reviewed to improve the blow over risk quantification using the developed tool based on the wind speed of the RWIS ESS. Integration between these two models is also promising. However, given the current status of ongoing Pikalert® updates for the CV Pilot project, fully exploring this option was not possible at this time.

In conclusion, the following recommendations were drawn from the work of this project:

- The RWIS ESS should be enhanced to cover the blow over hotspots identified by the hazard map within at least 10 km (6.2 miles) for accurate blow over risk evaluation with correlated consideration of the traffic volume of high-profile, light-weight vehicles.
- Numerical weather prediction (NWP) model products may be a feasible option to interpolate the wind field between the RWIS ESS.
- Blow over risk prediction is viable because the developed model can be coupled with the NWP systems (e.g. Rapid Refresh (RAP) numerical weather model, the High-Resolution Rapid Refresh (HRRR)).
- The model sensitivity can be adjusted by the factor of safety (FOS) in the vehicle stability model. Further study on the FOS determination is recommended to help work toward accurate decision support systems and better traveler information messages through Dynamic Message Signs (DMS).
- The Pikalart system may incorporate the computed blow over risk from this model as an additional predictor variable. Discussions with the Wyoming CV Pilot Team, including NCAR team members, should be pursued.

References

AASHTO. (2018). A Policy on Geometric Design of Highways and Streets, 7th Edition. In American Association of State Highway and Transportation Officials.

Ahmed, M. M., Yang, G., & Gaweesh, S. (2019). Development and assessment of a connected vehicle training program for truck drivers. Transportation research record, 2673(2), 113-126.

Alonso-Estébanez, A., del Coz Díaz, J. J., Álvarez Rabanal, F. P., and Pascual-Muñoz, P. (2017). Performance analysis of wind fence models when used for truck protection under crosswind through numerical modeling. Journal of Wind Engineering and Industrial Aerodynamics, 168(March), 20–31. https://doi.org/10.1016/j.jweia.2017.04.021

Alrejjal, A., Farid, A., and Ksaibati, K. (2021). A correlated random parameters approach to investigate large truck rollover crashes on mountainous interstates. Accident Analysis and Prevention, 159(June), 106233. https://doi.org/10.1016/j.aap.2021.106233

Anderson, A. R. S., Wiener, G., Linden, S., Petzke, W., Guevara, G. N., Boyce, B. C., and Pisano, P. (2016). The Pikalert®Vehicle Data Translator Updates and Applications. Proceedings of the 32nd Conference on Environmental Information Processing Technologies, New Orleans, LA, USA, 10–14.

Ayodele, T, Jimohn A, Munda, J and Agee J (2012). Wind distribution and capacity factor estimation for wind turbines in the coastal region of South Africa. Energy Conversion and Management, 64, 614–625. https://doi.org/10.1016/j.enconman.2012.06.007

Baker, C. J. (1986). A simplified analysis of various types of wind-induced road vehicle accidents. Journal of Wind Engineering and Industrial Aerodynamics, 22(1), 69–85. https://doi.org/10.1016/0167-6105(86)90012-7

Baker, C. J. (1988). High sided articulated road vehicles in strong cross winds. Journal of Wind Engineering and Industrial Aerodynamics, 31(1), 67–85. https://doi.org/10.1016/0167-6105(88)90188-2

Baker, C. J. (1994). The quantification of accident risk for road vehicles in cross winds. Journal of Wind Engineering and Industrial Aerodynamics, 52(C), 93–107. https://doi.org/10.1016/0167-6105(94)90041-8

Baker, C. J., Quinn, A. D., and Sterling, M. (2008). Wind impact on transportation and power supply systems. Report Prepared for the UK Meteorological Office, Project PB/P001421

Baker, C. J., and Reynolds, S. (1992). Wind-induced accidents of road vehicles. Accident Analysis and Prevention, 24(6), 559–575. https://doi.org/10.1016/0001-4575(92)90009-8

Balsom, M., Wilson, F. R., and Hildebrand, E. (2006). Impact of wind forces on heavy truck stability. Transportation Research Record, 1969, 115–120. https://doi.org/10.3141/1969-18

Bíl M, Andrášik R, Sedoník J, and Cícha V. (2018). ROCA – An ArcGIS toolbox for road alignment identification and horizontal curve radii computation. PLoS ONE, 13(12), 1–15. https://doi.org/10.1371/journal.pone.0208407

Carlo M, and Appendix I. (1996). EXTREME WIND DISTRIBUTION TAILS: A “PEAKS OVER THRESHOLD” APPROACH. 122(5), 539–547.

Chen, F., Peng, H., Ma, X., Liang, J., Hao, W., and Pan, X. (2019). Examining the safety of trucks under crosswind at bridge-tunnel section: A driving simulator study. Tunnelling and Underground Space Technology, 92(July), 103034. https://doi.org/10.1016/j.tust.2019.103034

Chen, S., and Chen, F. (2010). Simulation-based assessment of vehicle safety behavior under hazardous driving conditions. Journal of Transportation Engineering, 136(4), 304–315. https://doi.org/10.1061/(ASCE)TE.1943-5436.0000093

Chen, S. R., and Cai, C. S. (2004). Accident assessment of vehicles on long-span bridges in windy environments. Journal of Wind Engineering and Industrial Aerodynamics, 92(12), 991–1024. https://doi.org/10.1016/j.jweia.2004.06.002

Coleman, S. A., and Baker, C. J. (1994). An experimental study of the aerodynamic behaviour of high sided lorries in cross winds. Journal of Wind Engineering and Industrial Aerodynamics, 53(3), 401–429. https://doi.org/10.1016/0167-6105(94)90093-0

Curtis, J. and K. Grimes. (2004) Wyoming Climate Atlas. Office of the Wyoming State Climatologist, Laramie, WY.

Dookie, I., Rocke, S., Singh, A., and Ramlal, C. J. (2018). Evaluating wind speed probability distribution models with novel goodness of fit metric: a Trinidad and Tobago case study. International Journal of Energy and Environmental Engineering, 9(3), 323–339. https://doi.org/10.1007/s40095-018-0271-y

Federal Highway Administraiton (FHWA) (2021) Road Weather Management Program Website [Internet]. Office of Operations. https://ops.fhwa.dot.gov/weather/. Accessed September 15, 2021.

Gopalakrishna, D., Garcia, V., Ragan, A., English, T., Zumpf, S., Young, R., Ahmed, M., Kitchener, F. and Serulle, N.U. (2016), “Connected vehicle pilot deployment program phase 1, concept of operation (ConOps), ICF/Wyoming”, Report No. FHWA-JPO-16-287, U.S. Department of Transportation, Washington, DC.

Hibino, Y., and Ishida, H. (2003). Static analysis on railway vehicle overturning under crosswind. RTRI report, 39-44.

Hong, S. Y., and Lim, J. O. J. (2006). The WRF single-moment 6-class microphysics scheme (WSM6). J. Korean Meteor. Soc, 42(2), 129-151.

Hou, G., Chen, S., and Chen, F. (2019). Framework of simulation-based vehicle safety performance assessment of highway system under hazardous driving conditions. Transportation Research Part C: Emerging Technologies, 105(May), 23–36. https://doi.org/10.1016/j.trc.2019.05.035

Hovey, P. and DeFiore, T. (2003). Using Modern Computing Tools to Fit the Pearson Type III Distribution to Aviation Loads Data, DOT/FAA/AR-03/62, Office of Aviation Research, Washington, D.C. 20591

Imai, T., Fujii, T., Tanemoto, K., Shimamura, T., Maeda, T., Ishida, H., and Hibino, Y. (2002). New train regulation method based on wind direction andvelocity of natural wind against strong winds. Journal of wind engineering and industrial aerodynamics, 90(12-15), 1601-1610.

Kantar, Y. M., and Usta, I. (2008). Analysis of wind speed distributions: Wind distribution function derived from minimum cross-entropy principles as a better alternative to Weibull function. Energy Conversion and Management, 49(5), 962–973. https://doi.org/10.1016/j.enconman.2007.10.008

Kull, K. (2017). Wind gusts top 60 mph, Trucks topple on I-25 [Internet]. Wyoming Tribune Eagle. https://www.wyomingnews.com/news/local_news/wind-gusts-top-60-mph-trucks-topple-on-i-25/article_1bc2dcf6-ce8c-11e7-9dda-5baa8e983b17.html. Accessed September 15, 2021.

Kunieda, M. (1972). Theoretical study on the mechanics of overturn of railway rolling stock. Railway Technical Research Report, 793, 1-15.

Kusaka, H, H Kondo, Y Kikegawa, F Kimura (2001) A simple single-layer urban canopy model for atmospheric models: comparison with multi-layer and slab models, Boundary-Layer Meteorology 101 (3), 329-358.

Kyte, M., Shannon, P., and Kitchener, F. (2000). Idaho Storm Warning System Operational Test. Idaho Deparment of Transportation

LaChance, B. (2020, 11 13). High Wind, Winter Storm Warnings in Effect for Much of Wyoming through Saturday [Internet]. Retrieved from Oil City News: https://oilcity.news/community/2020/11/13/strong-winds-on-i-25-i-80-in-wyoming-gusts-reaching-near-70-mph-in-some-areas/ . Accessed September 15, 2021.

Liesman, J. S. (2005). An analysis of Wyoming truck crashes. In Masters Abstracts International(Vol. 45, No. 06).

McKnight, A. J., and Bahouth, G. T. (2009). Analysis of large truck rollover crashes. Traffic Injury Prevention, 10(5), 421–426. https://doi.org/10.1080/15389580903135291

McNeill, D., and Freiberger, P. (1994). Fuzzy logic: The revolutionary computer technology that is changing our world. Simon and Schuster.

Morrison, H., and Gettelman, A. (2008). A new two-moment bulk stratiform cloud microphysics scheme in the Community Atmosphere Model, version 3 (CAM3). Part I: Description and numerical tests. Journal of Climate, 21(15), 3642-3659.

National Research Council. (2010). Technologies and approaches to reducing the fuel consumption of medium-and heavy-duty vehicles. National Academies Press.

Ohara, N. (2017). Historical Winter Weather Assessment for Snow Fence Design Using a Numerical Weather Model.

Saiidi, M., and Maragakis, E. (1995). Identification of trigger wind velocities to cause vehicle instability : final report to the Nevada Department of Transportation.

Snæbjörnsson, J. T., Baker, C. J., and Sigbjörnsson, R. (2007). Probabilistic assessment of road vehicle safety in windy environments. Journal of Wind Engineering and Industrial Aerodynamics, 95(9–11), 1445–1462. https://doi.org/10.1016/j.jweia.2007.02.020

Synoptic Data. (2021). Synoptic Data API Services. https://developers.synopticdata.com

United States Department of Transportation (USDOT) (2018). Federal Motor Carrier Safety Administration.Large Truckand Bus Crash Facts 2016 [Internet]. USDOT, Washington, D.C. www.fmcsa.dot.gov/safety/data-and-statistics/large-truck-and-bus-crash-facts-2016. Accessed September 15, 2021.

United States Department of Transportation (USDOT) (2021). Connected Vehicle Pilot Deployment Program – Wyoming DOT Pilot [Internet]. Intelligent Transportation Systems Joint Program Office. https://www.its.dot.gov/pilots/pilots_wydot.htm. Accessed September 15, 2021.

U.S. Geological Survey (USGS) (1999). National Elevation Dataset, EROS Data Center.

Wang, B., and Xu, Y. L. (2015). Safety analysis of a road vehicle passing by a bridge tower under crosswinds. Journal of Wind Engineering and Industrial Aerodynamics, 137, 25–36. https://doi.org/10.1016/j.jweia.2014.11.017

Welch, B. (2018). The Truck Blowover Algorithm for the Pikalert ® System.

Wolfram Research. (2010). ExpGammaDistribution [Internet]. Wolfram Language Function. https://reference.wolfram.com/language/ref/ExpGammaDistribution.html Accessed September 15, 2021.

WYDOT. (2016a). Understanding Wyoming's High Winds [Internet]. WYDOT videos on YouTube. Available from: https://www.youtube.com/watch?v=dIql3dWIRB4andab_channel=WYDOTVIDEOS. Accessed September 15, 2021.

WYDOT. (2016b). Blow over Brochure [Internet]. Wyoming Department of Transportation. Available from: https://www.dot.state.wy.us/files/live/sites/wydot/files/shared/Public%20Affairs/brochures/blow-over%20brochure.pdf . Accessed September 15, 2021.

WYDOT. (2021a). WYDOT Commercial Vehicle Operator Portal website [Internet]. https://cvop.wyoroad.info/cvop/

WYDOT. (2021b). Statewide Weather Sensors [Internet]. https://wyoroad.info/pls/Browse/WRR.RWIS. Accessed September 15, 2021.

WYDOT. (2021c). Wyoming Connected Vehicle Pilot Website [Internet]. Wyoming Department of Transportation. https://wydotcvp.wyoroad.info/research.html. Accessed September 15, 2021.

WYDOT. (2021d). Wyoming Travel Information Service Website [Internet]. Wyoming Department of Trasnportation. https://wyoroad.info/. Accessed September 15, 2021.

Yamartino, R. J. (1984). A comparison of several "single-pass" estimators of the standard deviation of wind direction. Journal of Climate and Applied Meteorology, 23(9), 1362-1366.

Young, R., and Liesman, J. (2007a). Estimating the relationship between measured wind speed and overturning truck crashes using a binary logit model. Accident Analysis and Prevention, 39(3), 574–580. https://doi.org/10.1016/j.aap.2006.10.002

Young, R., and Liesman, J. (2007b). Intelligent transportation systems for operation of roadway segments in high-wind conditions. Transportation Research Record.2007;2000(1):1–7. https://doi.org/10.3141/2000-01

Young R, Offei E, Dai Q. (2010) High Wind Warning System for Bordeaux, Wyoming. WYDOT FHWA-WY-10/05F.

Young, R. K., Welch, B. M., and Siems-Anderson, A.R., (2018). Generating Weather Alerts Including High Wind Blowover Hazards Using PikAlert® for the Wyoming Connected Vehicle Pilot Project, TRB, under review

Young R; Welch B, Siems-Anderson A. (2019) Generating Weather Alerts Including High Wind Blow over Hazards Using Pikalert ® for the Wyoming Connected Vehicle Pilot Project. Proceedings from the 98th Annual Meeting of the Transportation Research Board, Washington, D.C., January 2019.

Zeng Z, Ziegler A., Searchinger T., Yang L. Chen A., Ju K. Piao S., Li L., Ciais P, Chen D., Lui J., Azorin-Molina C., Chappell A., Medvigy D., Wood E. (2019) A Reversal in Global Terrestrial Stilling and Its Implications for Wind Energy Production. Nature Climate Change, Vol 9, December 2019, pp. 979-985.

Appendix: Variable Glossary

α	Factor of safety (FOS)	A_y	Reference area from the side
b	Width of vehicle	C_D	Drag coefficient for crosswind
h	Height of vehicle	ω	Vehicle angular velocity
h_D	Height of center of drag force	R	Radius of curve
h_C	Height of center of centrifugal force	M	Mass of the vehicle
y_L	Length of the center of lift forces	V	Velocity of the vehicle
y_W	Length of the center of gravitational force	U_x	Headwind component of wind speed
L_x	Lift force due to headwind	U_y	Crosswind component of wind speed
L_y	Lift force due to crosswind	U_{obs}	Observed wind speed
D_y	Drag force	h_{obs}	Anemometer height
F_C	Centrifugal force	z_0	Roughness height
W	Gravitational force	d	Zero plane displacement
C_{Lx}	Lift coefficient for headwind	Ψ_R	Relative azimuth angle
C_{Ly}	Lift coefficient for crosswind	Ψ_W	Wind azimuth angle
ρ	Density of air	Ψ_V	Vehicle azimuth angle
A_x	Reference area from the front		